



**FACULTY
OF MATHEMATICS
AND PHYSICS**
Charles University

MASTER THESIS

Jan Střeleček

**Some funny small things looking for
counterdiabatic elements**

Supervisor of the master thesis: prof. RNDr. Pavel Cejnar, Dr.,
DSc.

Study programme: Theoretical physics

Study branch: hmmmmm

Prague 2022

I declare that I carried out this master thesis independently, and only with the cited sources, literature and other professional sources. It has not been used to obtain another or the same degree.

I understand that my work relates to the rights and obligations under the Act No. 121/2000 Sb., the Copyright Act, as amended, in particular the fact that the Charles University has the right to conclude a license agreement on the use of this work as a school work pursuant to Section 60 subsection 1 of the Copyright Act.

In date
Author's signature

Dedication. To Michal and Kuba for discussions

Computational resources were supplied by the project "e-Infrastruktura CZ" (e-INFRA LM2018140) provided within the program Projects of Large Research, Development and Innovations Infrastructures.

Title: Some funny small things looking for counterdiabatic elements

Author: Jan Střeleček

Institute:

Supervisor:

Abstract: Abstract.

Keywords: key words

Contents

| | |
|---|----|
| Some notes to the notation | 3 |
| Introduction | 4 |
| 1 Mathematical introduction | 5 |
| 1.1 Fiber bundle | 6 |
| 1.2 Vector Bundle | 6 |
| 1.2.1 Connection on vector bundles | 7 |
| 1.2.2 Metric on vector bundles | 7 |
| 1.3 Section | 7 |
| 1.4 Pull-back and push forward | 7 |
| 1.5 Covariant derivative and parallel transport | 8 |
| 1.6 Parallel transport on vector bundles | 8 |
| 1.7 Antisymmetric tensors and wedge product | 8 |
| 1.8 Geometry in 2 dimensions | 9 |
| 1.9 Riemannian geometry definitions | 9 |
| 1.10 Riemannian geometry theorems | 10 |
| 2 Physical introduction | 11 |
| 2.1 Transporting states | 13 |
| 2.2 Metric and geometric tensor | 15 |
| 2.2.1 Derivation of the geometric tensor | 17 |
| 2.3 Adiabaticity | 17 |
| 2.3.1 Slow transports | 17 |
| 2.4 Gauge potentials | 19 |
| 2.4.1 Classical gauge potential | 19 |
| 2.4.2 Quantum gauge potential | 20 |
| 2.4.3 Adiabatic gauge potential | 20 |
| 2.5 Counter-diabatic driving | 21 |
| 2.5.1 Explicit form | 22 |
| 2.6 Berry phase and curvature | 23 |
| 3 Geodesics | 24 |
| 4 Spin 1/2 | 26 |
| 4.1 Special case | 27 |
| 5 Lipkin-Meshkov Glick model | 29 |
| 5.1 Case $N = 3$ | 29 |
| 5.2 Case $N = 5$ | 36 |
| 5.3 Limit $N \rightarrow \infty$ | 40 |
| 5.4 Arbitrary N | 41 |

| | |
|---|-----------|
| 6 Two leve system | 44 |
| 6.0.1 Harmonic oscillator correspondence | 44 |
| 6.1 Geodesical driving | 45 |
| 6.1.1 Derivation of the fidelity | 46 |
| 6.1.2 Analysis of the infidelity formula | 47 |
| 6.1.3 Energy variance | 50 |
| 6.2 Linear driving | 51 |
| 6.2.1 Dependence on time | 52 |
| 6.2.2 Final fidelity | 53 |
| 6.2.3 Critical time T_c | 56 |
| 6.2.4 Coefficients ξ and κ | 57 |
| 6.2.5 Summary | 58 |
| 6.2.6 Energy variance | 59 |
| 6.3 Energy variance for two level system | 60 |
| 7 From the projective Hilbert space to state manifolds | 61 |
| 7.1 Projective Hilbert space | 61 |
| 7.2 Restriction to eigenstate manifolds | 62 |
| 8 The meaning of geodesics | 66 |
| 8.1 Transport using quenches | 66 |
| 9 The role of geodesics | 70 |
| 9.1 Minimizing the energy variance | 70 |
| Conclusion | 71 |
| Bibliography | 72 |
| List of Figures | 73 |
| A Appendix 1 | 76 |
| B Attachments | 77 |
| B.1 First Attachment | 77 |

Some notes to the notation

| Symbol | Meaning | Defining formula |
|---------------|---------------------------------|--|
| \mathcal{A} | Gauge (calibrational) potential | $\mathcal{A}_\mu = i\hbar\partial_\mu$ |
| \mathbb{N} | Natural numbers, without zero | |

Mathematical spaces will be denoted *mathcal* and operators with *hat*.

Introduction

1. Mathematical introduction

The modern approach to the closed system dynamics is using differential geometry formalism. Before we get to the quantum mechanics itself, lets define the formalism and recapitulate some definitions of this branch of mathematics. More detailed notes can be found for example in [Fecko, 2006].

Let's have a manifold \mathcal{M} and curves

$$\gamma : \mathbb{R} \xrightarrow{\text{open}} I \rightarrow \mathcal{M} \quad \xi \mapsto \gamma(\xi).$$

The space of functions is $\mathcal{F}(\mathcal{M}) \equiv \{f : \mathcal{M} \rightarrow \mathbb{R}\}$, where

$$f : \mathcal{M} \rightarrow U \xrightarrow{\text{open}} \mathbb{R} \quad x \mapsto f(x).$$

To define *vectors* on \mathcal{M} , we need to make sense of the *direction*. It is defined using curves satisfying

$$\begin{aligned} \gamma_1(0) &= \gamma_2(0) \equiv P \\ \frac{d}{dt} x^i(\gamma_1(t)) \Big|_{t=0} &= \frac{d}{dt} x^i(\gamma_2(t)) \Big|_{t=0}. \end{aligned}$$

Taking the equivalence class created by those two rules, sometimes noted as $[\gamma] = v$, we have element of the tangent space to \mathcal{M} . We will use standard notation for the tangent space to \mathcal{M} in some point xP as $\mathbb{T}_P\mathcal{M}$ and contangent space as $\mathbb{T}_P^*\mathcal{M}$. Unifying all those spaces over all x we get tangent and cotangent bundle, $\mathcal{T}\mathcal{M}$ and $\mathcal{T}^*\mathcal{M}$ respective. To generalize this notation to higher tensors, we denote $\mathbb{T}_P\mathcal{M} \in \mathcal{T}^1\mathcal{M}$, $\mathbb{T}_P^*\mathcal{M} \in \mathcal{T}_1\mathcal{M}$, thus the space of p -times contravariant and q -times covariant tensors is denoted $\mathcal{T}_q^p\mathcal{M}$.

Using the congruence of the curves on \mathcal{M} , the expression

$$\frac{d}{d\xi} f \circ \gamma(\xi) \Big|_{\xi=0} \tag{1.1}$$

has a good meaning and we can define the *derivative* in some $P \in \mathcal{M}$ as

$$\mathbf{v} : \mathcal{F}(\mathcal{M}) \rightarrow \mathbb{R} \quad f \mapsto \mathbf{v}[f] \equiv \frac{df(\gamma(\xi))}{d\xi} \Big|_P \equiv \partial_\xi \Big|_P f. \tag{1.2}$$

It holds, that $\mathbf{v} \in \mathbb{T}_P\mathcal{M}$ and can be expressed as the *derivative in direction*,¹ which can be understood in coordinates as

$$\mathbf{v}[f] = \frac{d}{d\mathbf{v}} f \circ \gamma(\xi) \Big|_{\xi=0} = v^\mu \frac{d}{dx^\mu} f(x) \Big|_P. \tag{1.4}$$

The directionnal derivative will be denoted

$$\nabla_v$$

¹The direction itself is usually denoted as

$$\frac{D}{d\alpha} \gamma(\xi), \tag{1.3}$$

where the big D notation is used to point out that it's not a classical derivative, but it maps curves to some entirely new space of directions.

and in basis $\mathbf{e}_i \equiv \partial/\partial x^i$ we will denote

$$\nabla = (\mathbf{e}_x, \mathbf{e}_y, \mathbf{e}_z).$$

To get some physical application, we need to define one strong structure on manifolds – differentiable metric tensor $g_{\mu\nu} \in \mathcal{T}_2^0 \mathcal{M}$ – so the covariant derivatives and parallel transport are well-defined everywhere.

1.1 Fiber bundle

We already know tangent and cotangent spaces. Thinking of manifold \mathcal{M} as a fiber, for which at any point x we create new manifold $\mathbb{T}_x \mathcal{M}$, we and unifying all those tangent spaces, we get so-called *vector bundle*.

Definition 1. *Structure $(\mathcal{E}, \mathcal{B}, \pi, \mathcal{F})$, for topological spaces \mathcal{E} (total space), \mathcal{B} (base space), \mathcal{F} (fibre) and a continuous surjection $\pi : \mathcal{E} \rightarrow \mathcal{B}$ satisfying a local triviality² is called a Fiber bundle (projection map). In addition, the \mathcal{B} is assumed to be connected³ and for every $x \in \mathcal{B}$, there is an open neighborhood $\mathcal{U} \subset \mathcal{B}$ (trivializing neighborhood) such that there exists a homeomorphism from \mathcal{U} to so-called product space*

$$\phi : \pi^{-1}(\mathcal{U}) \rightarrow \mathcal{U} \times \mathcal{F},$$

such that $\pi^{-1} \circ \pi(\mathcal{U}) = \mathcal{U}$.

The above mappings can be more clear from figure 1.1. Because projections of products are open maps, $\pi : \mathcal{E} \rightarrow \mathcal{B}$ must be open map. The meaning of

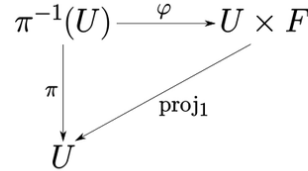


Figure 1.1: Mappings needed for the bundle definition.

definition is, that manifolds at every point $x \in \mathcal{F}$ are all locally diffeomorphic to each other.

1.2 Vector Bundle

Conversely, given a fiber bundle $(\mathcal{E}, \mathcal{X}, \pi, \mathcal{Rk})$ with a $GL(k)$ cocycle acting in the standard way on the fiber \mathcal{Rk} , there is associated a vector bundle. This is sometimes taken as the definition of a vector bundle

²local triviality

³can't be represented as a union of two disjoint sets

1.2.1 Connection on vector bundles

[Loring, 2017][chap. 10.1] Connection maps vector from tangent space to base manifold \mathcal{X} with some element from total space \mathcal{E} to total space

$$\Gamma : \mathcal{X} \times \mathcal{E} \rightarrow \mathcal{E}$$

such, that

- $\Gamma_X s$ is \mathcal{F} -linear in X and \mathbb{R} -linear in s
- Leibniz rule for $f \in \mathcal{C}^\infty$ is satisfied: $\Gamma_X(fs) = (Xf)s + f\Gamma_X s$

1.2.2 Metric on vector bundles

Map

$$g_{\mu\nu} : \mathcal{B} \times \mathcal{B} \rightarrow \mathbb{R}$$

1.3 Section

Section is a function

$$f : \mathcal{B} \rightarrow \mathcal{F},$$

such that $\pi(f(x)) = x$ for $\forall x \in \mathcal{B}$. This defines new manifold cutting throw \mathcal{E} .

Sectioning of fiber bundles creates vector spaces

1.4 Pull-back and push forward

Push-forward and pull-back are used to transport vectors and covectors between manifolds. Let's have two manifolds \mathcal{M}, \mathcal{N} , a smooth mapping ϕ and functions f, \tilde{f} such that

$$\begin{aligned} \phi : \mathcal{M} &\rightarrow \mathcal{N} & x &\mapsto \phi x \\ \tilde{f} : \mathcal{N} &\rightarrow \mathbb{R} & & \end{aligned}$$

Pull-back of the function then defines a new function $f : \mathcal{M} \rightarrow \mathbb{R}$ as

$$\phi^* : \mathcal{F}\mathcal{N} \rightarrow \mathcal{F}\mathcal{M} \quad \tilde{f} \mapsto f = (\phi^*\tilde{f})(x) \equiv \phi^*\tilde{f}(x) = \tilde{f}(\phi x).$$

Push-forward of a vector is defined as

$$\phi_* : \mathbb{T}_x \mathcal{M} \rightarrow \mathbb{T}_{\phi x} \mathcal{N} \quad \phi_* \frac{D\gamma(\xi)}{d\xi} \Big|_x = \frac{D\phi\gamma(\xi)}{d\xi} \Big|_x$$

and *pull-back of a covector* $\tilde{\alpha} \in \mathbb{T}_{\phi x} \mathcal{N}$ is

$$\phi^* : \mathbb{T}_{\phi x} \mathcal{N} \rightarrow \mathbb{T}_x \mathcal{M} \quad (\phi^*\tilde{\alpha})_\mu v^\mu \Big|_x = \tilde{\alpha}_\mu (\phi_* v)^\mu \Big|_{\phi x}.$$

If ϕ has a smooth inversion, i.e. it is a diffeomorphism, we can define pull-back of vectors as

$$\phi^* = \phi_*^{-1} \tag{1.5}$$

and push-forward of covectors

$$\phi_* = (\phi^{-1})^* \tag{1.6}$$

1.5 Covariant derivative and parallel transport

this section is probably not needed

Covariant derivative is generally... Metric covariant derivative is...

Parallel transport of vector $\mathbf{v} \in \mathbb{T}_p\mathcal{M}$ will be denoted $\text{par}_\gamma \mathbf{v} \in \mathbb{T}$

Affine connection can be expressed as

$$\Gamma_{\mu\nu}^\alpha = \frac{1}{2}g^{\alpha\beta}(g_{\beta\mu,\nu} + g_{\nu\beta,\mu} - g_{\mu\nu,\beta}), \quad (1.7)$$

where we used comma notation for the coordinate derivative. The covariant derivative of $\mathbf{a} \in \mathbb{T}_P\mathcal{M}$ is then defined

$$\frac{D\mathbf{a}^\mu}{dx^\nu} = a_{,\nu}^\mu - \Gamma_{\alpha\beta}^\mu x^\alpha a^\beta \quad (1.8)$$

and for $\boldsymbol{\alpha} \in \mathbb{T}_P^*\mathcal{M}$ it is

$$\frac{D\boldsymbol{\alpha}_\mu}{dx^\nu} = \alpha_{\mu,\nu} - \Gamma_{\mu\beta}^\alpha x^\beta \alpha_\alpha \quad (1.9)$$

The vector $v \in \mathbb{T}_P\mathcal{M}$ is said to be parallel transported along curve $\gamma(\lambda)$, if it's covariant derivative

$$\frac{Dv^\mu}{d\xi} = 0 \quad (1.10)$$

vanishes along γ .

1.6 Parallel transport on vector bundles

this is what we need Parallel transport of vector V along curve γ will be denoted

$$\text{par}_\gamma V.$$

It is

1.7 Antisymmetric tensors and wedge product

p -form $A \in \mathcal{T}_p\mathcal{M}$ is called *antisymmetric*, if changing the order of the indices has impact only on the sign, symbolically

$$A_{i_1 \dots i_p} = \text{sign}(\sigma) A_{i_{\sigma_1} \dots i_{\sigma_p}},$$

where σ is some permutation. *Antisymmetrisation* is defined as a normalized sum over all permutation

$$A^{[i_1 \dots i_p]} \equiv \frac{1}{p!} \sum_{\sigma} A^{[i_{\sigma_1} \dots i_{\sigma_p}]} \quad (1.11)$$

The *wedge product* of $A \in \mathcal{T}_p\mathcal{M}$ and $B \in \mathcal{T}_q\mathcal{M}$ is antisymmetrisation of the tensor product in the sense

$$A \wedge B \equiv \frac{(p+q)!}{p!q!} A^{[i_1 \dots i_p]} \otimes B^{i_1 \dots i_q} \quad (1.12)$$

1.8 Geometry in 2 dimensions

Most general object to start with is the *Riemann tensor*

$$R^\alpha_{\beta\gamma\delta} := \Gamma^\alpha_{\beta\delta,\gamma} - \Gamma^\alpha_{\beta\gamma,\delta} + \Gamma^\mu_{\beta\delta}\Gamma^\alpha_{\mu\gamma} - \Gamma^\mu_{\beta\gamma}\Gamma^\alpha_{\mu\delta}. \quad (1.13)$$

Ricci tensor can be defined as its contraction

$$R_{\alpha\gamma} := R^\mu_{\alpha\mu\gamma}, \quad (1.14)$$

which is second order symmetric tensor. *Ricci scalar* is defined as contraction of Ricci tensor

$$R := R^\mu_\mu. \quad (1.15)$$

This can be simplified for 2 dimensional manifold as

$$R = \frac{2}{g_{22}} \left(\Gamma^1_{22,1} - \Gamma^1_{12,2} + \Gamma^1_{11}\Gamma^1_{22} + \Gamma^1_{12}\Gamma^2_{22} - \Gamma^1_{21}\Gamma^1_{12} - \Gamma^1_{22}\Gamma^2_{12} \right). \quad (1.16)$$

Another possibility to express Ricci tensor, see Gutiérrez-Ruiz et al. [2021, eq. 6,7]

$$R = \frac{1}{\sqrt{|g|}} (\mathcal{A} + \mathcal{B}) \quad (1.17)$$

for

$$\mathcal{A} := \left(\frac{g_{12}}{g_{11}\sqrt{|g|}} g_{11,2} - \frac{1}{\sqrt{|g|}} g_{22,1} \right)_{,1} \quad (1.18)$$

$$\mathcal{B} := \left(\frac{2}{\sqrt{|g|}} g_{12,1} - \frac{1}{\sqrt{|g|}} g_{11,2} - \frac{g_{12}}{g_{11}\sqrt{|g|}} g_{11,1} \right)_{,2}. \quad (1.19)$$

This equation turned out to be more numerically unstable, therefore eq. 1.16 will be user later on.

1.9 Riemannian geometry definitions

Definition 2 (Riemannian manifold). *Manifold is called Riemannian, iff its equipped with positive definite metric tensor.*

Definition 3 (Connected manifold). *Manifold is connected, iff the distance between two points is infimum of the lengths of curves joining the two points.*

Definition 4 (Compact manifold). *Manifold is said to be compact if its every open cover has a finite subcover.*

Definition 5 (Geodesical completeness). *A manifold is said to be geodesically complete if its every geodesic can be extended to infinite values of their affine parameter.*

This condition holds if the space does not contain any singularities and its coordinate-independent notion.

Definition 6 (Geodesic maximality). *A manifold is said to be geodesically maximal if its eigter geodesically complete, or every non-complete geodesic (such that cannot be extended to infinite values of their affine parameter) ends in a singularity.*

Geodesic maximality is coordinate dependent notion, if the manifold is geodesically complete.

1.10 Riemannian geometry theorems

Theorem 1 (Von Neumann-Wigner). *(Von Neumann J, Wigner E. 1929. Physikalische Zeitschrift 30:467-470) This, sometimes called the Non-Crossing Theorem states, that the eigenvalues of Hermitian matrix driven by N continuous real parameters forms at maximum $N - 2$ dimensional submanifold.*

Theorem 2 (Hopf-Rinow Theorem). *For connected Riemannian manifold \mathcal{M} with the metric g , following are equivalent:*

- (\mathcal{M}, g) is geodesically complete, i.e. all geodesics are infinite
- (\mathcal{M}, g) is geodesically complete at some point P , i.e. geodesics going throw P are infinite
- (\mathcal{M}, g) satisfies the Heine-Borel property, i.e. every closed bounded set is compact
- (\mathcal{M}, g) is complete as a metric space.

See Petersen [1998][p.125].

Theorem 3 (Modified Hopf-Rinow Theorem). *For connected Riemannian manifold \mathcal{M} with the metric g , any two points of \mathcal{M} can be joined with a minimizing geodesic. See Gorodski [2012][Chapter 3].*

This generally means, that in a space with singularity exists such points, which cannot be connected with the rest of the manifold using geodesics. Term "event horizon" will be used for such segments of manifold, as is common in General relativity.

Theorem 4. *A compact Riemannian manifold is geodesically complete. See Gorodski [2012][Chapter 3].*

2. Physical introduction

Most parts of this chapter are inspired by [Kolodrubetz et al., 2017] and original notes [Berry, 1984], [Berry, 1989], [Berry, 2009]. Now we will assign some physical background to the structure defined in the first chapter. We will see, that the whole space structure is quite complicated, because it's of fiber structure, where every fiber is another fiber bundle. Luckily what we will be using later on are only some much easier Riemannian submanifolds.

Assume parameter $\lambda \in \mathcal{U} \subset \mathbb{R}^n$ controlling some Hamiltonian $\hat{H}(\lambda)$, which is bounded from below and the spectrum is discrete for the first $k > 1$ energies, will be clear later on. From this we can construct fiber bundle, such that at every point of base manifold $\lambda \in \mathcal{U}$, we construct fiber spanning all possible states of $\hat{H}(\lambda)$, thus the fiber structure can be according to section 1.1 written as

$$\left(\mathcal{H}_{full} := \bigcup_{\lambda} \mathcal{H}(\lambda), \mathcal{U} \subset \mathbb{R}^n, \pi, \mathcal{H}(\lambda) := \bigcup_{states} |\psi(\lambda)\rangle \right).$$

The projection is defined as $\pi(\lambda) : |\psi(\lambda)\rangle \mapsto \lambda$ and $\mathcal{H}(\lambda)$ is Hilbert space for all pure states of $\hat{H}(\lambda)$. Geometric intuition is displayed in fig. 2.1

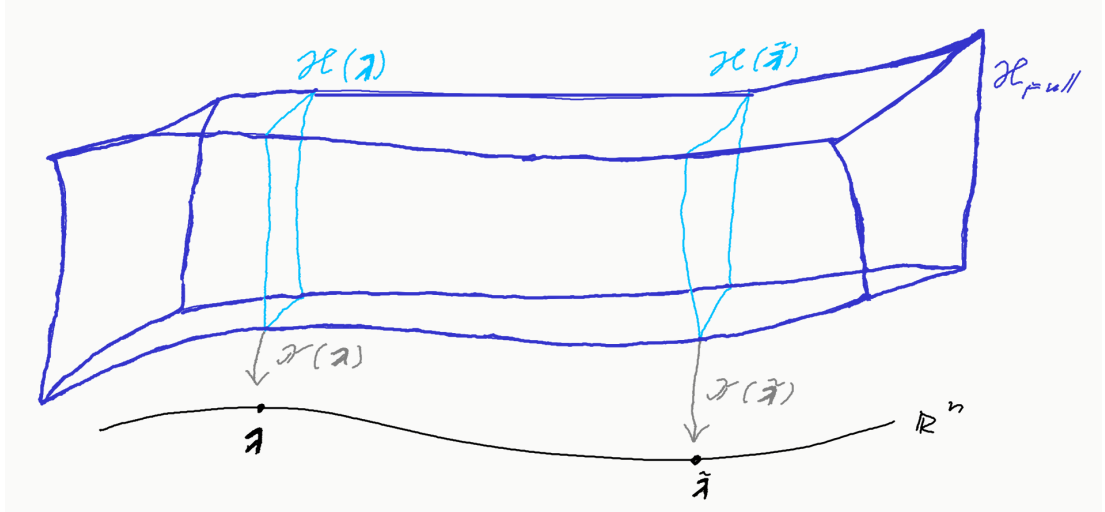


Figure 2.1: Fiber bundle over \mathbb{R}^n with Hilbert spaces $\mathcal{H}(\lambda)$ as individual fibers.

Because we are interested only in discrete part of spectrum¹, it will further on be referred to only as *spectrum*.

The states of the system evolve according to the Schrödinger equation

$$i\hbar d_t |\psi(\lambda(t))\rangle = \hat{H}(\lambda) |\psi(\lambda(t))\rangle, \quad (2.1)$$

which for eigenstates of instantaneous Hamiltonian reads as energy Schrödinger equation

$$\hat{H}(\lambda) |s(\lambda)\rangle = E_s(\lambda) |s(\lambda)\rangle. \quad (2.2)$$

For every $\mathcal{H}(\lambda)$ the first k energies can be sorted from the lowest to create discrete set $\sigma(\hat{H}(\lambda)) \equiv \{E_0, \dots, E_k\}$. Clearly, there exists a bijection between all fibers

¹Spectrum of the operator consists of discrete spectrum, calculable as eigenvalue problem, continuous and residual spectrum.

$\mathcal{H}(\lambda)$, thus we can define *section* \sec_s , mapping eigenstate corresponding to energy E_s to base manifold

$$\sec_s : |o(\lambda)\rangle \mapsto \mathcal{U} \subset \mathbb{R}^n,$$

which is also bijection. For $\forall s \in \{0, k\}$ we can create according to sec. 1.3 new *energy manifolds*

$$\mathcal{M}_s \subset \mathcal{M},$$

with special importance of the *ground state manifold* \mathcal{M}_0 , which will be used later on for adiabatic transports of ground states. Geometrical intuition is drawn on fig. 2.2. Because those manifolds were created by sectioning, they are considered to be vector spaces in a geometrical sense. This was expected, because they contain quantum states.

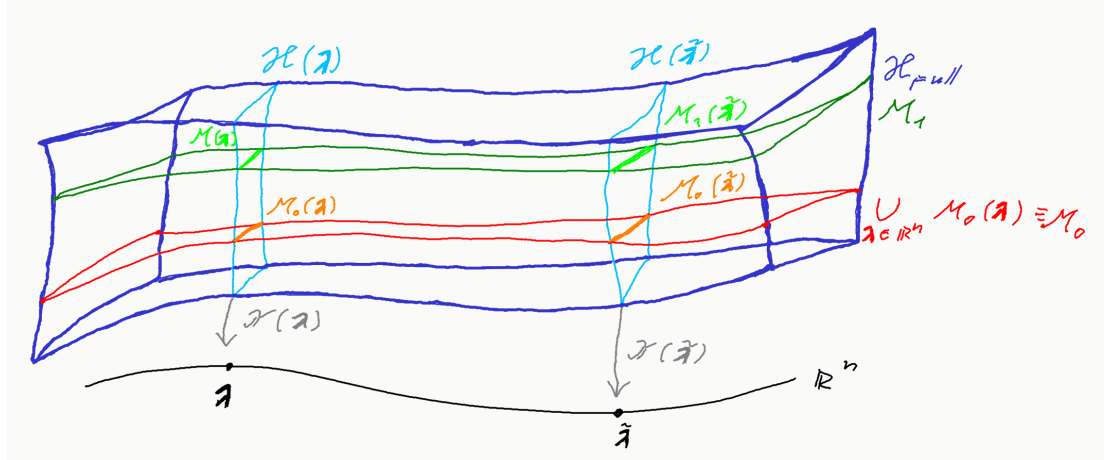


Figure 2.2: Geometrical intuition to transport on fiber manifold sections \mathcal{M}_i .

All Hilbert spaces above are considered to be spaces of *bare states* \mathcal{H} . In quantum mechanics, physical observables are related to the *space of rays*, defined as $\mathcal{PH} := \mathcal{H}/U(1)$, where elements of $U(1)$ are unitary transformations $e^{i\phi}$ for $\phi \in \mathbb{R}$ defining gauge symmetry between quantum states. The geometrical intuition is drawn for any λ on fig. 2.3.

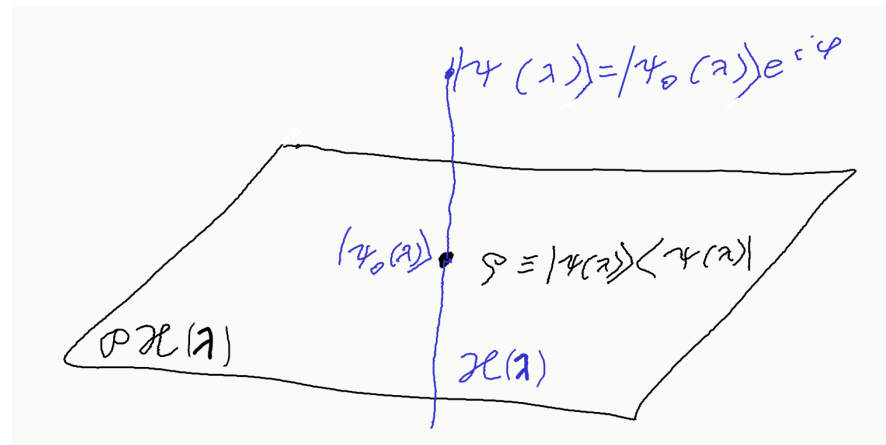


Figure 2.3: Space of bare states and its projection to space of rays $\mathcal{PH}(\lambda) := \mathcal{H}(\lambda)/U(1)$.

This means, that energy manifolds \mathcal{M}_s , generated by bare states, are again of fiber structure, defined as

$$(\mathcal{H}, \mathcal{PH}, \pi_{rays}, \{e^{i\phi} |\psi\rangle \text{ for } \phi \in \mathbb{R}\}),$$

where π_{rays} is just rule setting phase ϕ to zero. Because all \mathcal{M}_s are compact and connected, they are diffeomorphic to each other.

2.1 Transporting states

Let's now focus on decomposition of \mathcal{H}_{full} to different state manifolds \mathcal{M}_s , as displayed on figure 2.4.

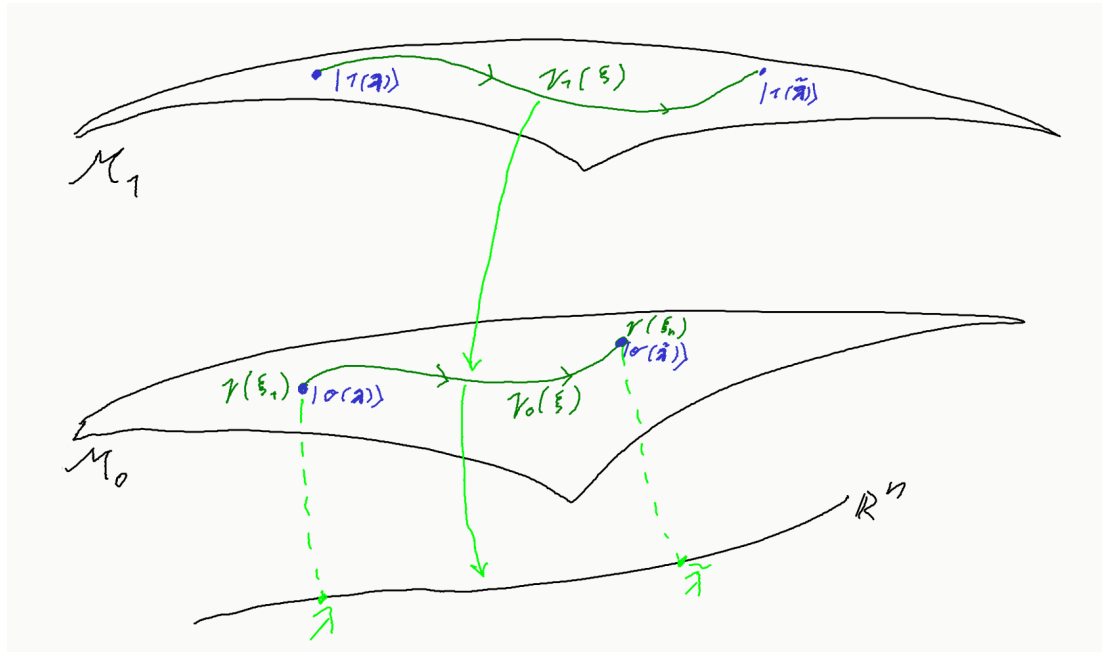


Figure 2.4: Geometrical intuition to transport on fiber manifold sections \mathcal{M}_s .

Changing state from eigenstate $|s(\lambda)\rangle$ to any pure state $|\psi(\tilde{\lambda})\rangle$, during some time period, is unitary transformation and can be thought of as *parallel transport on fiber bundle* between two vectors. Assuming the transport goes along curve $\{\gamma_s(\xi) | \xi \in [\xi_1, \xi_2] \subset \mathbb{R}\} \subset \mathcal{M}_s$ This can be written as

$$|\psi(t)\rangle \equiv \text{par}_{\gamma_s} |s(\lambda)\rangle = \exp\left(-\frac{i}{\hbar} \int_0^t E_s(\tau) d\tau\right) \exp(i\gamma_s(\xi)) |s(\lambda)\rangle. \quad (2.3)$$

The first exponential, the *dynamical phase*, is well known solution to energy Schrödinger equation 2.2 with $\lambda = \text{const}$ and depends only on time and energy of states during the transport. The second exponential is called *geometrical phase*. This phase is generally non-integrable, meaning it cannot be written simply as $\gamma_s(\lambda)$ and for some closed curve on \mathcal{M}

$$C = \{\lambda(\xi) | \xi \in [0, \Xi], \text{ such that } \lambda(0) = \lambda(\Xi)\} \quad (2.4)$$

we generally get $\text{par}_C |\psi(\lambda)\rangle \neq |\psi(\lambda)\rangle$. This property is sometimes more generally called an *anholonomy* and geometric intuition can be seen on fig. 2.5.

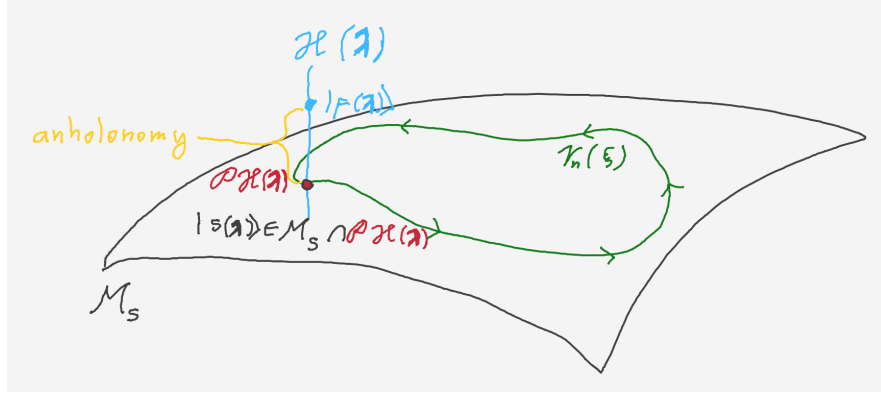


Figure 2.5: Parallel transporting around some closed curve C with anholonomy drawn in yellow.

For quantum states, the anholonomy can be measured as a non-zero angle between $|V\rangle$ and $\text{par}_C|V\rangle$, meaning

$$\langle V | \text{par}_C | V \rangle \neq 0.$$

Substituting general solution 2.3 to eq. 2.1 yields (see [Berry, 1984])

$$d_t \gamma(\lambda) = i \langle s(\lambda) | \partial_\mu s(\lambda) \rangle d_t \lambda^\mu(\lambda). \quad (2.5)$$

Integrating this equation around some closed curve C and assuming the dynamical phase to be zero, thus not exciting the system, we get

$$\gamma_n(C) = i \oint_C \langle s(\lambda) | \partial_\mu s(\lambda) \rangle d\lambda^\mu. \quad (2.6)$$

We see, that the geometric phase does not depend on energy or time, only on the sequence of Hamiltonians, which means it depends only on the path itself.

The problem of expressions above lies in $\partial_\lambda s(\lambda)$, which locally requires knowledge of single-valued basis $\{|0\rangle, \dots, |k\rangle\}$. This can be avoided in 3-dimensions using Stokes's theorem for S as the surface with boundary $\partial S = C$, for coordinate gradient ∇

$$\begin{aligned} \gamma_s(C) &= -\text{Im} \iint_C dS \cdot \nabla \times \langle s(\lambda) | \nabla n(\lambda) \rangle \\ &= -\text{Im} \iint_C dS \cdot \langle \nabla s(\lambda) | \times | \nabla s(\lambda) \rangle \\ &= -\text{Im} \iint_C dS \cdot \sum_{m \neq s} \langle \nabla s(\lambda) | m(\lambda) \rangle \times \langle m(\lambda) | \nabla s(\lambda) \rangle \\ &= -\iint_C dS \cdot V_s(\lambda) \end{aligned} \quad (2.7)$$

for

$$V_s(\lambda) = \text{Im} \frac{\langle s(\lambda) | \nabla_\lambda \hat{H}(\lambda) | m(\lambda) \rangle \times \langle m(\lambda) | \nabla_\lambda \hat{H}(\lambda) | s(\lambda) \rangle}{(E_m(\lambda) - E_s(\lambda))^2} \quad (2.8)$$

where the element of summation $m = s$ in third step of derivation is real, therefore has no influence on γ_s and can be omitted. The last equivalence holds, because

if we differentiate the Schrödinger equation 2.2, we get for any $|s\rangle, |m\rangle \in \mathcal{M}$

$$\begin{aligned} \nabla \hat{H} |s(\boldsymbol{\lambda})\rangle + \hat{H} |\nabla s(\boldsymbol{\lambda})\rangle &= E_s |\nabla s(\boldsymbol{\lambda})\rangle \\ \langle m(\boldsymbol{\lambda}) | \nabla \hat{H} |s(\boldsymbol{\lambda})\rangle + \langle m(\boldsymbol{\lambda}) | E_m |\nabla s(\boldsymbol{\lambda})\rangle &= \langle m(\boldsymbol{\lambda}) | \nabla \hat{H} |s(\boldsymbol{\lambda})\rangle \\ \langle m(\boldsymbol{\lambda}) | \nabla s(\boldsymbol{\lambda})\rangle &= \frac{\langle m(\boldsymbol{\lambda}) | \nabla \hat{H} |s(\boldsymbol{\lambda})\rangle}{E_m(\boldsymbol{\lambda}) - E_s(\boldsymbol{\lambda})}, \quad s \neq m, \end{aligned} \quad (2.9)$$

where we used $|\nabla s\rangle \equiv \nabla |s\rangle$. or just use Feynman-Hellman equations, quantum geometric tensor pedagogical, page 5 Comparing the first expression in eq. 2.7 with its last one and extending it to real numbers, we get

$$V_s(\boldsymbol{\lambda}) = \nabla \times \langle s(\boldsymbol{\lambda}) | \nabla m(\boldsymbol{\lambda}) \rangle, \quad (2.10)$$

defining vector potential of $V_s(\boldsymbol{\lambda})$. In addition, it extends our definition from single valued basis to any solution of 2.2, thus instead of ground state manifold, we can use any \mathcal{M}_s .

As was mentioned, the above procedure from eq. 2.6 was performed only for three-dimensional space. Proper generalization to n-dimensional space would yield, see [Berry, 1984],

$$\gamma_s(C) = - \iint_C dS \cdot \text{Im} \frac{\langle s(\boldsymbol{\lambda}) | d\hat{H}(\boldsymbol{\lambda}) | m(\boldsymbol{\lambda}) \rangle \wedge \langle m(\boldsymbol{\lambda}) | d\hat{H}(\boldsymbol{\lambda}) | s(\boldsymbol{\lambda}) \rangle}{(E_m(\boldsymbol{\lambda}) - E_s(\boldsymbol{\lambda}))^2}, \quad (2.11)$$

which will not be needed in this thesis.

2.2 Metric and geometric tensor

As a playground for this chapter, we will choose the ground state manifold \mathcal{M}_0 , but it can be easily generalized to any energy states manifold \mathcal{M}_s . From now on we will use natural units, so $\hbar = 1$.

Let's first look at \mathcal{PM}_s , which is needed to be *gauge independent*. Gauge dependence in quantum mechanics means, that the change in phase factor ϕ of some state $|o(\boldsymbol{\lambda})\rangle \in \mathbb{T}_{\boldsymbol{\lambda}}\mathcal{M}$ induces the change

$$|o(\boldsymbol{\lambda})\rangle \mapsto e^{i\phi(\boldsymbol{\lambda})} |o(\boldsymbol{\lambda})\rangle \implies \langle o(\boldsymbol{\lambda}) | \nabla o(\boldsymbol{\lambda}) \rangle \mapsto \langle o(\boldsymbol{\lambda}) | \nabla o(\boldsymbol{\lambda}) \rangle + i \nabla \phi(\boldsymbol{\lambda}) \quad (2.12)$$

For $\phi(\boldsymbol{\lambda}) \in \mathcal{C}^2$ we see from eq. 2.10, that gauge independent choice would be for infinitesimal change for example

$$f = \langle o(\boldsymbol{\lambda} + \delta\boldsymbol{\lambda}) | o(\boldsymbol{\lambda}) \rangle, \quad (2.13)$$

sometimes referred to as the *fidelity of a ground state*². We can see it's physical meaning imagining *quantum quench* (rapid change of some Hamiltonian parameters), in which case f^2 is the probability that system will remain in the new

²Generalization for any mixed state is for two density matrices σ, ρ as

$$f := \left(\text{Tr} \sqrt{\sqrt{\rho} \sigma \sqrt{\rho}} \right)$$

ground state. $1 - f^2$ is therefore probability of exciting the system during this quench, which leads to the definition of *distance on \mathcal{M}_0* ³

$$ds^2 \equiv 1 - f^2 = 1 - |\langle o(\lambda + \delta\lambda) | o(\lambda) \rangle|^2. \quad (2.14)$$

We can easily check, that the axioms of metric defined using distance as bilinear form s between elements $|\psi\rangle, |\phi\rangle \in \mathcal{M}_0$ are for **closed systems** satisfied:

- identity of indiscernibles $s(|\psi\rangle, e^{i\alpha}|\psi\rangle) = 0 \Leftrightarrow |\psi\rangle = |\phi\rangle, \alpha \in \mathbb{R}$,
- symmetry for any two states $|\psi\rangle, |\phi\rangle$ is implied by $|\langle\psi|\phi\rangle| = |\langle\phi|\psi\rangle|$
- triangle inequality: $s(|\psi\rangle, |\psi_2\rangle) < s(|\psi\rangle, |\psi\rangle_1) + s(|\psi_1\rangle, |\psi_2\rangle)$ for any $|\psi_1\rangle$.

Because $1 - f^2 > 0$, the first term of Taylor expansion is zero, thus we have for a metric tensor

$$ds^2 = g_{\mu\nu} d\lambda^\mu d\lambda^\nu + \mathcal{O}(\lambda^3). \quad (2.15)$$

Let's define the metric on the space of states \mathcal{M}_0 and then see, how it corresponds to fidelity. This metric is called the *Geometric tensor*, and can be expressed as

$$\chi_{\mu\nu} := \langle \partial_\mu o | \partial_\nu o \rangle_c \equiv \langle \partial_\mu o | \partial_\nu o \rangle - \langle \partial_\mu o | o \rangle \langle o | \partial_\nu o \rangle, \quad (2.16)$$

where shortened notation $\partial_\nu := \frac{\partial}{\partial \lambda^\nu}$ was used.

It is practical to decompose it the geometric tensor

$$\chi_{\mu\nu} \equiv g_{\mu\nu} - i \frac{1}{2} \nu_{\mu\nu}, \quad (2.17)$$

where the *Fubini-Study tensor*⁴, as it's called, is metric on \mathcal{PM}_0 and can be expressed as

$$g_{\mu\nu} = \frac{\chi_{\mu\nu} + \chi_{\nu\mu}}{2} = \text{Re} \langle \partial_\mu o | \partial_\nu o \rangle_c = \text{Re} \sum_{o \neq j} \frac{\langle o | \frac{\partial \mathcal{H}}{\partial \lambda^\mu} | j \rangle \langle j | \frac{\partial \mathcal{H}}{\partial \lambda^\nu} | o \rangle}{(E_o - E_j)^2}, \quad (2.18)$$

and the *curvature tensor* a.k.a. *Berry curvature* is

$$\nu_{\mu\nu} = i(\chi_{\mu\nu} - \chi_{\nu\mu}) = \text{Im} \langle o | [\overleftarrow{\partial}_\nu, \partial_\mu] | o \rangle_c = -2 \text{Im} \sum_{o \neq j} \frac{\langle o | \frac{\partial \mathcal{H}}{\partial \lambda^\mu} | j \rangle \langle j | \frac{\partial \mathcal{H}}{\partial \lambda^\nu} | o \rangle}{(E_o - E_j)^2}, \quad (2.19)$$

where $\overleftarrow{\partial}_\nu$ affects the covector on the left.

³d notation is in differential geometry assumed to be an exterior differential. On functions, it acts as $d : \mathcal{F}\mathcal{M} \rightarrow \mathcal{T}_1\mathcal{M}$ and intuitively corresponds to total differential from functional analysis.

⁴In some literature, this is called Geometric tensor

2.2.1 Derivation of the geometric tensor

To prove the correspondence of geometric tensor, described by eq. 2.16, to distance on \mathcal{M}_0 , see eq. 8.1, we start with eigenstate $|o(\boldsymbol{\lambda})\rangle \in \mathcal{M}_0 \cap \mathcal{H}(\boldsymbol{\lambda})$. Changing parameters $\boldsymbol{\lambda}$ to $\boldsymbol{\lambda} + \delta\boldsymbol{\lambda}$ results in Hamiltonian \hat{H}_f with eigenstates $|s(\boldsymbol{\lambda} + \delta\boldsymbol{\lambda})\rangle \in \mathcal{M}_s \cap \mathcal{H}(\boldsymbol{\lambda} + \delta\boldsymbol{\lambda})$, meaning it can be excited. Probability amplitude of going to such state is

$$\begin{aligned} a_s &= \langle s(\boldsymbol{\lambda} + \delta\boldsymbol{\lambda})|o(\boldsymbol{\lambda})\rangle \approx \delta\lambda^\mu \langle \partial_\mu s(\boldsymbol{\lambda})|o(\boldsymbol{\lambda})\rangle \\ &= -\delta\lambda^\mu \langle s(\boldsymbol{\lambda})|\partial_\mu|o(\boldsymbol{\lambda})\rangle. \end{aligned} \quad (2.20)$$

If we introduce the *gauge potential*, aka *calibration potential*, as⁵

$$\hat{\mathcal{A}}_\mu \equiv i\partial_\mu, \quad (2.21)$$

the probability amplitude can be expressed as

$$a = i \langle s(\boldsymbol{\lambda})|\hat{\mathcal{A}}_\mu|o(\boldsymbol{\lambda})\rangle \delta\lambda^\mu, \quad (2.22)$$

which has meaning of matrix elements of the gauge potential. Probability of the excitation i.e. transition to any state $s > 0$ from ground state is then (omitting the $\boldsymbol{\lambda}$ dependence in notation)

$$\begin{aligned} \sum_{s \neq 0} |a_s|^2 &= \sum_{s \neq 0} \delta\lambda^\mu \delta\lambda^\nu \langle o|\hat{\mathcal{A}}_\mu|s\rangle \langle s|\hat{\mathcal{A}}_\nu|o\rangle + \mathcal{O}(|\delta\lambda^3|) \\ &= \delta\lambda^\mu \delta\lambda^\nu \langle o|\hat{\mathcal{A}}_\mu \hat{\mathcal{A}}_\nu|o\rangle_c =: \delta\lambda^\mu \delta\lambda^\nu \chi_{\mu\nu} + \mathcal{O}(|\delta\lambda^3|), \end{aligned} \quad (2.23)$$

where last term defines the geometric tensor.

2.3 Adiabaticity

Adiabatic transformation is such a transformation from \mathcal{M} to \mathcal{M} , which does not excite the system, meaning the fidelity $f = 1$. Generally it can be achieved by two ways – infinitely slow transformation of states, or adding some *counter-diabatic elements* to the Hamiltonian to counter the excitation.

In this chapter, we will be dealing with the system described by the finite-dimensional Hamiltonian $\hat{H}(\boldsymbol{\lambda})$ which drives the system according to Schrödinger equation from some initial state $|s(\boldsymbol{\lambda})\rangle$ to $|s(\tilde{\boldsymbol{\lambda}})\rangle$ along the path $\gamma(\lambda)$. Before going through the details of adiabatic transformations, let's define its meaning properly.

Definition 7 (Adibaticity). *Slow change of parameters driving Hamiltonian in a sense, that it does not excite the system and allows the system to return to the same energetic state after circulation around any closed path on the manifold with fidelity $f = 1$.*

2.3.1 Slow transports

[Kolodrubetz et al., 2017][chap. 2.3] As was mentioned in the introduction of this chapter, one way to change the system parameters without exciting it is to change the driving parameter slowly enough. The meaning of the word "slow" clears up next theorem.

⁵In SI units, the gauge potential is $\hat{\mathcal{A}}_\mu \equiv i\hbar\partial_\mu$

Theorem 5 (Adiabatic theorem). *For Hamiltonian \hat{H} varying in the time range T , the solution of the Schrödinger equation*

$$\hat{H}(\lambda) |\psi_n(\lambda)\rangle = E_n(\lambda) |\psi_n(\lambda)\rangle$$

with initial condition in x -representation $\langle x|\psi(t=0\rangle = \psi_n(x, 0)$ can be approximated as

$$||\psi(\lambda) - \psi_{ad}(\lambda)|| \approx o\left(\frac{1}{T}\right) \quad (2.24)$$

for adiabatic state

$$|\psi_{ad}\rangle = e^{\theta_n(\lambda)} e^{\gamma_n(\lambda)} |\psi(\lambda)\rangle, \quad (2.25)$$

where we define nongeometrical phase induced by energy transitions,

$$\theta_n(\lambda) \equiv -\frac{1}{\hbar} \int_0^t E_n(\tau) d\tau$$

and geometrical phase, also called Berry phase

$$\gamma_n(\lambda) \equiv \int_0^t \underbrace{i \langle \psi_n(\tau) | \partial_t \psi_n(\tau) \rangle}_{\nu_n(\tau)} d\tau.$$

Proof. TBD (is on wikipedia :)

□

Assume differentiable and non-singular Hamiltonian $\hat{H}(\boldsymbol{\lambda})$ with degenerate basis $\{|m, \boldsymbol{\lambda}\rangle\}_m$ called the *adiabatic basis*. This is generally the family of adiabatically connected eigenstates⁶ The transition amplitude between states for adiabatic change is

$$0 = \langle m(\boldsymbol{\lambda}) | \hat{H} | n(\tilde{\boldsymbol{\lambda}}) \rangle \quad \text{for } n \neq m, \forall \boldsymbol{\lambda}, \forall \tilde{\boldsymbol{\lambda}}. \quad (2.26)$$

This can be driven along some curve $\gamma(\lambda)$, i.e. differentiated by ∂_t :

$$\begin{aligned} 0 &= \langle \partial_t m(\boldsymbol{\lambda}) | \hat{H}(\tilde{\boldsymbol{\lambda}}) | n(\tilde{\boldsymbol{\lambda}}) \rangle + \langle m(\boldsymbol{\lambda}) | \underbrace{\partial_t \hat{H}(\tilde{\boldsymbol{\lambda}})}_{\approx \partial_t \hat{H}(\boldsymbol{\lambda})} | n(\tilde{\boldsymbol{\lambda}}) \rangle + \langle m(\boldsymbol{\lambda}) | \hat{H}(\tilde{\boldsymbol{\lambda}}) | \partial_t n(\tilde{\boldsymbol{\lambda}}) \rangle \\ &= E_n(\lambda) \langle \partial_t m(\boldsymbol{\lambda}) | n(\tilde{\boldsymbol{\lambda}}) \rangle + E_m(\lambda) \langle m(\boldsymbol{\lambda}) | \partial_t n(\tilde{\boldsymbol{\lambda}}) \rangle + \langle m(\boldsymbol{\lambda}) | \partial_t \hat{H}(\tilde{\boldsymbol{\lambda}}) | n(\tilde{\boldsymbol{\lambda}}) \rangle \\ &= (E_m(\lambda) - E_n(\lambda)) \underbrace{\langle m | \partial_t(\tilde{\boldsymbol{\lambda}}) \rangle}_{-\frac{i}{\hbar} \langle m | \hat{\mathcal{A}}_t | n(\tilde{\boldsymbol{\lambda}}) \rangle} + \langle m | \partial_t \hat{H} | n(\tilde{\boldsymbol{\lambda}}) \rangle. \end{aligned} \quad (2.27)$$

This can be rewritten in matrix form as

$$i\hbar \partial_t \hat{H} = [\hat{\mathcal{A}}_t, \hat{H}] - i\hbar \hat{M}_t \quad \text{for } \hat{M}_t \equiv - \sum_n \frac{\partial E_n(\lambda)}{\partial t} |n(\lambda)\rangle \langle n(\lambda)|. \quad (2.28)$$

\hat{M} is diagonal in energetic basis and its elements has meaning of *generalized force*. We can easily see that $[\hat{H}, \hat{M}] = 0$, implying

$$[\hat{H}, i\hbar \partial_t \hat{H} - [\hat{\mathcal{A}}_t, \hat{H}]] = 0. \quad (2.29)$$

This can be used as the definition for *counter-diabatic potential* $\hat{\mathcal{A}}_t$, because it was obtained from only one assumption – adiabaticity. The strength of this equation lies in fact, that it finds counter-diabatic potential without the need of Hamiltonian diagonalization.

⁶In the case of energy level crossing, the eigenstates are not unified, because transition between them is not adiabatical.

2.4 Gauge potentials

In section 2.2.1 we introduced the gauge potential without proving its gauge meaning, but only stating its correspondence to transition probability, see eq. 2.22. *Gauge transformations*, in classical mechanics called *canonical*, can be defined such, that they *preserve Lagrangian of the system under local transformations from some Lie group*. This implies, that gauge transformed Hamiltonian $\hat{H}(\boldsymbol{\lambda})$ and $\hat{H}(\boldsymbol{\lambda} + d\boldsymbol{\lambda})$ commutes with its canonically transformed version⁷

$$[\hat{H}(\boldsymbol{\lambda}), \hat{H}(\boldsymbol{\lambda} + d\boldsymbol{\lambda})] = 0. \quad (2.30)$$

To understand the meaning of gauge symmetries, let's first consider classical system and then move to quantum mechanics.

2.4.1 Classical gauge potential

In the Hamiltonian classical mechanics, we assume the manifold \mathcal{M} as subset of the phase space defined by Hamiltonian $H = H(p_i, q_i)$, where momentum p_i and position q_i are assumed to form the orthogonal basis of the phase space

$$\{q^i, p_j\} = \delta_j^i, \quad (2.31)$$

which also defines *calibrational freedom* in their choice. *Canonical transformations* then by definition preserve this formula. Using the *Poisson bracket*, defined as

$$\{A, B\} := \frac{\partial A}{\partial q^j} \frac{\partial B}{\partial p_j} - \frac{\partial B}{\partial q^j} \frac{\partial A}{\partial p_j}, \quad (2.32)$$

we will examine continuous canonical transformations generated by gauge potential \mathcal{A}_λ

$$q^j(\lambda + \delta\lambda) = q^j(\lambda) - \frac{\partial \mathcal{A}_\lambda(\mathbf{p}, \mathbf{q})}{\partial p_j} \delta\lambda \Rightarrow \frac{\partial q^j}{\partial \lambda} = -\frac{\partial \mathcal{A}_\lambda}{\partial p_j} = \{\mathcal{A}_\lambda, q^j\} \quad (2.33)$$

$$p_j(\lambda + \delta\lambda) = p_j(\lambda) - \frac{\partial \mathcal{A}_\lambda(\mathbf{p}, \mathbf{q})}{\partial q^j} \delta\lambda \Rightarrow \frac{\partial p_j}{\partial \lambda} = -\frac{\partial \mathcal{A}_\lambda}{\partial q^j} = \{\mathcal{A}_\lambda, p_j\}. \quad (2.34)$$

Substituting this to relations of orthogonality 2.31, we get

$$\{q^j(\lambda + \delta\lambda), p_j(\lambda + \delta\lambda)\} = \delta_j^i + \mathcal{O}(\delta\lambda^2). \quad (2.35)$$

If λ is time parameter and $\mathcal{A}_t = -H$, equations 2.33,2.34 are identical to the Hamilton equations

$$\begin{aligned} \dot{q}^j &= -\{H, q^j\} = \frac{\partial H}{\partial p_j} \\ \dot{p}_j &= -\{H, p_j\} = -\frac{\partial H}{\partial q^j}. \end{aligned} \quad (2.36)$$

Because the Hamiltonian is generator of the movement in the phase space (\mathbf{q}, \mathbf{p}) , we can interpret \mathcal{A}_t as the generators of the movement on \mathcal{M} . Other specific choice might be $\lambda = X^i$, which gives us the momentum components $\mathcal{A}_{X^i} = p_i$.

Generally every gauge symmetry is generated by its gauge potential and corresponds to some conserved property, as theorem of Emma Nöether states.

⁷This can be easily reformulated to the world of classical physics, where the commutator is replaced by Poisson bracket.

2.4.2 Quantum gauge potential

[Kolodrubetz et al., 2017][chap. 2.2] The role of Poisson brackets in quantum mechanics is taken by commutators, canonical transformations are called *unitary transformations* and calibration freedom is hidden in the choice of basis. Now let's find some special basis transformations \hat{U} between initial system S and the transformed \tilde{S} . Both of them describe the system with Hamiltonian $\hat{H}(\boldsymbol{\lambda})$ with eigenstates $|n(\boldsymbol{\lambda})\rangle$ and eigenstate manifolds $\mathcal{M}_n \equiv \cup_{\boldsymbol{\lambda}}\{|n(\boldsymbol{\lambda})\rangle\}$.

From fiber structure goes⁸, that any state of $\hat{H}(\boldsymbol{\lambda})$ for $\forall \boldsymbol{\lambda} \in U \subset \mathbb{R}^n$ can be decomposed as

$$|\psi(\boldsymbol{\lambda})\rangle \equiv \sum_n \psi_n(\boldsymbol{\lambda}) |n\rangle \quad (2.37)$$

for some coordinate independent basis $\{|n\rangle\}_n$. Then there exist unitary transformation

$$\hat{U}(\boldsymbol{\lambda}) : \tilde{S} \rightarrow S, \quad \hat{U}(\boldsymbol{\lambda}) |m(\boldsymbol{\lambda})\rangle = |n\rangle. \quad (2.38)$$

where scalar parameter t is assumed to be changing along the path $\gamma(t)$, corresponding to situation on fig. 2.4. This satisfies

$$i\hbar \partial_t \hat{U}(t) = \hat{H}(t) \hat{U}(t) \quad (2.39)$$

for \hat{H} the full Hamiltonian of the system and any point on $\tilde{\gamma}(t)$, along which the partial derivative is taken.

The wave function $|\psi\rangle$ in S can be decomposed using Schmidt decomposition⁹

$$|\psi(\boldsymbol{\lambda})\rangle = \sum_{m,n} \psi_n(\boldsymbol{\lambda}) |m(\boldsymbol{\lambda})\rangle \underbrace{\langle m(\boldsymbol{\lambda})|n\rangle}_{U_{mn}(\boldsymbol{\lambda})} = \sum_m \underbrace{\tilde{\psi}_m(\boldsymbol{\lambda})}_{\langle m(\boldsymbol{\lambda})|\psi_n|n\rangle} |m(\boldsymbol{\lambda})\rangle, \quad (2.40)$$

where $U_{mn}(\boldsymbol{\lambda})$ are matrix elements of unitary transformation $\hat{U}(\boldsymbol{\lambda})$. In this work, we will be interested only in the gauge transformations preserving energy of the system.

2.4.3 Adiabatic gauge potential

Adiabatic gauge potentials, sometimes just *adiabatic potentials*, are generators of unitary transformations, so we can define them analogically to the classical case

$$i\hbar \partial_\lambda |\tilde{\psi}(\boldsymbol{\lambda})\rangle = i\hbar \partial_\lambda \left(\hat{U}^+(\boldsymbol{\lambda}) |\psi\rangle \right) = \underbrace{i\hbar \left(\partial_\lambda \hat{U}^+(\boldsymbol{\lambda}) \right)}_{-\tilde{\mathcal{A}}_\lambda} \hat{U}(\boldsymbol{\lambda}) |\tilde{\psi}(\boldsymbol{\lambda})\rangle. \quad (2.41)$$

The adiabatic potential $\tilde{\mathcal{A}}_\lambda$ can be transformed to non-tilde system as

$$\begin{aligned} \hat{\mathcal{A}}_\lambda &= \hat{U}(\boldsymbol{\lambda}) \tilde{\mathcal{A}}_\lambda \hat{U}^+(\boldsymbol{\lambda}) = -i\hbar \hat{U}(\boldsymbol{\lambda}) \left(\partial_\lambda \hat{U}^+(\boldsymbol{\lambda}) \right) = \\ &= -i\hbar \partial_\lambda \left(\underbrace{U^+(\boldsymbol{\lambda}) U(\boldsymbol{\lambda})}_1 \right) - \left(\partial_\lambda U(\boldsymbol{\lambda}) \right) U^+(\boldsymbol{\lambda}) = i\hbar \left(\partial_\lambda U(\boldsymbol{\lambda}) \right) U^+(\boldsymbol{\lambda}). \end{aligned} \quad (2.42)$$

⁸especially from the fact, that all spaces $\hat{H}(\boldsymbol{\lambda})$ are isomorphic to each other

⁹The Schmidt decomposition can be performed in finite dimension, or if the Hamiltonian is compact, which is not automatic in quantum mechanics. What's more, the Hamiltonian is usually not even bounded. Anyway, for simple systems with bounded energy we can assume so.

From this we get the equations for adiabatic potential in two systems

$$\hat{\mathcal{A}}_\lambda = i\hbar(\partial_\lambda U(\boldsymbol{\lambda}))U^+(\boldsymbol{\lambda}) \quad (2.43)$$

$$\tilde{\hat{\mathcal{A}}}_\lambda = -i\hbar(\partial_\lambda \hat{U}^+(\boldsymbol{\lambda}))\hat{U}(\boldsymbol{\lambda}) \quad (2.44)$$

which can be shown to be Hermitian

$$\tilde{\hat{\mathcal{A}}}_\lambda^+ = i\hbar U(\boldsymbol{\lambda})^+(\partial_\lambda \hat{U}(\boldsymbol{\lambda})) = -i\hbar(\partial_\lambda \hat{U}(\boldsymbol{\lambda})^+)\hat{U}(\boldsymbol{\lambda}) = \tilde{\hat{\mathcal{A}}}_\lambda, \quad (2.45)$$

analogically for non-tilde potential. Using the eigenbasis of \hat{H} , the matrix elements are

$$\langle n | \tilde{\hat{\mathcal{A}}}_\lambda | m \rangle = i\hbar \langle n | \hat{U}(\boldsymbol{\lambda})^+ \partial_\lambda \hat{U}(\boldsymbol{\lambda}) | m \rangle = i\hbar \langle n(\boldsymbol{\lambda}) | \partial_\lambda | m(\boldsymbol{\lambda}) \rangle. \quad (2.46)$$

and because

$$\langle n(\boldsymbol{\lambda}) | \hat{\mathcal{A}}_\lambda | m(\boldsymbol{\lambda}) \rangle = \langle n | \tilde{\hat{\mathcal{A}}}_\lambda | m \rangle, \quad (2.47)$$

we get

$$\hat{\mathcal{A}}_\lambda = i\hbar \partial_\lambda. \quad (2.48)$$

Adiabatic gauge transformations are class of gauge transformations with fidelity $f = 1$. This means, that if the system is driven by Hamiltonian $\hat{H}(\boldsymbol{\lambda})$ with fidelity $f < 1$, there exists such adiabatic potential \mathcal{A}_λ , that driving of the same system using $\hat{H} - \mathcal{A}_\lambda$ has fidelity $f = 1$.

The adiabatic gauge potentials can then be understood as affine connections defining the parallel transport on fiber bundle, if we define covariant derivative as

$$D_\mu = \partial_\mu + i\hat{\mathcal{A}}_\mu, \quad (2.49)$$

which yields $D_\mu |\psi_n\rangle = 0$ for every eigenstate, which yields, that the transport of eigenvalues on \mathcal{M}_0 is parallel. $\hat{\mathcal{A}}_\mu$ is generally defined 2.43, which generally gives non-zero covariant derivative for states not belonging to \mathcal{M}_0 .

Finding of those potentials has many practical applications, so let's introduce one analytical procedure of finding them.

2.5 Counter-diabatic driving

[Kolodrubetz et al., 2017][page 15–17] The main idea of a counter-diabatic driving is, that any excitation of the system can be countered by adding so called *counter-diabatic potential* to the Hamiltonian. Consider again any eigenstate $|\psi(t)\rangle$ of the Hamiltonian $\hat{H} = \hat{H}(\lambda)$ driven along the curve $\gamma(\lambda(t))$ on \mathcal{M}_0 depending on time t , during which the fidelity $f \neq 0$. Because the system is not measured during the trip, it can't be stated if or if not it was excited, but the main goal here is to make fidelity zero, which is iff \tilde{H} is diagonal. For diagonalizable Hamiltonian, there exist a transformation, see eq. 2.38, for which the fidelity will be zero. Such a transformation does not have to be unique, but we can choose any one of them. This can be seen more clearly from direct transformation of the Schrödinger equation.

The Schrödinger equation

$$i\hbar \frac{d}{dt} |\psi(\lambda)\rangle = \hat{H}(\lambda) |\psi(\lambda)\rangle \quad (2.50)$$

can be transformed using

$$\hat{U}(\lambda)^+ |\psi(\lambda)\rangle = |\tilde{\psi}(\tilde{\lambda})\rangle, \quad (2.51)$$

for which $\tilde{H} := \hat{U}^+ \hat{H} \hat{U}$ is diagonal, leading to

$$i\hbar \frac{d}{dt} (\hat{U}(\tilde{\lambda}) |\tilde{\psi}(\tilde{\lambda})\rangle) = \hat{H}(\lambda) \hat{U}(\tilde{\lambda}) |\tilde{\psi}(\tilde{\lambda})\rangle \quad (2.52)$$

$$i\hbar \frac{d\lambda}{dt} \partial_\lambda \hat{U}(\tilde{\lambda}) |\tilde{\psi}(\tilde{\lambda})\rangle + i\hbar \hat{U}(\tilde{\lambda}) \frac{d}{dt} |\tilde{\psi}(\tilde{\lambda})\rangle = \hat{H}(\lambda) \hat{U}(\tilde{\lambda}) |\tilde{\psi}(\tilde{\lambda})\rangle. \quad (2.53)$$

This can be rewritten using adiabatic potential from eq. 2.48, using *dot* notation for time derivatives and omitting the points in which the objects are evaluated, as

$$i\hbar \frac{d}{dt} |\tilde{\psi}\rangle = \left[\hat{U}^+ \hat{H} \hat{U} - \dot{\lambda} \tilde{\mathcal{A}}_\lambda \right] |\tilde{\psi}\rangle = \left[\tilde{H} - \dot{\lambda} \tilde{\mathcal{A}}_\lambda \right] |\tilde{\psi}\rangle =: \tilde{H}_m |\tilde{\psi}\rangle, \quad (2.54)$$

where the term $-\dot{\lambda} \tilde{\mathcal{A}}_\lambda$ is called *Galilean* and \tilde{H}_m is the Hamiltonian in transformed system. Because \tilde{H} is diagonal, it drives $|\tilde{\psi}\rangle$ with fidelity $f = 1$. This means that for any driving defined by $\hat{H}(\lambda(t))$, which defines the unitary transformation \hat{U} , there exists such *counter-diabatic potential* $\hat{\mathcal{A}}_\lambda$, that $\tilde{H}_m + \dot{\lambda} \hat{\mathcal{A}}_\lambda$ has $f = 1$.

This procedure does not directly tell us how to calculate the counter-diabatic potential, only states its existence. For many simple cases the calculation can be done analytically, but most often some approximation methods are needed.

2.5.1 Explicit form

If we now consider the parametrization with time $t := t$, \hat{U} can be explicitly expressed according to **ansatz** in eq. 2.3 as

$$\hat{U}(t) = \sum_n \exp \left(\frac{i}{\hbar} E_n(\tau) d\tau - \int_0^t \langle s(\tau) | \partial_\tau n(\tau) \rangle d\tau \right) |s(t)\rangle \langle s(0)|. \quad (2.55)$$

Inserting to eq. 2.39, we get explicit form of the Hamiltonian, which can be decomposed into the diagonal form of the original Hamiltonian and a counter-diabatic potential

$$\hat{H}(t) = \sum_n |n\rangle E_n \langle n| + i\hbar \sum_n |\partial_\lambda n\rangle \langle n| - \langle n | \partial_\lambda n \rangle |n\rangle \langle n| =: \hat{H}_0(t) + \hat{H}_1(t), \quad (2.56)$$

for shortened notation $|n\rangle \equiv |n(t)\rangle$, analogically for bras. Using

$$\hat{H}_0(t) |n\rangle = E_n |n\rangle \quad \Rightarrow \quad \langle m | \partial_\lambda n \rangle = \frac{\langle m | \partial_\lambda \hat{H}_0 | n \rangle}{E_n - E_m} \quad (2.57)$$

we have explicit formula

$$\hat{H}_1(t) = i\hbar \sum_{m \neq n} \frac{|m\rangle \langle m | \partial_\lambda \hat{H}_0 | n \rangle \langle n|}{E_n - E_m} \quad (2.58)$$

2.6 Berry phase and curvature

Let's now consider only the ground state manifold, because it will be used later on. Thought every step can be easily generalized to any state manifold \mathcal{M}_m .

On the ground state manifold $\mathcal{M}_0 \equiv \cup_{\lambda} \{|o(\lambda)\rangle\}$, the *Berry connection* is defined as

$$A_\mu(\lambda) \equiv \langle o(\lambda) | \hat{A}_\mu | o(\lambda) \rangle = -i\hbar \langle o(\lambda) | \partial_\mu | o(\lambda) \rangle, \quad (2.59)$$

which uses the decomposition of λ to some basis, thus it empowers us to take derivatives in any direction in the base manifold \mathbb{R}^n and thus the geometric tensor can be written as

$$\chi_{\mu\nu}(\lambda) = \partial_\mu A_\nu(\lambda) - \partial_\nu A_\mu(\lambda) \quad (2.60)$$

and the *Berry phase*¹⁰ as the integral of a connection along some closed curve \mathcal{C}

$$\phi_B \equiv - \oint_{\mathcal{C}} A_\mu(\lambda) d\lambda^\mu = \int_{\mathcal{S}} \chi_{\mu\nu}(\lambda) d\lambda^\mu \wedge d\lambda^\nu, \quad (2.63)$$

where we used the Stokes theorem for some area \mathcal{S} with boundary $\partial\mathcal{S} = \mathcal{C}$.

Berry phase is usually zero, except for the cases, when the curve goes around some geometric tensor singularity, meaning $Ind_a \gamma(\lambda) > 0$. Those singularities appear in the system due to energy spectrum degeneracies, in the case of ground state manifold when $E_1 - E_0 = 0$. Those points are called *diabolic*, because of their shape in the (λ, χ) parameter space.¹¹

¹⁰The reasonability of this definition can be seen, if we assume the ground state of a free particle $\langle \mathbf{x} | i(\lambda) \rangle = i(\mathbf{x}, \lambda) = |i(\mathbf{x})| e^{i\phi(\lambda)}$, then the Berry connection is

$$A_\mu = - \int d\mathbf{x} |i(\mathbf{x}, \lambda)|^2 \partial_\mu \phi(\lambda) = -\partial_\mu \phi(\lambda) \quad (2.61)$$

and Berry phase

$$\phi_B = \oint_{\mathcal{C}} \partial_\mu \phi d\lambda^\mu, \quad (2.62)$$

which represents total phase accumulated by the wave function. It is really the analogy for Berry phase in classical mechanics, which for example in the case Foucault pendulum on one trip around the Sun makes $\phi_B = 2\pi$

¹¹<https://en.wikipedia.org/wiki/Diabolo>

3. Geodesics

Of special importance in theory of the ground state manifold are geodesics. It is not yet clear what role they have in general, but in some special cases its well known, see ?. The holy grail of this theory would be to find path with the lowest excitation amplitude, which is not an easy task.

Let's have a geodesic $\mathcal{G}(t)$ and some curve $\gamma(t)$ on the ground stat manifold, spanning between points P_i and P_f during some time t_f , meaning

$$\mathcal{G}(0) = \gamma(0) = P_i \in \mathcal{M}_0, \quad \mathcal{G}(t_f) = \gamma(t_f) = P_f \in \mathcal{M}_0.$$

Excitation amplitude during infinitesimal quench is ds , therefore $\sum_i \Delta s_i$ summed along path $\gamma(t)$ is the amplitude of transport along that path. This can be more rigorously expressed by functional

$$s_\gamma = \int_{\gamma(t)} ds = \int_0^{t_f} \sqrt{g_{\mu\nu} \dot{\lambda}^\mu \dot{\lambda}^\nu} dt \quad (3.1)$$

This is the entity, which is minimal if γ is a geodesic. Before moving on, lets quickly review the proof of this statement.

Geodesics minimize the distance on manifold. Functional of distance is

$$s = \int \mathcal{L}(t, \lambda^\mu, \dot{\lambda}^\mu) dt \quad (3.2)$$

for

$$\mathcal{L} = \sqrt{g_{\mu\nu} \dot{\lambda}^\mu \dot{\lambda}^\nu}. \quad (3.3)$$

Using Euler-Lagrange equations

$$\frac{d\mathcal{L}}{d\lambda^\mu} - \frac{d}{dt} \frac{d\mathcal{L}}{d\dot{\lambda}^\mu} = 0, \quad (3.4)$$

we get for $g_{\mu\nu} = g_{\mu\nu}(\lambda^\mu)$ second order differential equation

$$\ddot{\lambda}^\mu + \Gamma^\mu_{\alpha\beta} \dot{\lambda}^\alpha \dot{\lambda}^\beta = 0 \quad \Gamma^\mu_{\alpha\beta} = \frac{1}{2} g^{\mu\kappa} (g_{\kappa\alpha,\beta} + g_{\kappa\beta,\alpha} - g_{\beta\alpha,\kappa}), \quad (3.5)$$

which is the Geodesic equation. \square

Excitation probability along the path γ can be formally written as $F = \sum_i \Delta s_i^2$, which cannot be simply calculated as s^2 . Because $\Delta s_i > 0$, we have

$$\begin{aligned} \sum_i \Delta s_i^2 &< (\sum_i \Delta s_i)^2 \\ F &< s^2. \end{aligned} \quad (3.6)$$

This doesn't necessarily mean, that fidelity along geodesic will be minimal ($F(\mathcal{G}) < F(\gamma)$), because we didn't rule out the scenario

$$F(\gamma) < F(\mathcal{G}) < s_{\mathcal{G}}^2 < s_\gamma^2.$$

This means, that the geodesic equation cannot be used for fidelity minimization and some new insight is needed. The functional, which needs to be minimized is

$$F = \int \int g_{\mu\nu} d\lambda^\mu d\lambda^\nu = \int_{t_i}^{t_f} \underbrace{\int_{t_i}^{\tau} g_{\mu\nu} \frac{d\lambda^\mu}{dt} \frac{d\lambda^\nu}{dt} dt}_{\mathcal{L}(\lambda^\mu, \dot{\lambda}^\mu, \tau)} d\tau. \quad (3.7)$$

Using Euler-Lagrange equations, again for time independent $g_{\mu\nu} = g_{\mu\nu}(\lambda^\mu)$, leads to

$$\int_{t_i}^{t_f} \left[g_{\mu\nu,\kappa} \dot{\lambda}^\mu \dot{\lambda}^\nu - \frac{d}{dt} \left[g_{\mu\nu} (\delta_\kappa^\mu \dot{\lambda}^\nu + \dot{\lambda}^\mu \delta_\kappa^\nu) \right] \right] dt = 0 \quad (3.8)$$

which needs to be zero for integration over any subset (t_i, t_f) leading to zero condition for the integrand itself, which leads to geodesic equation 3.5, as in the case of distance on manifold.

Polkovnikov for some special case: They play a role of "maximum fidelity at any time" transport, meaning at any given time t the fidelity on corresponding point on geodesics will be less than of γ

$$F(\mathcal{G}(t)) < F(\gamma(t)).$$

4. Spin 1/2

The Hamiltonian for a single spin in a magnetic field \mathbf{B} is

$$H = -\mu \mathbf{B} \cdot \mathbf{S} \quad (4.1)$$

for spin 1/2 we have using sigma matrices

$$S = \frac{\hbar}{2} (\sigma_x, \sigma_y, \sigma_z) \equiv \frac{\hbar}{2} \left(\begin{pmatrix} 0 & 1 \\ 1 & 0 \end{pmatrix}, \begin{pmatrix} 0 & -i \\ i & 0 \end{pmatrix}, \begin{pmatrix} 1 & 0 \\ 0 & -1 \end{pmatrix} \right) \quad (4.2)$$

The coordinate system can be oriented such that $\mathbf{B} = (0, 0, B_z)$ and eigenfunctions of the spin are thus in spherical coordinates θ, ϕ and x-representation

$$u_1 = \begin{pmatrix} \cos \frac{\theta}{2} e^{-i\phi} \\ \sin \frac{\theta}{2} \end{pmatrix}; \quad u_2 = \begin{pmatrix} -\sin \frac{\theta}{2} e^{-i\phi} \\ \cos \frac{\theta}{2} \end{pmatrix} \quad (4.3)$$

For both of these states the Berry connection can be defined using 2.59

$$A^{(u_1)} = \begin{pmatrix} \langle u_1 | \frac{du_1}{d\theta} \rangle \\ \langle u_1 | \frac{du_1}{d\phi} \rangle \end{pmatrix}; \quad A^{(u_2)} = \begin{pmatrix} \langle u_2 | \frac{du_2}{d\theta} \rangle \\ \langle u_2 | \frac{du_2}{d\phi} \rangle \end{pmatrix} \quad (4.4)$$

and geometric tensor using 2.16 we have

$$\chi_{ij}^{(u_k)} = \langle \partial_i u_k | \partial_j u_k \rangle - \langle \partial_i u_k | u_k \rangle \langle u_k | \partial_j u_k \rangle \quad (4.5)$$

implying

$$\chi^{(u_1)} = \begin{pmatrix} \frac{1}{4} & \frac{i}{4} \sin \theta \\ -\frac{i}{4} \sin \theta & \frac{\sin^2 \theta}{4} \end{pmatrix}; \quad \chi^{(u_2)} = \begin{pmatrix} \frac{1}{4} & -\frac{i}{4} \sin \theta \\ \frac{i}{4} \sin \theta & \frac{\sin^2 \theta}{4} \end{pmatrix}. \quad (4.6)$$

It's real part is according to 2.18 the metric tensor

$$g^{(u_1)} = g^{(u_2)} = \begin{pmatrix} \frac{1}{4} & 0 \\ 0 & \frac{\sin^2 \theta}{4} \end{pmatrix} \quad (4.7)$$

For two state system, the metric tensor is always the same for both states. (just guessing now :). Berry curvature can be easily calculated as minus imaginary part of the geometric tensor.

From the metric the Ricci curvature and Gaussian curvature are

$$R = \begin{pmatrix} 1 & 0 \\ 0 & \frac{1}{4} \sin^2 \theta \end{pmatrix} \quad (4.8)$$

$$K = \frac{1}{8}(1 + \sin^4 \theta) \quad (4.9)$$

If the magnetic field is positive, u_1 is the ground state. The metric on \mathcal{M}_0 is then $g^{(u_1)}$ calculated above. During some arbitrary change of magnetic field whilst not measuring the state of the system, it can be transported from $|\psi_i\rangle := |u_1\rangle$ to some new ground state by changing the magnetic field direction, as shown on fig. 4.1

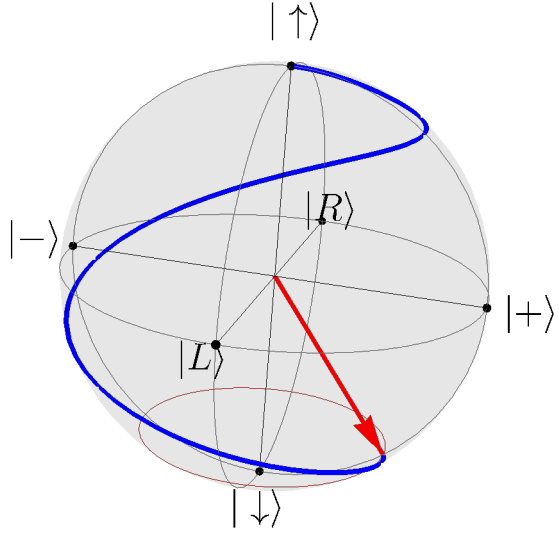


Figure 4.1: Bloch sphere for the eigenstate u_1 with the initial direction of magnetic field $\mathbf{B} = (0, 0, B_z)$ transported along $\gamma = \{(\phi, \sqrt{\phi}) | \phi \in [0, 2\pi]\}$ (blue). The final orientation of the magnetic field is marked red and the states on the Bloch sphere correspond to initial eigenstate.

It's pedagogical to point out the correspondence to figure 2.4, where $\mathcal{M}_0 = \cup_{\lambda} \{|u_1\rangle\}$, $\mathcal{M}_1 = \cup_{\lambda} \{|u_2\rangle\}$, $|o(\lambda)\rangle = u_1(\mathbf{B} = B(0, 0))$ and $|o(\tilde{\lambda})\rangle = u_1(\mathbf{B} = B(2\pi, \sqrt{2\pi}))$, written in spherical coordinates.

If the transport is made infinitesimally slow with respect to time t , after every step $d\theta$ the eigensystem has to be calculated, and we find out that the system collapses into instantaneous $u_1(t)$ state of $\mathcal{H}(t)$, so the fidelity at any θ is $f_0(\theta) = 1$ and $ds^2(\theta) = 1 - f_0^2 = 0$. Opposite to the adiabatic transport would be the quantum quench, meaning the orientation of \mathbf{B} is changed instantly resulting in a final state

$$|f\rangle = \alpha |u_1\rangle + \beta |u_2\rangle, \quad \text{for } \frac{\alpha}{\beta} = e^{-i\phi} \tan \frac{\theta}{2}, \quad \alpha^2 + \beta^2 = 1. \quad (4.10)$$

This yields probability of staying in the state u_1 after quench is $f_q = \langle u_1 | f \rangle = \alpha$ and $s = 1 - \alpha$.

4.1 Special case

Assume again transport of $|u_1\rangle$ by rotating the magnetic field along the path $\gamma = \{(0, \theta) | \theta \in [0, \pi/2]\}$, as drawn on figure 4.2. The fidelity for infinitesimal speed is at every point on the path $f_0 = 1$ and for quantum quench $f_q = 1/2$.

Now let's calculate the fidelity for some finite time transport.

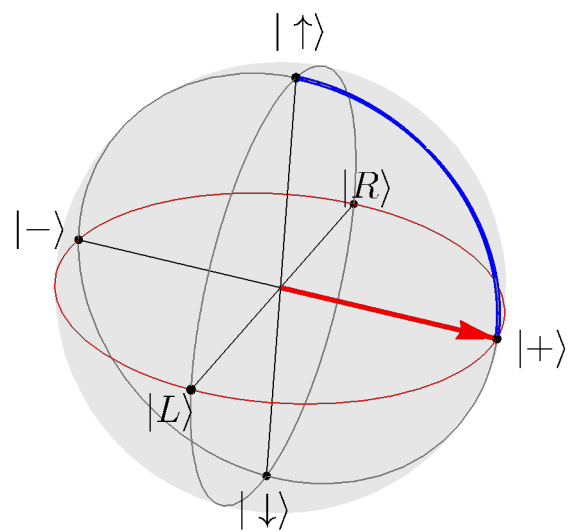


Figure 4.2: Bloch sphere for the eigenstate u_1 with the initial direction of magnetic field $\mathbf{B} = (0, 0, B_z)$ transported along $\gamma = \{(0, \theta) | \theta \in [0, \pi/2]\}$ (blue). The final orientation of the magnetic field is marked red and the states on the Bloch sphere correspond to initial eigenstate.

5. Lipkin-Meshkov Glick model

The aim of this text is to analyze Hamiltonian

$$\hat{H} = \hat{J}_3 + \lambda \hat{V}_1 + \chi \hat{V}_2 + \chi^2 \hat{V}_3, \quad (5.1)$$

where

$$\hat{V}_1 = -\frac{1}{2j} \hat{J}_1^2 \quad (5.2)$$

$$\hat{V}_2 = -\frac{1}{2j} [\hat{J}_1(\hat{J}_3 + j\mathbb{1}) + (\hat{J}_3 + j\mathbb{1})\hat{J}_1] \quad (5.3)$$

$$\hat{V}_3 = -\frac{1}{2j} (\hat{J}_3 + j\mathbb{1})^2. \quad (5.4)$$

Using the Spherical harmonics basis $\{|j, m\rangle\}$ for quantum numbers j as the angular momentum and m its projection on the direction of \hat{J}_3 and defining

$$\hat{J}_{\pm} := \frac{1}{2}(\hat{J}_1 \pm i\hat{J}_2), \quad (5.5)$$

we get the matrix elements

$$\langle j'm' | \hat{J}^2 | jm \rangle = j(j+1)\delta_{j'j}\delta_{m'm} \quad (5.6)$$

$$\langle j'm' | \hat{J}_3 | jm \rangle = m\delta_{j'j}\delta_{m'm} \quad (5.7)$$

$$\langle j'm' | \hat{J}_{\pm} | jm \rangle = \sqrt{(j \mp m)(j \pm m + 1)}\delta_{j'j}\delta_{m'm \pm 1}, \quad (5.8)$$

where $\delta_{a'b}$ is Kronecker delta. Hamiltonian in eq. 5.1 can then be written as

$$\begin{aligned} \hat{H} = & J_3 - \frac{\lambda}{8j}(J_+ + J_-)^2 - \frac{\chi}{4j} [(J_+ + J_-)(J_3 + j\mathbb{1}) + (J_3 + j\mathbb{1})(J_+ + J_-)] \\ & - \frac{\chi^2}{2j} (J_3 + j\mathbb{1})^2, \end{aligned} \quad (5.9)$$

which has pentadiagonal matrix representation. During the whole paper, $j = N/2$ will be used.

The behavior of dimensions $N = 1$ and $N = 2$ are fundamentally different from higher dimensions and, therefore, the discussion will start at $N = 3$, followed by $N = 5$. Then the limit $N \rightarrow \infty$ will be taken along with the generalization of some characteristics to an arbitrary dimension. Due to the complexity of our Hamiltonian, it is not possible to prove every statement analytically. Some numerical methods, supported by some basic theorems, are needed. All figures and simulations were calculated in Mathematica.

5.1 Case $N = 3$

The lowest dimension behaving similarly to higher N is 3 with the matrix represented Hamiltonian

$$\hat{H} = \begin{pmatrix} -\frac{\lambda+6}{4} & -\frac{\chi}{2\sqrt{3}} & -\frac{\lambda}{2\sqrt{3}} & 0 \\ -\frac{\chi}{2\sqrt{3}} & \frac{(-7\lambda-4\chi^2-6)}{12} & -\chi & -\frac{\lambda}{2\sqrt{3}} \\ -\frac{\lambda}{2\sqrt{3}} & -\chi & \frac{(-7\lambda-16\chi^2+6)}{12} & -\frac{5\chi}{2\sqrt{3}} \\ 0 & -\frac{\lambda}{2\sqrt{3}} & -\frac{5\chi}{2\sqrt{3}} & -\frac{\lambda}{4} - 3\chi^2 + \frac{3}{2} \end{pmatrix}. \quad (5.10)$$

The spectrum of this Hamiltonian can be calculated analytically using some substitutions G, F, D, E , see Appendix A, as

$$E_0 = \frac{1}{12} \left(G - F - \frac{\sqrt{D - E}}{2} \right) \quad (5.11)$$

$$E_1 = \frac{1}{12} \left(G - F + \frac{\sqrt{D - E}}{2} \right) \quad (5.12)$$

$$E_2 = \frac{1}{12} \left(G + F - \frac{\sqrt{D + E}}{2} \right) \quad (5.13)$$

$$E_3 = \frac{1}{12} \left(G + F + \frac{\sqrt{D + E}}{2} \right). \quad (5.14)$$

Eigenvectors can also be written analytically, but doing it here would be redundant. On sections $\lambda = 1$ and $\chi = 1$, see Figures 5.1 resp. 5.2, it can be seen the general behaviour of the spectrum, where the energies get close to each other somewhere around the center of our coordinate system $(\lambda; \chi)$ and then separate monotonously to never meet again. In addition, the spectrum is symmetrical for $\chi \leftrightarrow -\chi$.

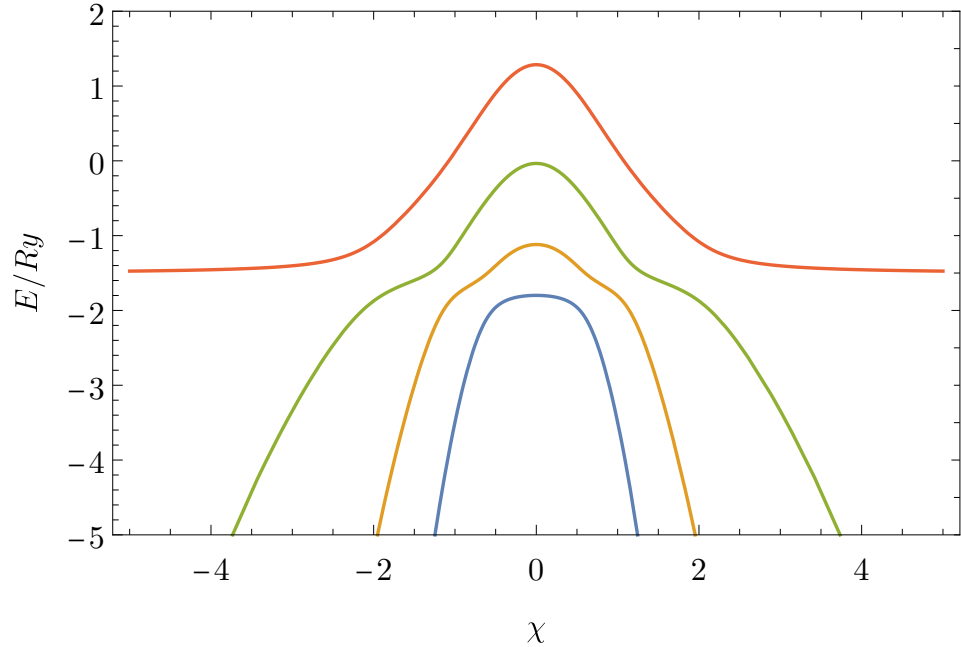


Figure 5.1: Energy for the case $N = 3$, section $\lambda = 1$

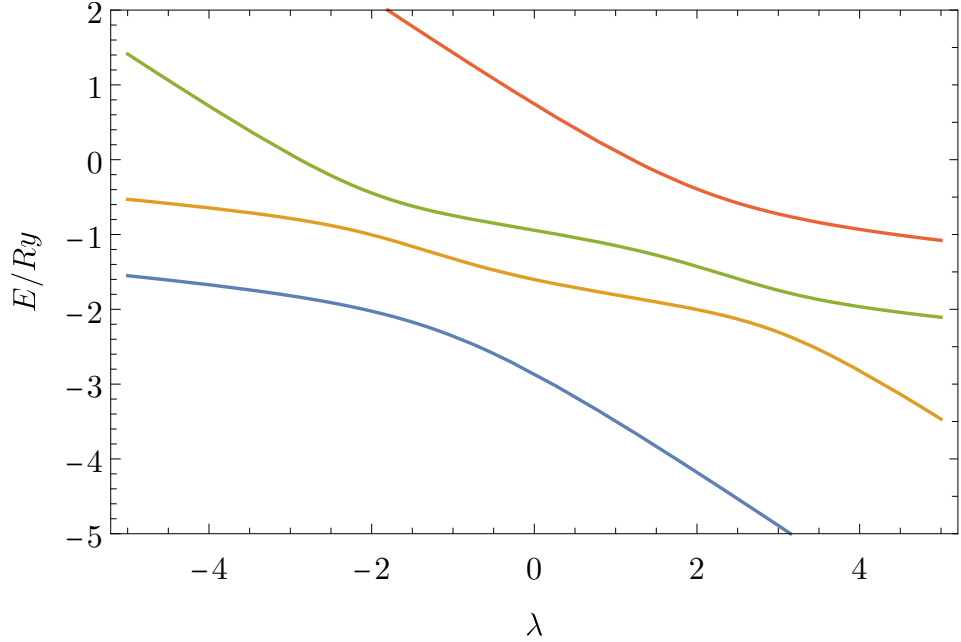


Figure 5.2: Energy for the case $N = 3$, section $\chi = 1$

From the Equations 5.11, 5.12 can be seen that there might exist degeneracy between every two neighboring energy levels¹. Specifically, for $E_0 = E_1$ for $D = E$, which for real values λ , χ has two solutions

$$(\lambda_d, \pm\chi_d) = \left(-\frac{1}{2}; \sqrt{\frac{3}{5}} \right).$$

Point-like characteristics correspond to Theorem 1, which states that Hamiltonian driven by two real parameters can be degenerated only on 0-dimensional manifolds.

If the energy spectrum is degenerate and the metric tensor diverges, see individual elements in Fig. 5.3, its determinant also diverges, as shown in Fig. 5.4, along with Christoffel symbols in Fig. 5.5. Note that the metric tensor determinant is positive definite, thus the manifold is Riemannian. Further on, it reflects the symmetry $\chi \leftrightarrow -\chi$, except for elements g_{12} , Γ_{121} , Γ_{211} , and Γ_{222} , which switch their sign.

¹If substituted letters were real numbers, degeneracies would exist between every two neighboring energy levels. The problem here, that for functions G, F, D, E the solution might not exist. Even though we will see that it's probably not that case and degeneracy exist between every two neighboring energy levels.

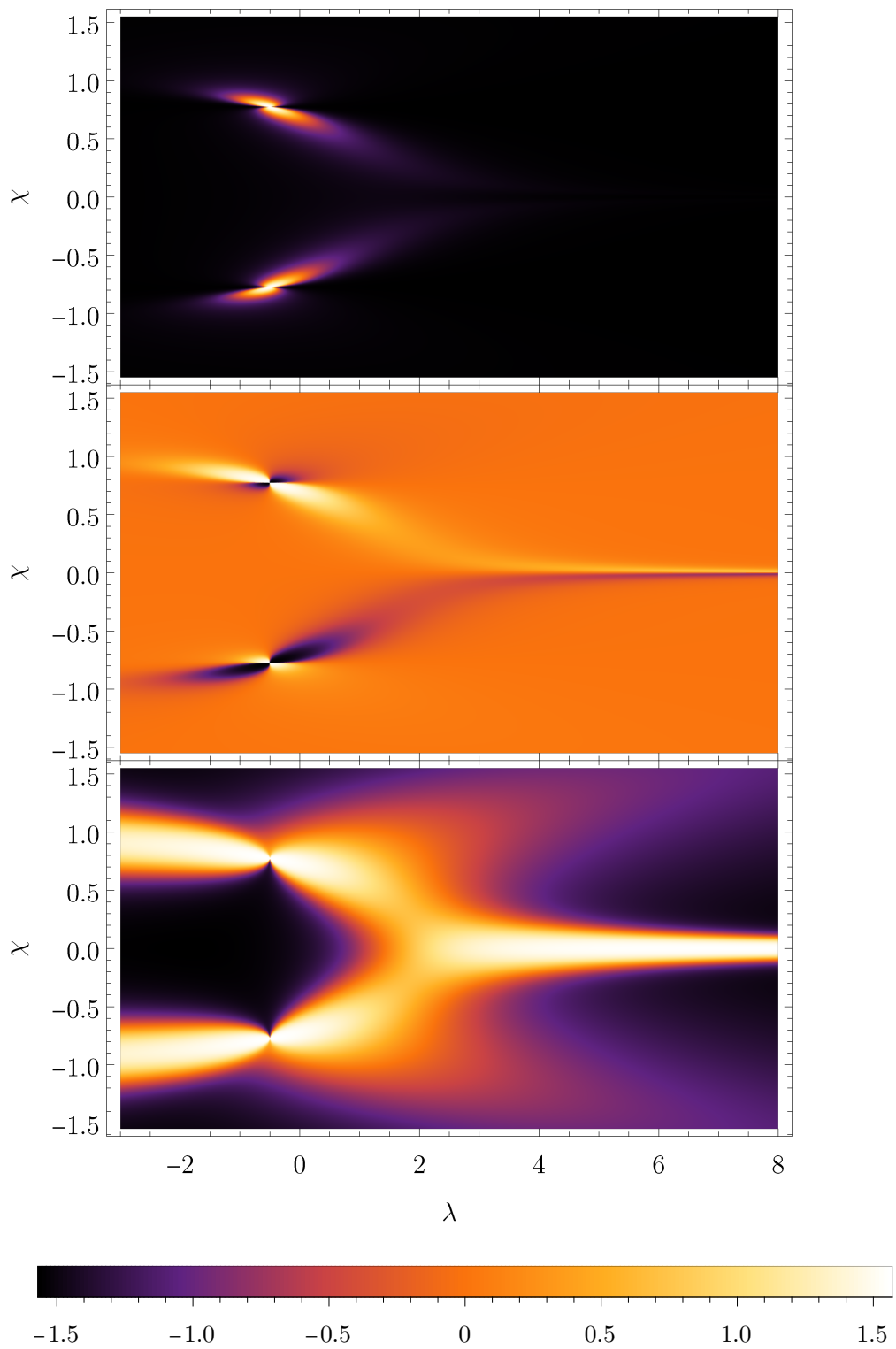


Figure 5.3: Arctangent of metric tensor elements for the case $N = 3$. From the top: $\text{Arctan}(g_{11})$, $\text{Arctan}(g_{12}) = \text{Arctan}(g_{21})$, $\text{Arctan}(g_{22})$

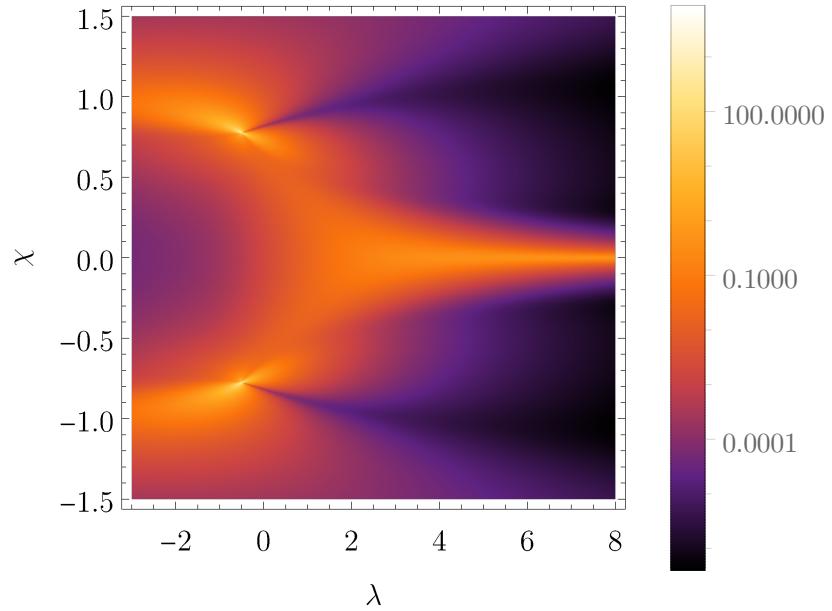


Figure 5.4: Metric tensor determinant in a parameter space for $N = 3$.

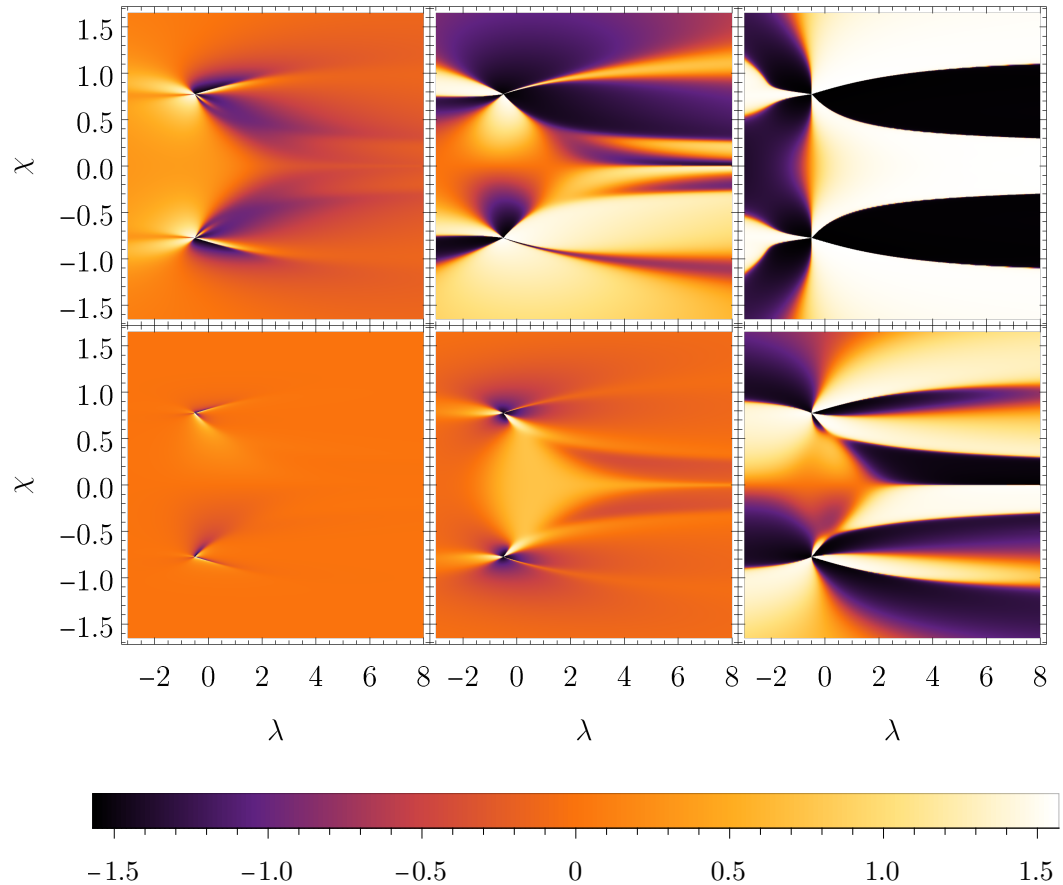


Figure 5.5: 1.0 Arctangent of Christoffel symbols for the case $N = 3$. First row from left: $\text{Arctan}(\Gamma_{111})$, $\text{Arctan}(\Gamma_{121})$, $\text{Arctan}(\Gamma_{122})$. Second row from left: $\text{Arctan}(\Gamma_{211})$, $\text{Arctan}(\Gamma_{221})$, $\text{Arctan}(\Gamma_{222})$.

Due to metric tensor degeneracy, the space is not geodesically maximal. To see that the singularity is not the only *coordinate one*², the Ricci scalar can be calculated, see Fig. 5.6. Divergent Ricci scalar implies the existence of a *physical singularity*. This can be seen from the sections in χ -direction drawn in Fig. 5.7, which at coordinate $(\lambda_d; \chi_d)$ diverges, implying the singularity is *physical*.

The presence of singularities means that our ground state manifold is geodesically incomplete and according to Theorem 3 there exist some geodesically unreachable coordinates.

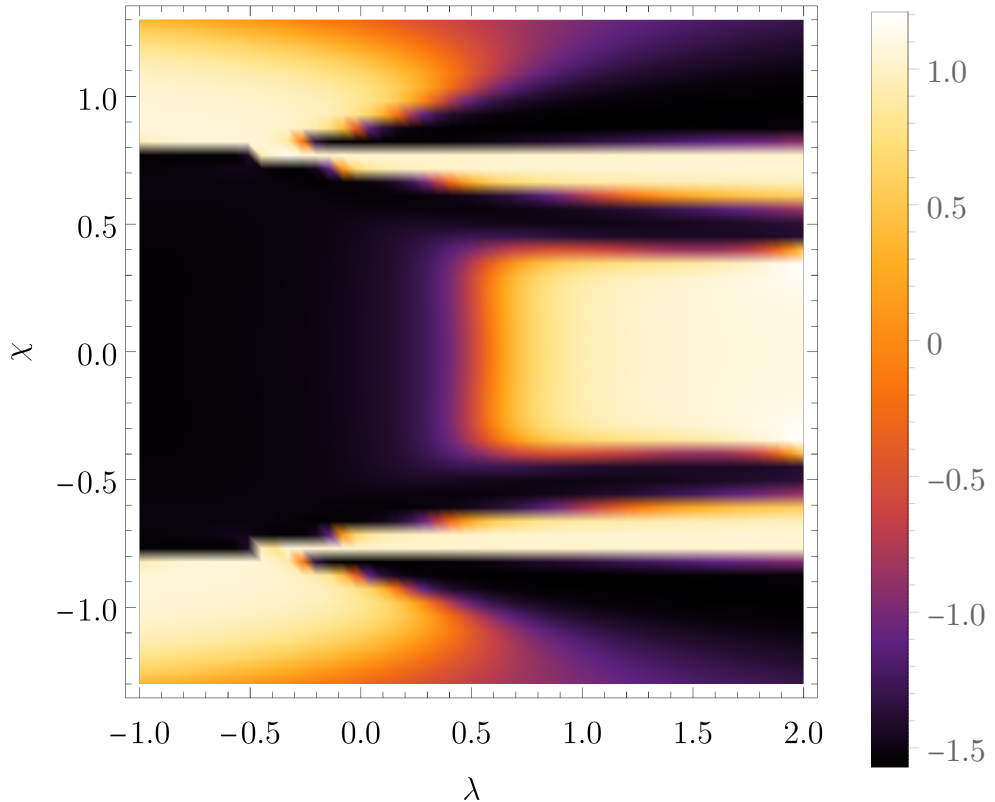


Figure 5.6: Arctangent of Ricci curvature for the case $N = 3$. [Excuse the resolution, I will make better calculation in Metacentrum later.](#)

²Coordinate singularity is present only in some coordinates. This is different from so called *physical singularity*, which is present in every choice of the coordinate system.

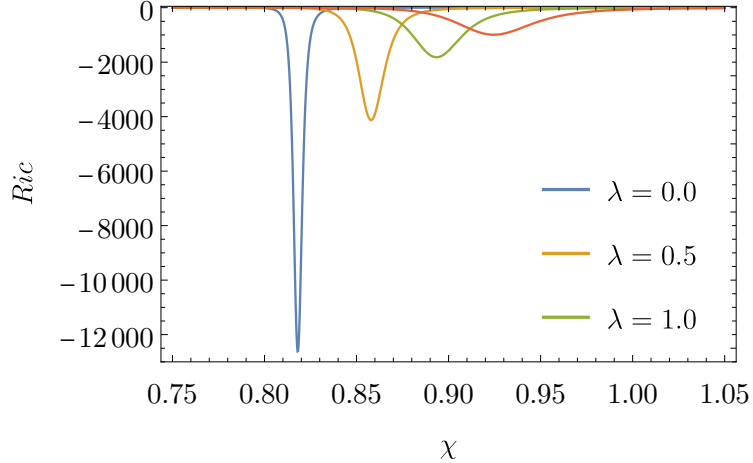


Figure 5.7: Ricci curvature sections for three different $\lambda = const.$

The system characteristics can be seen more clearly from geodesics, i.e., by solving the initial value problem with conditions

$$(\lambda(t_i); \chi(t_i)) = (\lambda_i; \chi_i)$$

$$\left. \left(\frac{d\lambda(t)}{dt}; \frac{d\chi(t)}{dt} \right) \right|_{t_i} = (\lambda'_i; \chi'_i),$$

where t_i means *initial time*.

Results for these geodesics starting at $(\lambda; \chi) = (0; 0)$, $(\lambda', \chi') = (\cos \theta; \sin \theta)$ for $\theta \in [-0.63; 0.63]$ and $\theta \in [\pi - 0.225; \pi + 0.225]$ with step $\Delta\theta = 0.01$, can be seen in Fig. 5.8. Other values θ result in a close approach of the geodesics to the singularity, making the calculations numerically unstable. The fact that geodesics lean towards singularities is well known from the theory of General Relativity (GR). The main difference here is that our "test particle" seems to be partially repulsed by the singularity. The analogy with GR would therefore fail because of the nonexistence of negative mass and gravitational dipoles. The better analogy would be electromagnetism, which has a downside in the fact that one does not usually use the metric structures in this theory. Comparison of those two intuitive examples can be seen in Fig. 5.9. The geodesic behavior is not caused only by the singularity but also by a large Ricci curvature leaning to the right from it. This means that the distance across this gap is also large, leading to the strong tendency of the geodesics to go around the singularity rather than crossing it, which is again seen in Fig. 5.8.

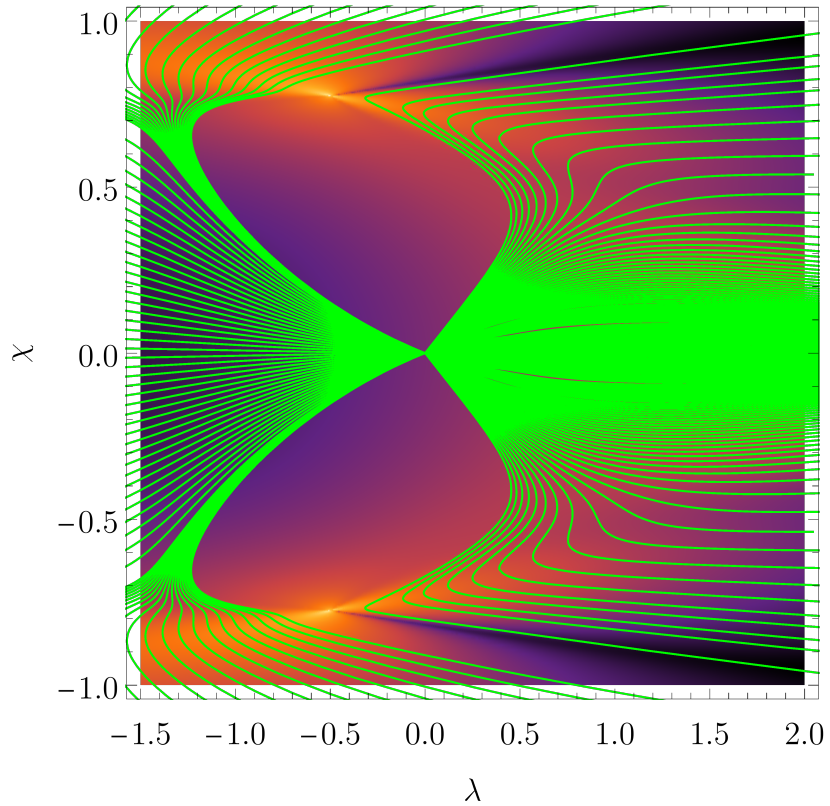


Figure 5.8: Geodesics for the case $N = 3$ starting from $(\lambda_i; \chi_i) = (0; 0)$ with $(\lambda'_i; \chi'_i) = (\cos \theta; \sin \theta)$, parametrized by angle θ .

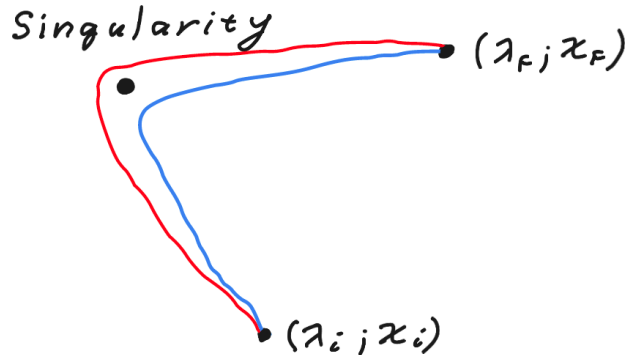


Figure 5.9: Comparing geodesics with repulsing (blue) and attracting (red) metric tensor divergence in the spherical symmetrical space.

5.2 Case $N = 5$

Few characteristics in arbitrary dimension can be shown for the case $N = 5$. First are the degeneracies between different energy levels, which can be seen in Fig. 5.10. One can see that only $E_0 = E_1$ the degeneracy lies on the separatrix and all others are distributed around. The $\chi \leftrightarrow -\chi$ symmetry holds for all of them.

Another fact, which is good to realize, is how the space itself looks like. This is best seen from the metric tensor determinant, fig. 5.11.

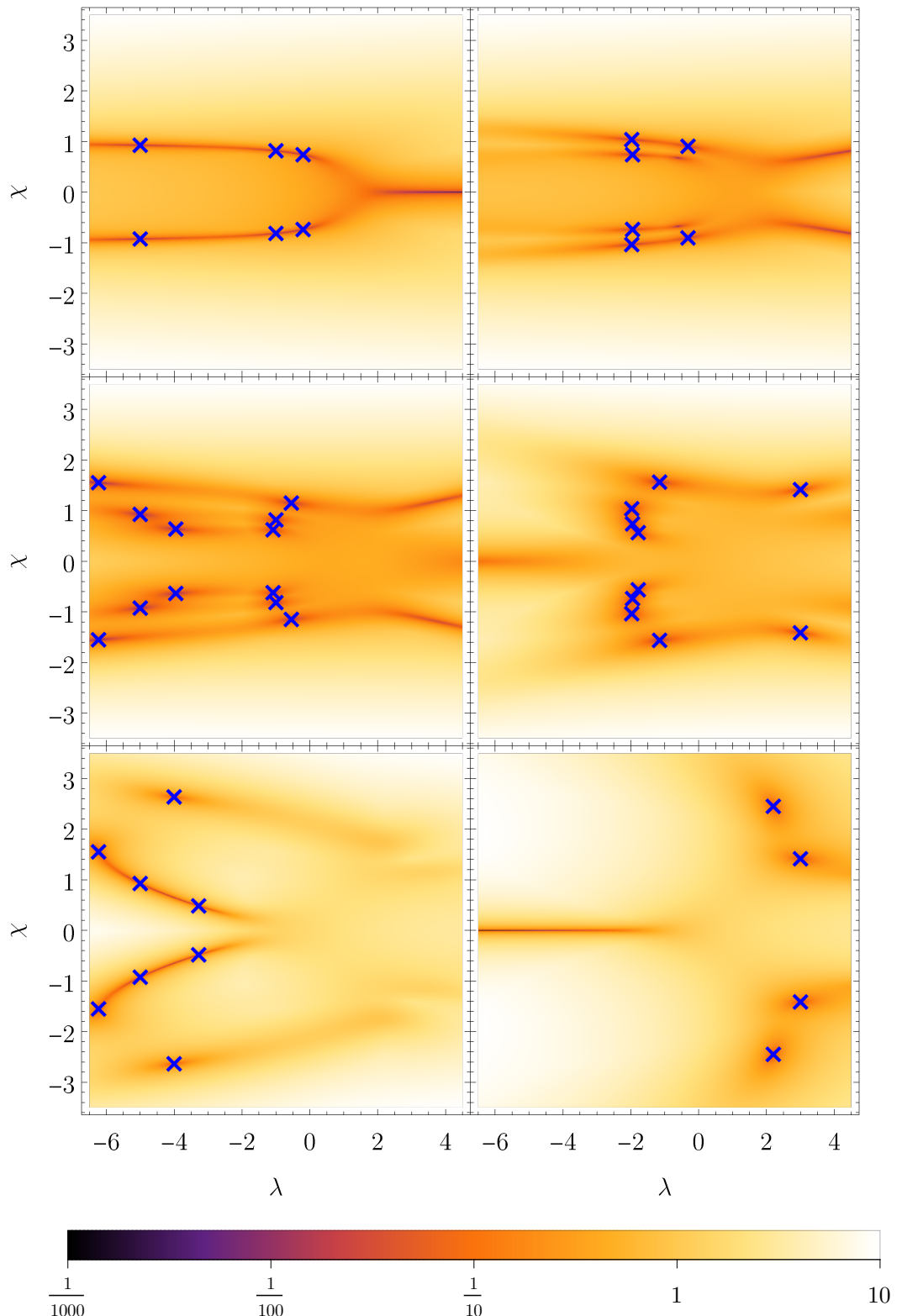


Figure 5.10: Energy differences between neighboring energy levels for $N = 5$. First row: $E_1 - E_0$, $E_2 - E_1$, second row: $E_3 - E_2$, $E_4 - E_3$, third row: $E_5 - E_4$, $E_6 - E_5$.

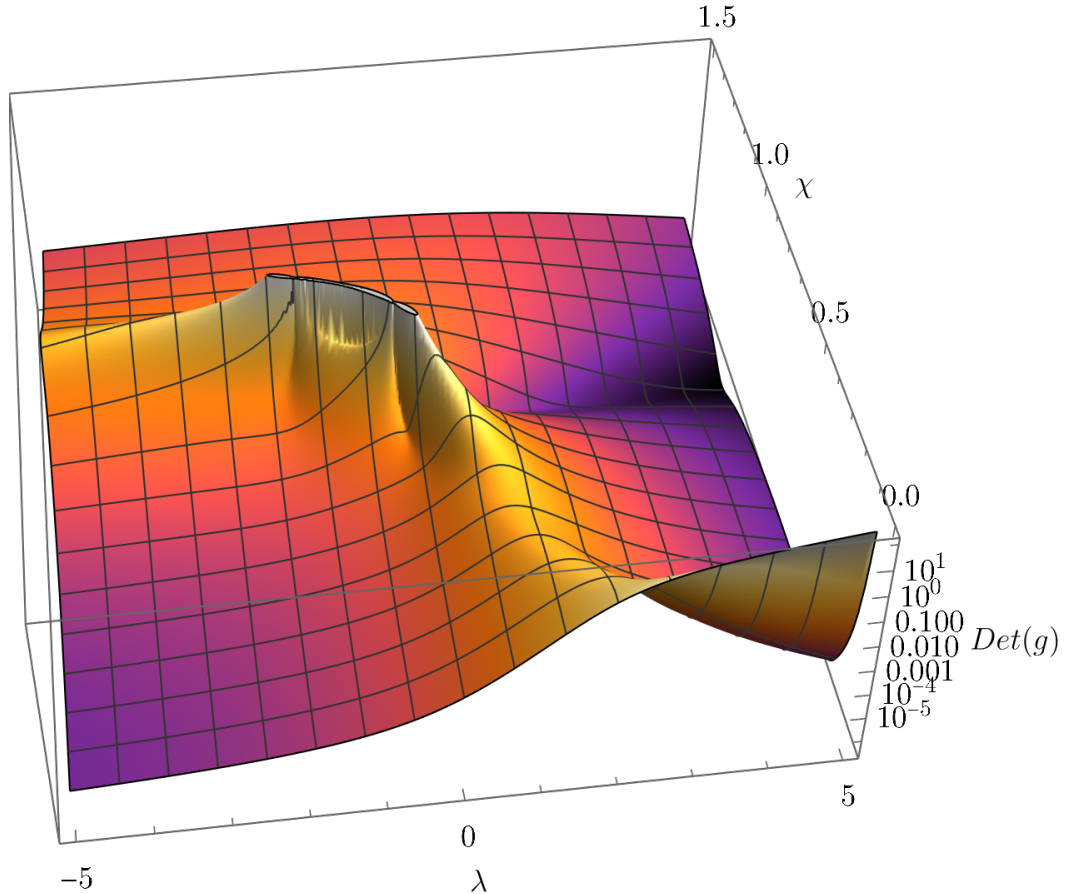


Figure 5.11: Metric tensor determinant for the case $N = 5$.

Geodesics for the case $N = 5$ starting from the point $(0; 0)$ have the characteristics already seen in the case $N = 3$. However, when starting at $(\lambda; \chi) = (1; 0)$, the behavior around the singularity is not the only interesting thing happening. As can be seen in Fig. 5.12, the geodesics tend to deflect themselves from the area with high curvature around the axis $\chi = 0$, which happens even for other initial conditions, just that for $(0; 0)$ it is not so apparent. Small irregularity can be seen in Fig. 5.8 around $(0.5; 0.1)$. This implies that the geodesic equation might have at least two solutions as candidates for the globally shortest path between two points.³ Example of three solutions between two points can be seen in Fig. 5.13.

³The existence of singularities implies that there are infinitely many solutions, because they can bounce between singularities, or go around one of them any number of times. Those are surely not the globally shortest paths, which we are interested in.

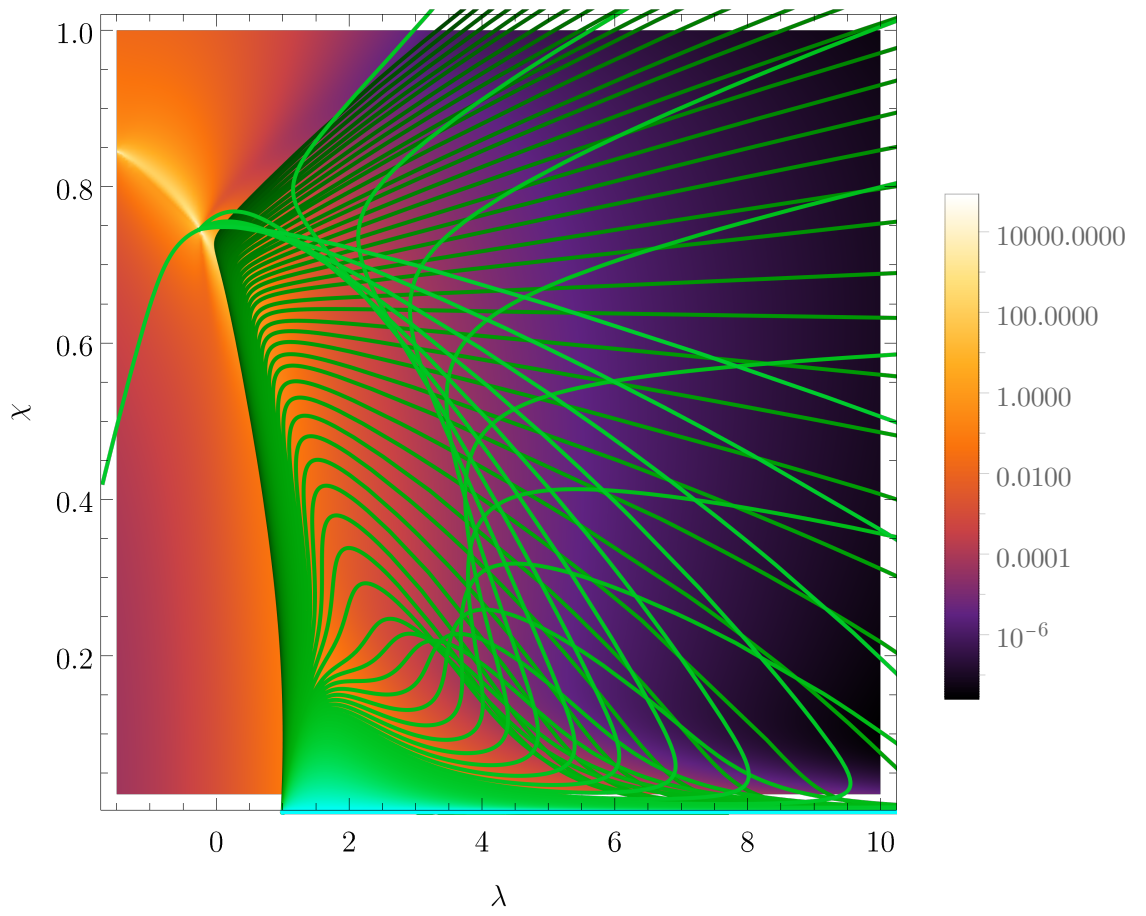


Figure 5.12: Geodesics for the case $N = 5$, starting from the point $(1; 0)$. The numerics around the singularity breaks down, but the solution is close to the drawn one, i.e. they will pass close to the singularity and continue to the left.

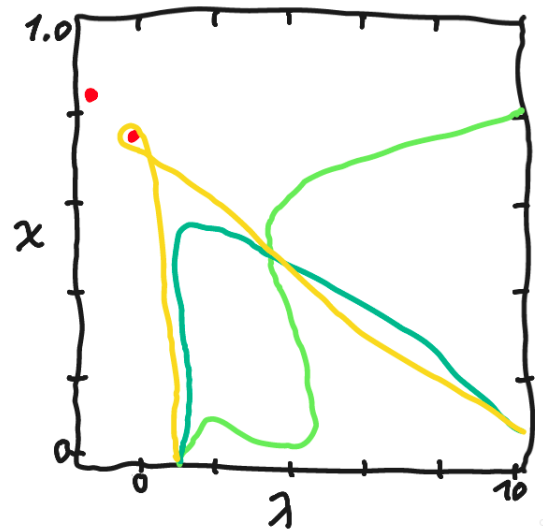


Figure 5.13: Three possible solutions between points $(1; 0)$ and $(4; 0.5)$. The length of the yellow one is surely longer than other two, but the difference between green vs. blue solution is not clear on the first sight.

5.3 Limit $N \rightarrow \infty$

The limit $N \rightarrow \infty$ can be applied to the Hamiltonian in Eq. 5.1 using Holstein-Primakoff mapping for bosonic operators⁴

$$\mathcal{H} := \lim_{j \rightarrow \infty} \frac{\hat{H}}{2j}, \quad (5.15)$$

resulting in classical Hamiltonian

$$\begin{aligned} \mathcal{H}(x, p) = & -\frac{1}{2} + \frac{1-\lambda}{2}x^2 + \frac{\lambda-\chi^2}{4}x^4 - \frac{\chi x^3}{2}\sqrt{2-x^2-p^2} - \frac{\chi^2}{4}p^4 \\ & + \frac{p^2}{4} \left[2 + (\lambda - 2\chi^2)x^2 - 2\chi x\sqrt{2-x^2-p^2} \right]. \end{aligned} \quad (5.16)$$

Finding minimas in its derivatives, we get the *separatrix*

$$\chi^2 = \frac{\lambda - 1}{\lambda - 2}, \quad (5.17)$$

which represents the phase transition in the limit $N \rightarrow \infty$. In our case, the transition is of first order everywhere, except in $(\lambda; \chi) = (1; 0)$, where it has order two. The separatrix is shown in Fig. 5.14 compared to minimum between the ground state and the first excited state $E_1 - E_0$ for $N = 3$ case. With increasing N , it converges to the separatrix line.

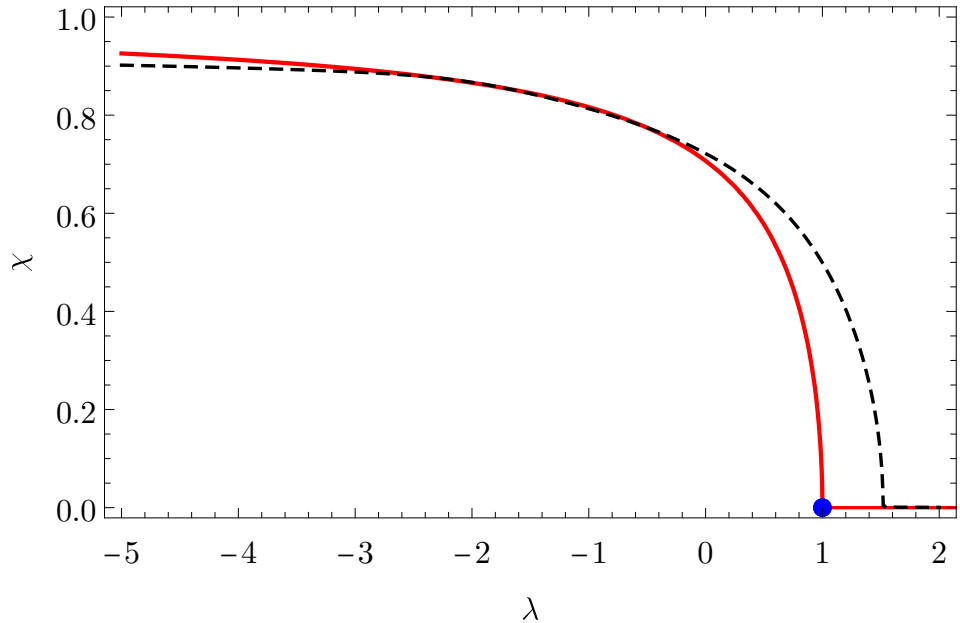


Figure 5.14: First order phase transition – Separatrix (red), second order transition (blue point) compared to minimum between the ground state and first excited state in $N=3$ case (black, dashed).

⁴Felipe did this and I have no idea how

5.4 Arbitrary N

For higher dimensions we see the same characteristic behaviour in the energy spectrum sections, see the example in Fig. 5.15, 5.16 for the $N = 10$ case. Between all energy levels there is at least one avoided crossing and between zeroth and the first there are $N - 2$ crossings for N odd and $N - 3$ for N even, which I have no idea how to prove, but it looks like it might be true.

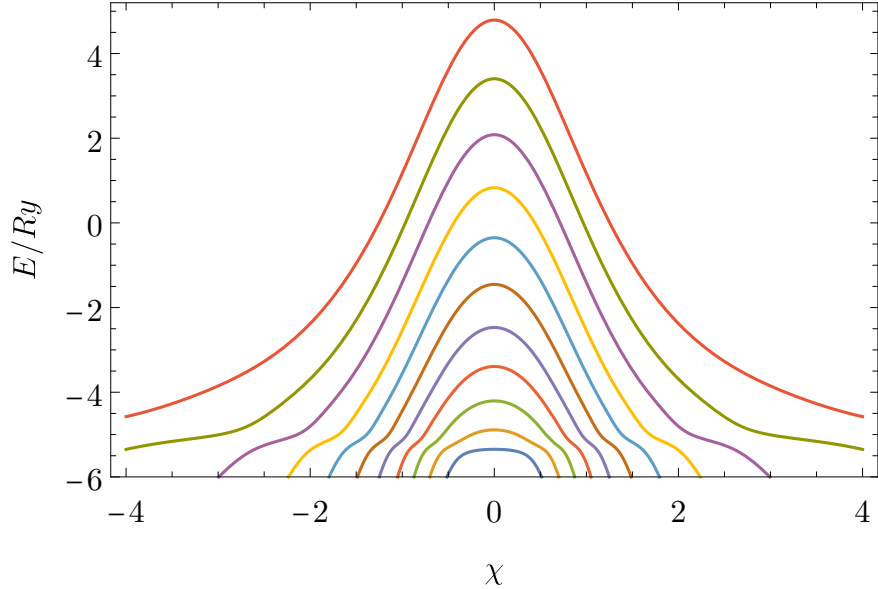


Figure 5.15: Energy spectrum as function of χ , for $\lambda = 1$ and $N = 10$.

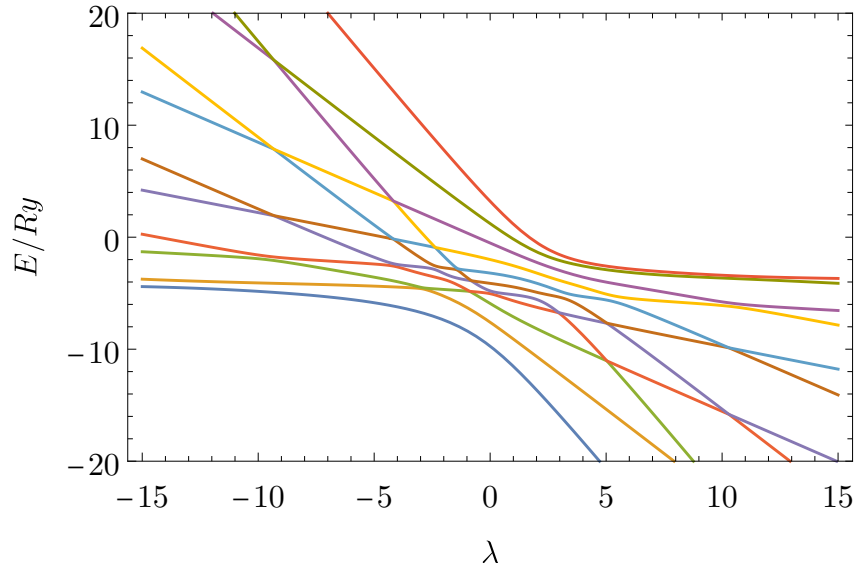


Figure 5.16: Energy spectrum as a function of λ , for $\chi = 1$ and $N = 10$.

Special attention was given to the spectrum degeneracies between the zeroth and the first energy level, because those influence the metric tensor and geodesics. Their exact calculation is numerically costly, and only the first few cases, namely,

$N \in \{3, 4, 5, 6, 7\}$, were calculated, see Tab. 5.1. Those were later proven up to a numerical precision for cases $N \leq 1000$.

| N | $(\lambda_l; \pm \chi_l)$ | $(\lambda_2; \pm \chi_2)$ | $(\lambda_r; \pm \chi_r)$ |
|-----|--------------------------------------|---------------------------------------|---------------------------------------|
| 3 | $(-\frac{1}{2}; \sqrt{\frac{3}{5}})$ | | |
| 4 | $(-3; \sqrt{\frac{4}{5}})$ | | $(-\frac{1}{3}; \sqrt{\frac{4}{7}})$ |
| 5 | $(-\frac{3}{2}; \sqrt{\frac{5}{7}})$ | | $(-\frac{1}{4}; \sqrt{\frac{5}{9}})$ |
| 6 | $(-5; \sqrt{\frac{6}{7}})$ | $(-1; \sqrt{\frac{2}{3}})$ | $(-\frac{1}{5}; \sqrt{\frac{6}{11}})$ |
| 7 | $(-\frac{5}{2}; \sqrt{\frac{7}{9}})$ | $(-\frac{3}{4}; \sqrt{\frac{7}{11}})$ | $(-\frac{1}{6}; \sqrt{\frac{7}{13}})$ |

Table 5.1: Singularities between the zeroth and first energy levels for dimensions 3–7. Subscript $l(r)$ means the most *left(right)-wise* positioned coordinates in the (λ, χ) -plot.

The observed formula for (λ_l, χ_l) and (λ_r, χ_r) , i.e., those with minimal, resp. maximal λ coordinate is

$$(\lambda_l; \pm \chi_l) = \begin{cases} \left(1 - \frac{N}{2}; \sqrt{\frac{N}{N+2}}\right) & , N \geq 3, N \text{ is odd} \\ \left(1 - N; \sqrt{\frac{N}{N+1}}\right) & , N \geq 3, N \text{ is even} \end{cases} \quad (5.18)$$

$$(\lambda_r; \pm \chi_r) = \left(\frac{1}{1-N}; \sqrt{\frac{N}{2N-1}} \right) , N \geq 3. \quad (5.19)$$

Dimensions 3 to 10 are shown in Fig. 5.17. In addition, the degeneracies between the zeroth and the first energy levels belong to the separatrix described by Eq. 5.17. Due to this, the position of the singularities is constrained to the separatrix between points $(\lambda_l, \pm \chi_l)$ and $(\lambda_r, \pm \chi_r)$.

In the limit $N \rightarrow \infty$ they converge to

$$\lim_{N \rightarrow \infty} (\lambda_l; \pm \chi_l) = (-\infty, 1)$$

$$\lim_{N \rightarrow \infty} (\lambda_r; \pm \chi_r) = \left(0, \frac{1}{\sqrt{2}}\right).$$

One would expect the whole separatrix to be divergent, thus the left limit to be in the $-\infty$, as it is, and the right one to be at the point $(\lambda; \chi) = (1; 0)$, which is not the case. This might mean that some new singularities are being constructed right of λ_r and I will look at it. In addition, because for $N \rightarrow \infty$ there is an infinite number of singularities and because the whole separatrix is divergent, they need to be dense.

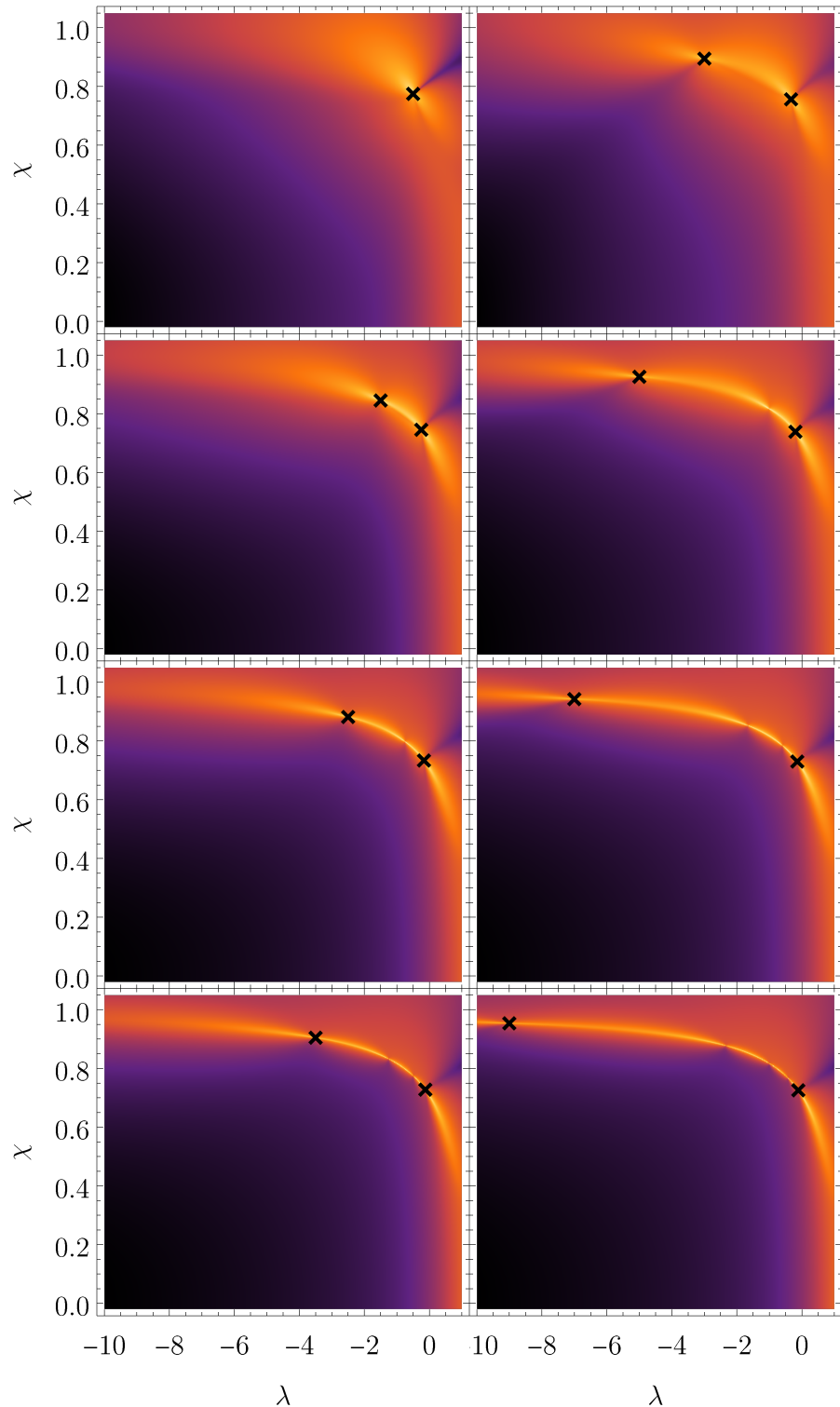


Figure 5.17: Spectrum degeneracy between E_0 and E_1 . Hamiltonian dimensions are 1,3,5,7 in the first column and 2,4,6,8 in the second column. Black crosses mark most left-wise and right-wise singularity and the background corresponds to the metric tensor determinant. Other singularities are also well visible in the determinant.

6. Two leve system

Let's have a Hamiltonian

$$\hat{H}(t) = \begin{pmatrix} \Omega(t) & \Delta(t) \\ \Delta(t) & -\Omega(t) \end{pmatrix} \quad (6.1)$$

for $\Omega : \mathbb{R}^+ \rightarrow \mathbb{R}$, $\Delta : \mathbb{R}^+ \rightarrow \mathbb{R}$. Its spectrum is

$$E_1(t) = -E_0(t) = \sqrt{\Omega^2(t) + \Delta^2(t)} \quad (6.2)$$

and using the basis

$$\mathcal{B} := \left\{ |0\rangle \equiv \begin{pmatrix} 0 \\ 1 \end{pmatrix}, |1\rangle \equiv \begin{pmatrix} 1 \\ 0 \end{pmatrix} \right\}, \quad (6.3)$$

we get the eigenvectors

$$|0(t)\rangle = N_+ \begin{pmatrix} \frac{E_0(t)+\Omega(t)}{\Delta(t)} \\ 1 \end{pmatrix}; \quad |1(t)\rangle = N_- \begin{pmatrix} \frac{E_1(t)+\Omega(t)}{\Delta(t)} \\ 1 \end{pmatrix} \quad (6.4)$$

for normalization constants $N_{\pm} = \left(\left(\frac{\pm E_0(t)+\Omega(t)}{\Delta(t)} \right)^2 + 1 \right)^{-1/2}$.

The goal will be to find *fidelity* $F := |\langle 0(t)|\psi(t)\rangle|^2$ of different driving protocols. For this we need to solve time Schrödinger equation

$$\hat{H}(t)|\psi(t)\rangle = i \frac{d}{dt} |\psi(t)\rangle \quad (6.5)$$

with time varying Hamiltonian. For 2-dimentional system with $|\psi(t)\rangle =: (a(t), b(t))^T$ we get the system of *two coupled differentials equations of the 1. order with non-constant coefficients*

$$\Omega(t)a(t) + \Delta(t)b(t) = i\dot{a}(t) \quad (6.6)$$

$$\Delta(t)a(t) - \Omega(t)b(t) = i\dot{b}(t) \quad (6.7)$$

with normalization

$$a^2(t) + b^2(t) = 1, \quad \forall t \in [0, T_f]. \quad (6.8)$$

and initial value

$$\begin{pmatrix} a(0) \\ b(0) \end{pmatrix} = |0(0)\rangle. \quad (6.9)$$

6.0.1 Harmonic oscillator correspondence

The Equations 6.6, 6.7 have no general analytical solution, with exceptions of a few easy protocols $\hat{H}(t)$. Still we can find some general behavior.

N-dimensional Schrödinger equation can be rewritten to *one differential equation of N^{th} order with non-constant coefficients*. In our two dimensional case, this equation corresponds to *damped harmonic oscillator without external force*

$$0 = \ddot{a}(t) + \gamma(t)\dot{a}(t) + \omega^2(t)a(t) \quad (6.10)$$

$$\gamma(t) := -\frac{\dot{\Delta}(t)}{\Delta(t)} \quad (6.11)$$

$$\omega^2(t) := i \left(\dot{\Omega}(t) - \frac{\dot{\Delta}(t)}{\Delta(t)} \Omega(t) \right) + \Delta^2(t) + \Omega^2(t). \quad (6.12)$$

Along with normalization condition 6.8 and initial conditions

$$\begin{pmatrix} a(0) \\ b(0) \end{pmatrix} = |0(t)\rangle; \quad \dot{a}(0) = -i(\Omega(0)a(0) + \Delta(0)b(0)). \quad (6.13)$$

Note that in this form $\Delta \neq 0$. This is not problem due to system symmetry $\Delta \leftrightarrow \Omega$, which means we can change the driving by interchanging Δ and Ω on any problematic intervals.

Classical mechanics correspondence

From the perspective of classical mechanics, meaning $x(t) := a(t)$ is a position in a phase space (\mathbf{x}, \mathbf{p}) , we can write classical Lagrangian from Eq. 6.10 as

$$\mathcal{L} = \frac{1}{2} \exp\left(\int_0^t \gamma(s)ds\right) (\dot{x}^2 - \omega^2(t)x^2) \quad (6.14)$$

Proof. The correspondence of Lagrangian 6.14 with Eq. 6.10 can be shown by direct evaluation of Euler-Lagrange equations

$$\begin{aligned} \frac{\partial \mathcal{L}}{\partial x} - \frac{d}{dt} \frac{\partial \mathcal{L}}{\partial \dot{x}} &= 0 \\ \frac{1}{2} \exp\left(\int_0^t \gamma(s)ds\right) (-2\omega^2(t)x) - \frac{d}{dt} \left(\exp\left(\int_0^t \gamma(s)ds\right) \dot{x} \right) &= 0 \\ -\omega^2(t)x - \gamma(t)\dot{x} - \ddot{x} &= 0, \end{aligned} \quad (6.15)$$

where derivation along upper bound $F(x) := \int_0^{g(x)} f(t)dt \Rightarrow F'(x) = f(g(x))g'(x)$ for $f(t) \in L^1(0, g(x))$ and differentiable function g , was used. \square

6.1 Geodesical driving

As was mentioned, the Schrödinger equation has no general analytical solution, except a few easy protocols $\hat{H}(t)$. One of them is *Geodesical protocol*.

Define driving in 3-dimensional space (the reason will be the urge to rewrite it using $\hat{\sigma}$ matrices)

$$d(t) \equiv \begin{pmatrix} \Omega(t) \\ \Xi(t) \\ \Delta(t) \end{pmatrix} := \begin{pmatrix} -s \cos(\omega(T_f)t) \\ 0 \\ s \sin(\omega(T_f)t) \end{pmatrix} \quad (6.16)$$

parametrized by time $t \in [0, 1]$ and with use of *speed regulating function* $\omega(T_f) := \pi/T_f$. This means, the driving will always be along half-sphere, as in Fig. 6.8.

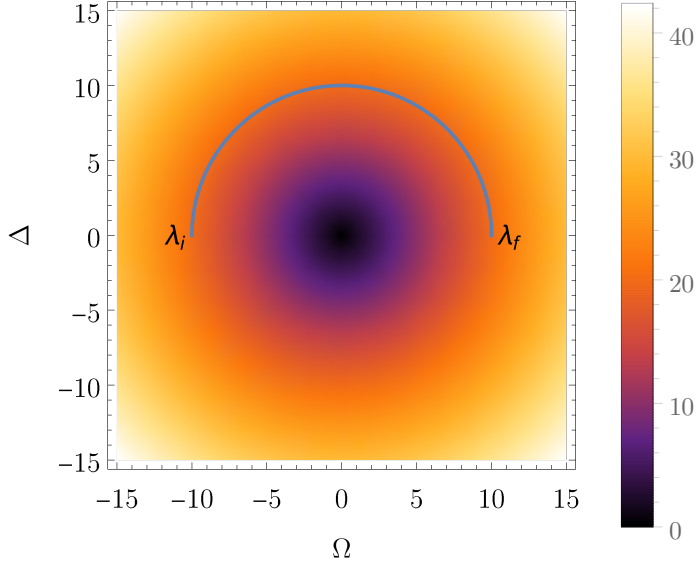


Figure 6.1: Driving along the geodesic. λ_i and λ_f are initial resp. final parameters. DensityPlot shows the difference between Hamiltonian eigenvalues.

6.1.1 Derivation of the fidelity

Because the Hamiltonian can be rewritten using Pauli matrices

$$\hat{H}(t) = \begin{pmatrix} -s \cos(t\omega) & s \sin(t\omega) \\ s \sin(t\omega) & s \cos(t\omega) \end{pmatrix} = \Delta(t)\sigma_x + \Omega(t)\sigma_z = d(t).\hat{\sigma} \quad (6.17)$$

one can see that changing from the [original frame](#) to [moving frame of reference](#) (let's omit the final time dependence $\omega = \omega(T_f)$ for a while)

$$\psi(t) =: e^{\frac{i\omega}{2}\hat{\sigma}_y t} \tilde{\psi}(t) \quad (6.18)$$

reflects rotational symmetry of the problem. This change of reference frame transforms Schrödinger equation

$$\begin{aligned} \hat{H}(t)\psi(t) &= i\psi'(t) \\ \hat{H}(t)e^{\frac{i\omega}{2}\hat{\sigma}_y t} \tilde{\psi}(t) &= ie^{\frac{i\omega}{2}\hat{\sigma}_y t} \left(\frac{i\omega\hat{\sigma}_y}{2} \right) \tilde{\psi}(t) + ie^{\frac{i\omega}{2}\hat{\sigma}_y t} \tilde{\psi}'(t) \\ \underbrace{\left(e^{-\frac{i\omega}{2}\hat{\sigma}_y t} \hat{H}(t) e^{\frac{i\omega}{2}\hat{\sigma}_y t} + \frac{\omega}{2} \hat{\sigma}_y \right)}_{\hat{H}(t)} \tilde{\psi}(t) &= i\tilde{\psi}'(t). \end{aligned} \quad (6.19)$$

Therefore we can equivalently solve the Fidelity problem in this new coordinate system.

Hamiltonian in the moving frame is

$$\tilde{H} = \begin{pmatrix} -s & -i\omega(T_f)/2 \\ i\omega(T_f)/2 & s \end{pmatrix}, \quad (6.20)$$

which is time independent. The Schrödinger equation can now be easily solved using evolution operator

$$\hat{U}(t) = e^{-i\tilde{H}t} = \begin{pmatrix} \cos\left(\frac{t}{2}q(T_f)\right) + \frac{2is\sin\left(\frac{t}{2}q(T_f)\right)}{q(T_f)} & -\frac{\omega(T_f)\sin\left(\frac{t}{2}q(T_f)\right)}{q(T_f)} \\ \frac{\omega(T_f)\sin\left(\frac{t}{2}q(T_f)\right)}{q(T_f)} & \cos\left(\frac{t}{2}q(T_f)\right) - \frac{2is\sin\left(\frac{t}{2}q(T_f)\right)}{q(T_f)} \end{pmatrix}, \quad (6.21)$$

for $q(T_f) = \sqrt{4s^2 + \omega(T_f)^2}$.

In the original frame we get the evolution of the state $\psi(0)$

$$\psi(t) = e^{\frac{i\omega}{2}\hat{\sigma}_y t} \hat{U}(t) \tilde{\psi}(0) = \underbrace{e^{\frac{i\omega}{2}\hat{\sigma}_y t}}_{\hat{U}(t)} \hat{U} e^{-\frac{i\omega}{2}\hat{\sigma}_y t} \underbrace{e^{\frac{i\omega}{2}\hat{\sigma}_y t} \tilde{\psi}(0)}_{\psi(0)}. \quad (6.22)$$

Then the evolved wavefunction is

$$|\psi(t)\rangle = \begin{pmatrix} \cos\left(\frac{t}{2}q(T_f)\right) + \frac{2is\cos(t\omega(T_f))\sin\left(\frac{t}{2}q(T_f)\right)}{q(T_f)} \\ \frac{(\omega(T_f) - 2is\sin(t\omega(T_f)))\sin\left(\frac{t}{2}q(T_f)\right)}{q(T_f)} \end{pmatrix} \quad (6.23)$$

and the ground state

$$|0(t)\rangle = \mathcal{N} \begin{pmatrix} -\cot\left(\frac{t}{2}\omega(T_f)\right) \\ 1 \end{pmatrix}, \quad (6.24)$$

for a normalization constant $\mathcal{N} := |\langle 0(t) | 0(t) \rangle|^{-1}$. Fidelity during the transport is then¹

$$F = |\langle 0(t) | \psi(t) \rangle|^2, \quad (6.25)$$

An explicit formula for fidelity in time t and geodesic driving with final time T_f is then

$$F(t, T_f) = \frac{\pi^2 \left(\cos\left(t\sqrt{\frac{\pi^2}{T_f^2} + 4s^2}\right) + 1 \right) + 8s^2 T_f^2}{2 \sin^4\left(\frac{\pi t}{2T_f}\right) \left(4s^2 T_f^2 + \pi^2\right) \left(\left|\cot\left(\frac{\pi t}{2T_f}\right)\right|^2 + 1\right)^2}. \quad (6.26)$$

The domain can be extended to $t \in [0, T_f]$, $T_f \in [0, \infty]$ because

$$\lim_{t \rightarrow 0} F = 1, \quad \lim_{T_f \rightarrow 0} F = 0.$$

Sometimes the *Infidelity*, defined as $I := 1 - F$, will be used. Its meaning is the *probability of excitation of the state*.

6.1.2 Analysis of the infidelity formula

Fidelity for some fixed final time is just oscillating curve close to 1. For $T_f = 10$ it can be seen on Fig. 6.2. The *final fidelity* (at $t = T_f$) dependence on final time T_f can be seen on Fig. 6.3 and 6.4.

¹If we would calculate the fidelity in the **comoving frame**, we would get exactly one. This is the essence of counterdiabatic driving.

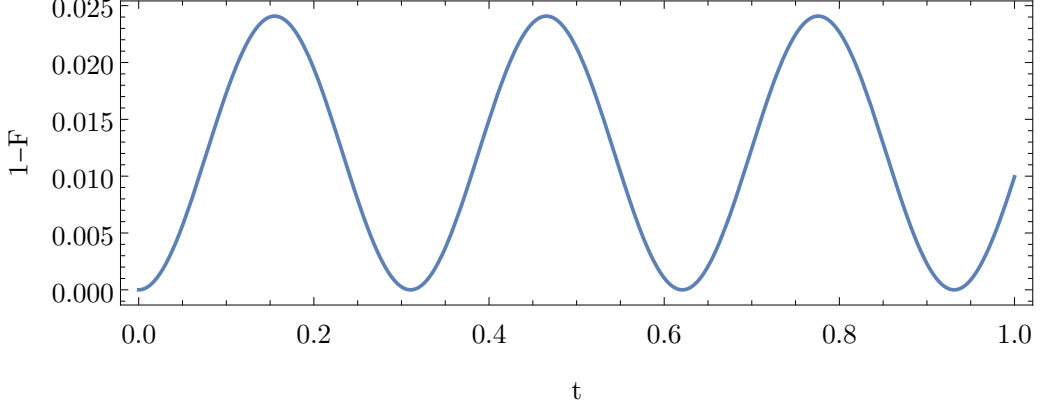


Figure 6.2: Infidelity in time for final time $T_f = 1$ for geodesical driving.

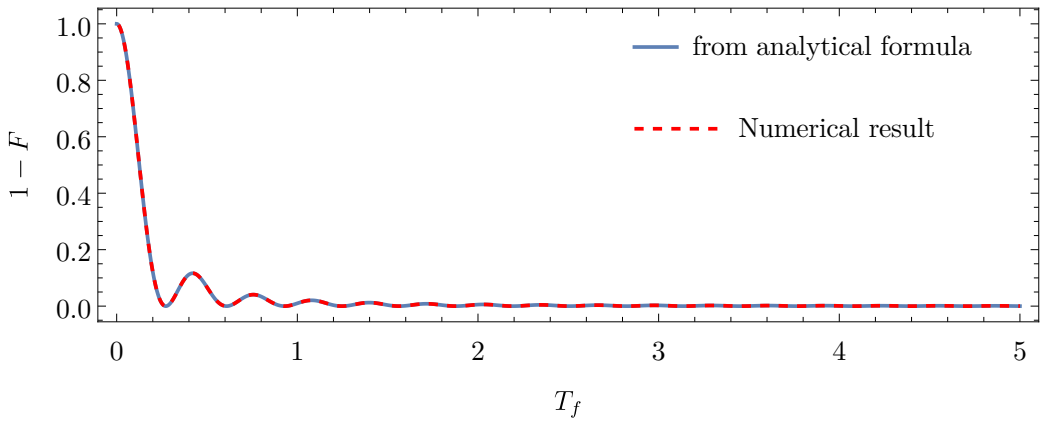


Figure 6.3: Final infidelity dependence on final time T_f for geodesical driving.

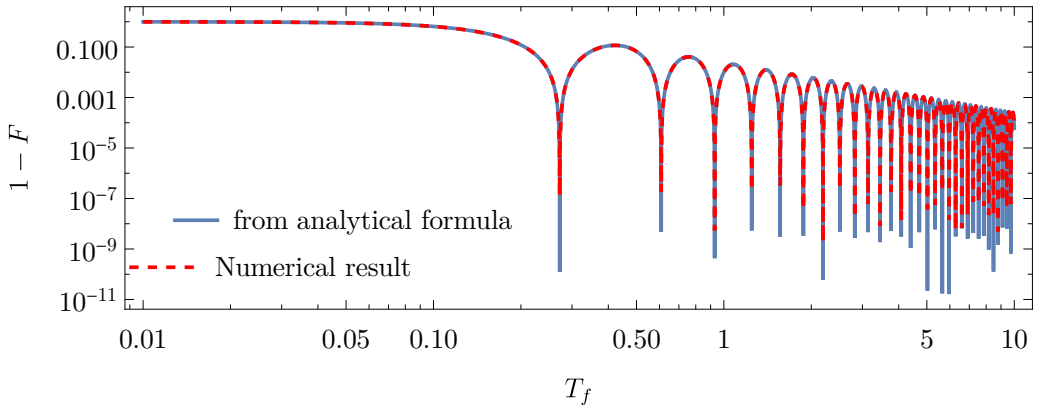


Figure 6.4: Infidelity dependence on final time in log-log scale. We can observe difference in numerical evaluation of different firmulas in the height of spikes.

From the fidelity Eq. 6.26 goes that $F = 1$ is equivalent to

$$\cos \left(\sqrt{T_s^2 + \pi^2} \right) = 1, \quad (6.27)$$

for $T_s := 2sT_f$. The solution to this equation is

$$T_s = \sqrt{(2\pi k)^2 - \pi^2} \text{ for } k \in \mathbb{N}. \quad (6.28)$$

This can be checked numerically, see Fig. 6.5. Because $F = 1$ has solutions 6.28, its dependence on final time in logarithmic scale has spikes going to 0, see Fig. 6.4, and their density is linear in T_f .

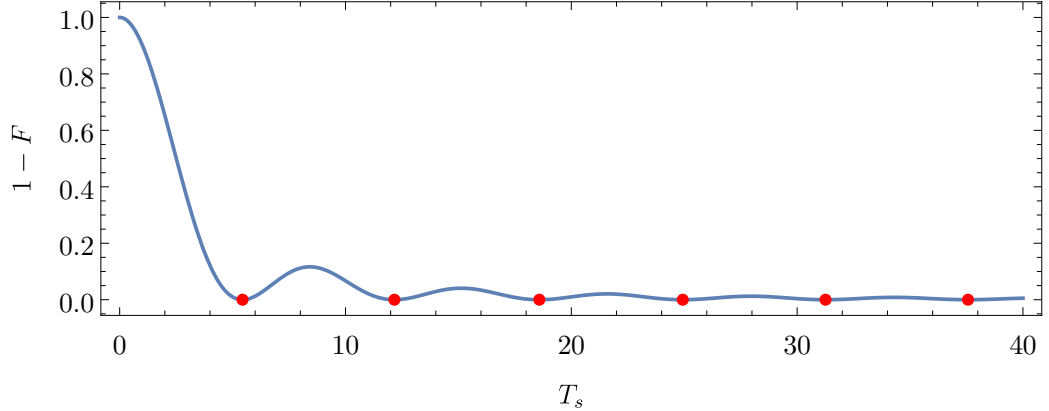


Figure 6.5: Rescaled final infidelity $T_s := 2sT_f$ dependence on final time. Red points are for $F = 1$.

Fidelity as a function of time and final time can be seen in Figures 6.6. Note that only $t < T_f$ has physical meaning.

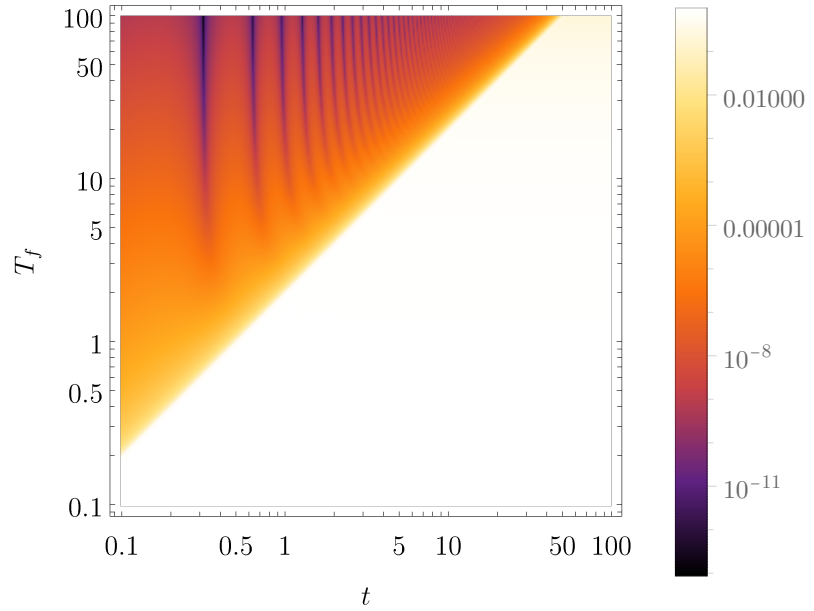


Figure 6.6: Fidelity dependence on time and final time in log log scale. Note that only $t < T_f$ has physical meaning.

6.1.3 Energy variance

Evaluating the fidelity for geodesical driving gives a function of time t and final time T_f

$$\begin{aligned} \delta E^2 = & \frac{s^2}{2q^2} \left[\left[16s^4 + 2s^2 \left((\omega^2 - 8s^2) \cos(2t\omega) - 8\omega^2 \cos^2(t\omega) \cos(t\sqrt{q}) \right) \right. \right. \\ & + 14s^2\omega^2 + \omega^4 \Big] - \omega^2 \left((2s^2 + \omega^2) \cos(2t\omega) - 2s^2 \right) \cos(2tq) \\ & \left. \left. + 8s^2\omega q \sin(2t\omega) \sin(tq) + \omega^3 q \sin(2t\omega) \sin(2tq) \right], \right] \end{aligned} \quad (6.29)$$

see the definition of q under Eq. 6.21. Its value as can be seen on Fig. 6.7. Note that only $t < T_f$ has a physical meaning, therefore the dependence is smooth along the whole geodesical driving protocols.

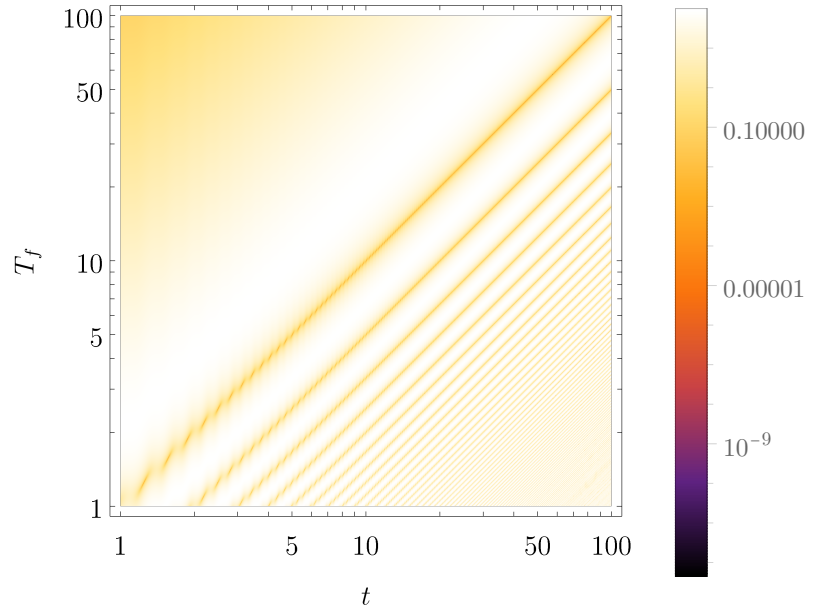


Figure 6.7: Energy variance for geodesical driving protocol.

6.2 Linear driving

Another analytically solvable driving is of type

$$\Omega(t) = \Omega_{sc} \left(\frac{2t}{T_f} - 1 \right), \quad \Delta(t) = \Delta_{sc}, \quad \text{for } \Omega_{sc} = 10, \Delta_{sc} = 1, \quad (6.30)$$

see Fig. 6.8.

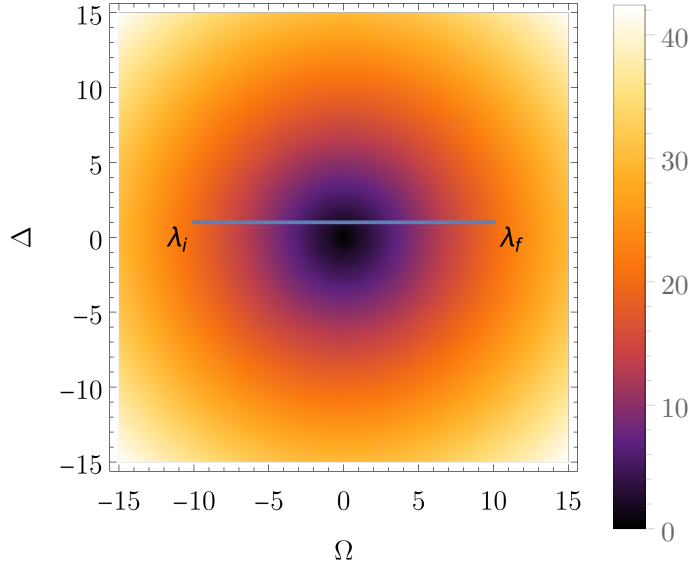


Figure 6.8: Driving along the linear path. $\lambda_i = (-10; 1)$ and $\lambda_f = (10; 1)$ are initial resp. final parameters. DensityPlot shows the difference between Hamiltonian eigenvalues.

From linear driving definition 6.30 and energy dependence 6.2 we have

$$\dot{\Delta}(t) = 0; \quad \Delta(t) \stackrel{\Delta(t) > 0}{=} \sqrt{\frac{E_{dif}^2(t)}{4} - \Omega^2(t)}; \quad E_{dif} := E_1 - E_0. \quad (6.31)$$

Substituting to functions from the Harmonic oscillator (Eq. 6.11, 6.12) we get

$$\gamma(t) = 0 \quad (6.32)$$

$$\omega^2(t) = i \frac{2\Omega_{sc}}{T_f} + \frac{\Omega_{sc}}{4} \left(\frac{2t}{T_f} - 1 \right)^2 + \frac{\Delta_{sc}^2}{4} = i \frac{2\Omega_{sc}}{T_f} + \frac{E_{dif}^2(t)}{4}. \quad (6.33)$$

Corresponding differential equation of second order is

$$a''(t) + \omega^2(t)a(t) = 0, \quad (6.34)$$

which is of Weber differential equation type² with Parabolic Cylinder functions³ as solution, see report from Felipe.

²<https://mathworld.wolfram.com/WeberDifferentialEquations.html>

³<https://mathworld.wolfram.com/ParabolicCylinderFunction.html>

6.2.1 Dependence on time

The fidelity in time can be seen on Fig. 6.9. For $t \approx T_f/2$ Hamiltonian parameters change quickly which leads to fast state excitation. Then the Harmonic oscillator damping gets involved and oscillations are quickly going to zero, never disappearing entirely.

We can see that the final fidelity decreases with longer final time, which correctly leads to adiabatic driving $\lim_{T_f \rightarrow \infty} F = 0$. For short final times we can observe so called quench, $\lim_{T_f \rightarrow 0} F = 1$. The interesting phenomenon on this image are the oscillations around $t = T_f/2$, which have higher relative amplitude to the final infidelity and bigger frequency with longer final time.

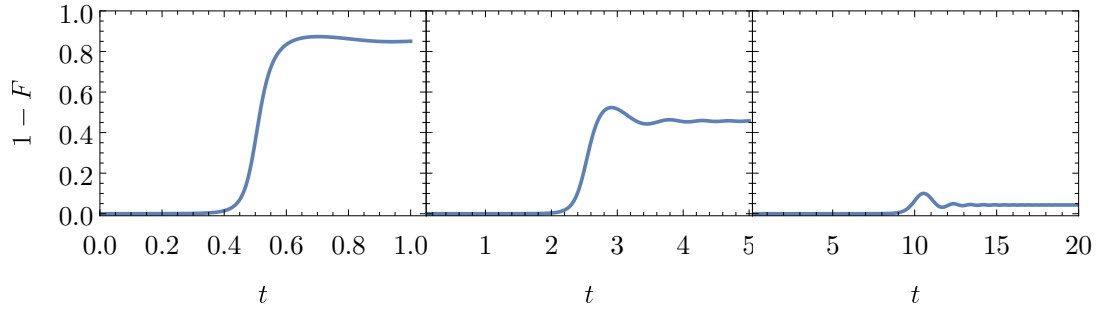


Figure 6.9: Infidelity in time for three final times $T_f \in \{1, 5, 20\}$ for the linear driving.

Because in the Harmonic oscillator $\gamma(t) = 0$, the oscillations of $a(t)$ are not damped. What we are observing is fidelity

$$F(t) := |\langle 0(t) | \psi(t) \rangle|^2 =: |\alpha(t)a(t) + \beta(t)b(t)|^2,$$

where the a, b represents the evolved state and α, β evolved ground state in the initial eigenbasis \mathcal{B} , see Eq. ???. The important notice is that the ground state is not generally constant. In our case is the ground state described by Eq. 6.4 and is slowly interchanging its value from the first to the second element of the vector $|0(t)\rangle$, see Fig. 6.10. This means that at the beginning of driving, the projection to the ground state selects $b(t)$. Then it's getting more influenced by $a(t)$ until almost only $a(t)$ influences the fidelity. **still dont see the damping here xd**

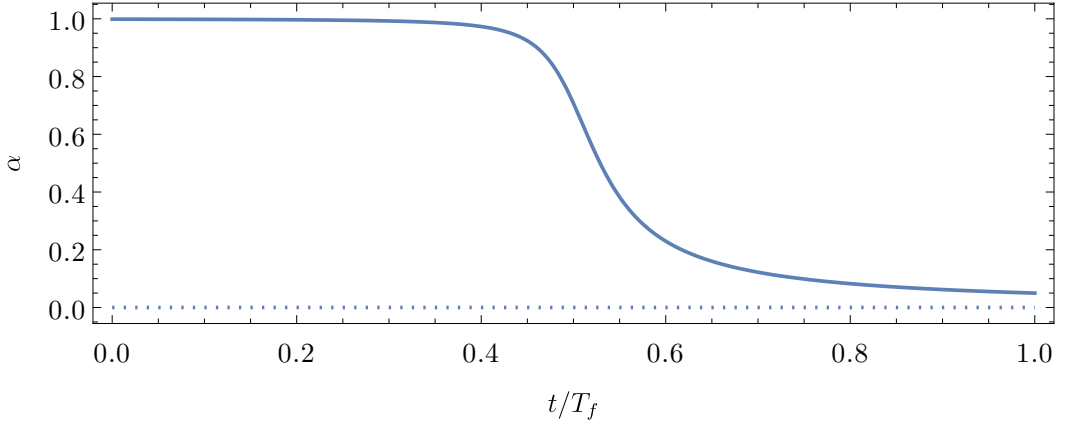


Figure 6.10: Value of first element of the ground state vector $\alpha \equiv |0(t)\rangle_1$ during linear driving.

Similarly, the oscillations cannot be analyzed only from $\omega^2(t)$ described by Eq. 6.33. General dependence of the frequency is not important for now and we will be interested only on the end of the driving. Let's assume⁴

$$\frac{1}{N_+} |0(t)\rangle_1 = \frac{E_0(t) + \Omega(t)}{\Delta(t)} \gg 1 = \frac{1}{N_+} |0(t)\rangle_2. \quad (6.35)$$

Writing $|\psi(t)\rangle =: (a(t), b(t))$, we get the fidelity approximation at the end of driving

$$F_{end} = \left| N_+ \left(\frac{E_0(t) + \Omega(t)}{\Delta(t)} a(t) + b(t) \right) \right|^2 \approx a^2(t). \quad (6.36)$$

Therefore when t is getting close to T_f the fidelity is oscillating with frequency 6.12.

6.2.2 Final fidelity

Because the oscillations after fast parameter change in the Hamiltonian never disappear entirely, we must observe those oscillations even at the final time. *Final fidelity* (meaning the fidelity at final time T_f) has dependence on T_f as can be seen in Fig. 6.11. Because after the final time $T_f^{\Delta_{sc}=1} \approx 120$ the values are so small, we can observe some fine structure of the fidelity, along with numerical error artifacts.

⁴Even though kets are vectors, we are forced to write indices down to avoid confusion with powers.

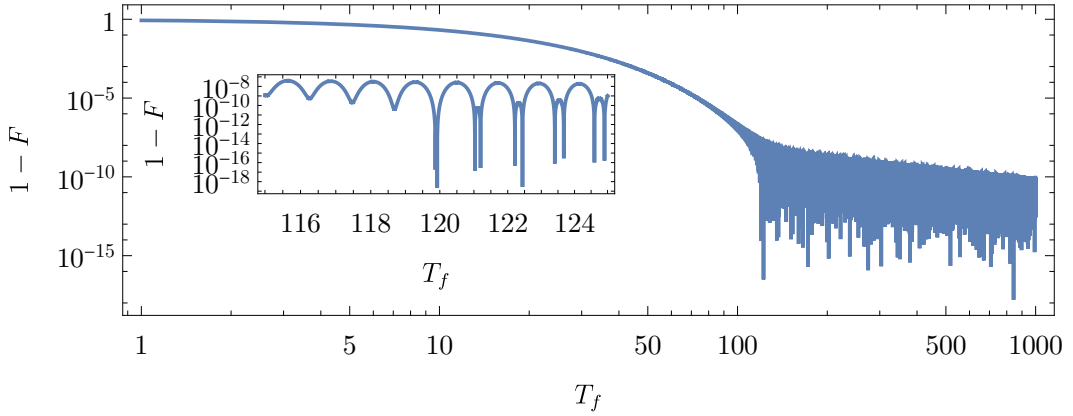


Figure 6.11: Final infidelity as a function of T_f with zoom on transitional part.

First of all, the numerical precision of this calculation was found to be around 10^{-14} . This means that the oscillations we see on Fig. 6.11 are of physical origin with some additional numerical error. In fact these small oscillations are the remnants of the fast excitation during close approach of energy levels, see Fig. 6.9.

Average final fidelity

We can eliminate the effect of oscillations by averaging over time. For that we define the *average final infidelity*

$$\langle 1 - F \rangle_p(T_f) := \frac{1}{(1-p)T_f} \int_{pT_f}^{T_f} F(t) dt. \quad (6.37)$$

It turned out that averaging over 1 % or 10 % of the driving (i.e. taking $\langle 1 - F \rangle_{0.9}$, resp $\langle 1 - F \rangle_{0.99}$) gave approximately the same results for long enough drivings. The same result can be obtained from calculating the fidelity for $T_f = \text{konst} < \infty$ at time $t \rightarrow \infty$. Even though this has no physical meaning, the analytical continuation of the harmonic oscillator solution leads to the Fidelity value around which the oscillations occur **here I have some numerical problems in mathematica, $t = 10T_f$ calculates OK, but going higher leads to error**. The result can be seen on Fig. 6.12.

Using this we can describe the driving using three regimes⁵:

- *exponential/fast-driving regime* – $\langle 1 - F \rangle_p = \exp(-\xi T_f)$, $\xi \in \mathbb{R}^+$
- *transitional regime* – happens around *critical time* T_c . **smoothening is not enough to remove the oscillations**
- *polynomial/close-adiabatic regime* – $\langle 1 - F \rangle_p \propto T_f^{-\kappa}$ for $\kappa \in \mathbb{R}^+$.

⁵The coefficient p is assumed to be small enough not to cover the biggest oscillations after $t = T_f/2$ and big enough to average over sufficient number of oscillations. $p \in [0.6T_f, 0.999T_f]$

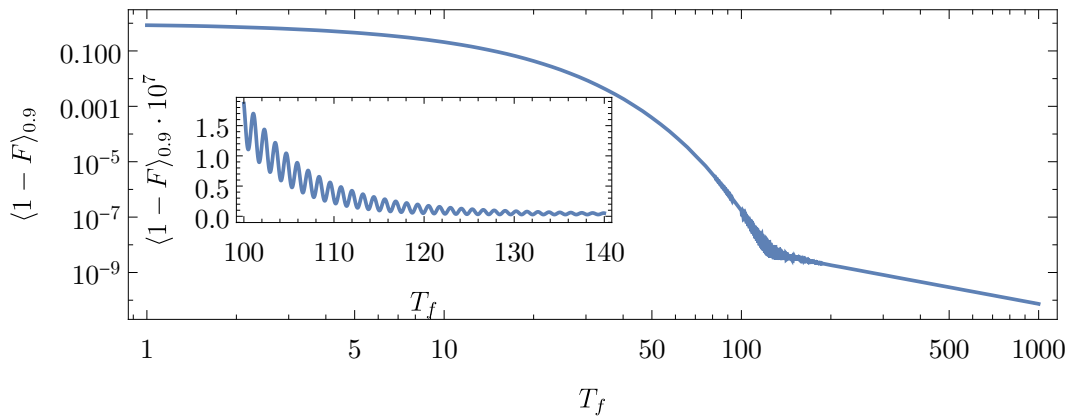


Figure 6.12: Final infidelity as a function of T_f in log log scale with linear scaled plot inserted.

The reason for different behavior in slow and fast driving protocols comes from the fact that oscillations do not disappear entirely for $t = T_f$. By comparing the infidelity for t close to T_f , Fig. 6.13, 6.14, we see that for $T_f < T_c$ the oscillations are smaller than the final infidelity and $1 - F \neq 0$. For $T_f > T_c$ the oscillations amplitude is bigger than final infidelity. **at least numerical proof would be nice here**

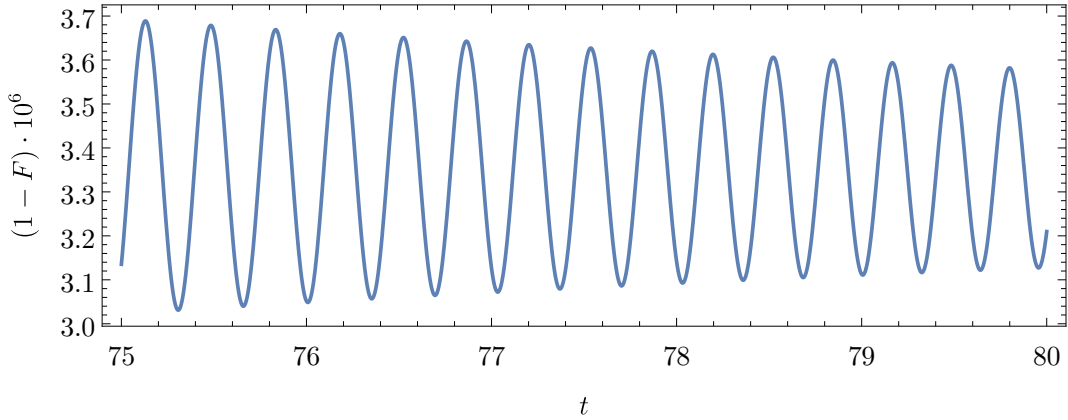


Figure 6.13: Final infidelity as a function of t for fast-driving regime, $T_f = 80 < T_c$.

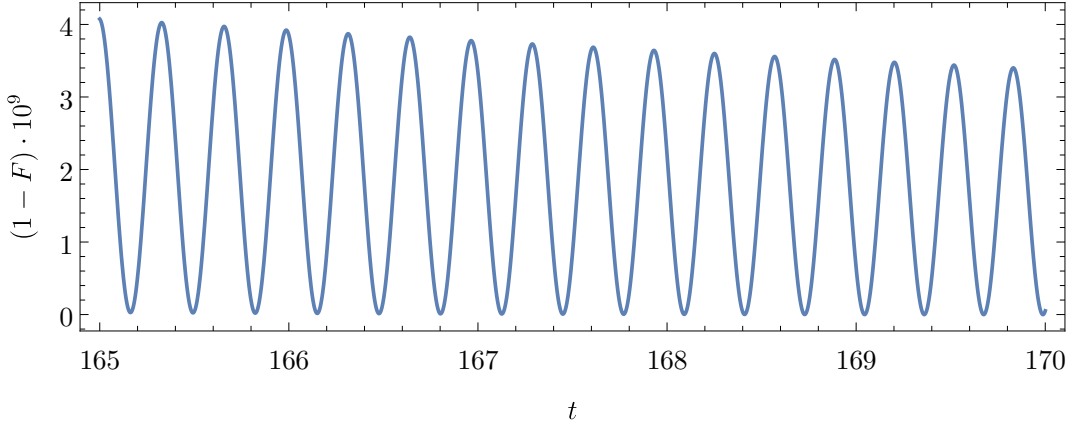


Figure 6.14: Final infidelity as a function of t for close-adiabatic regime. $T_f = 170 > T_c$

Two questions now arise. What are the coefficients ξ and κ and on which intervals in T_f these transitions hold?

6.2.3 Critical time T_c

The critical time T_c is the point where the fidelity dependence on final time becomes polynomial. We have showed that for

$$\text{for } \begin{cases} T_f < T_c \\ T_f > T_c \end{cases} \quad \text{the oscillations amplitude } A \text{ is } \begin{cases} A < 1 - F_{final} \\ A > 1 - F_{final} \end{cases}. \quad (6.38)$$

On Fig. 6.15 we can see the dependence of critical time as the point of transition between *smooth* and *chaotic* regimes, on $\Delta = \Delta_s c$ for the linear driving. The fine structure, see Fig. 6.16, is caused by the oscillatory character of the final fidelity. The approximated dependence is

$$T_c \propto \Delta_{sc}^{-2} \quad (6.39)$$

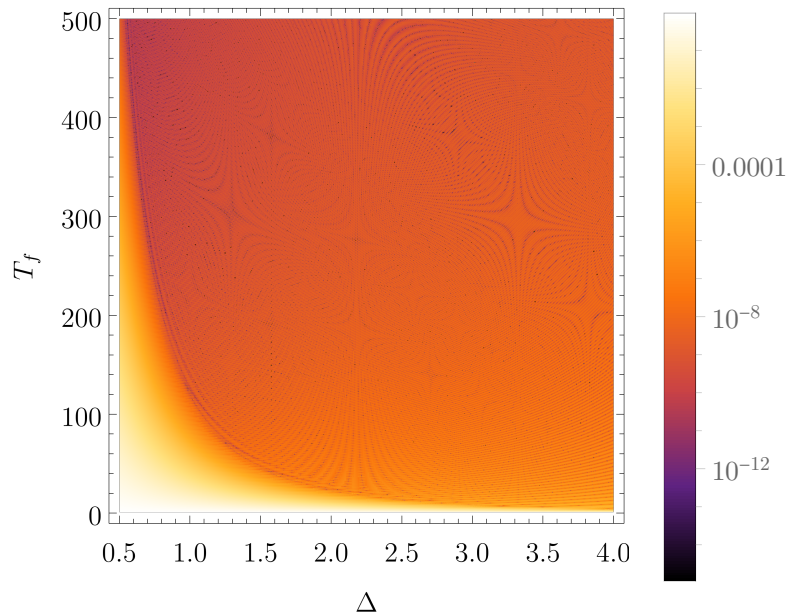


Figure 6.15: Final infidelity as a function of Δ and T_f and its three regimes. Zoomed boundary between them can be seen on 6.16.

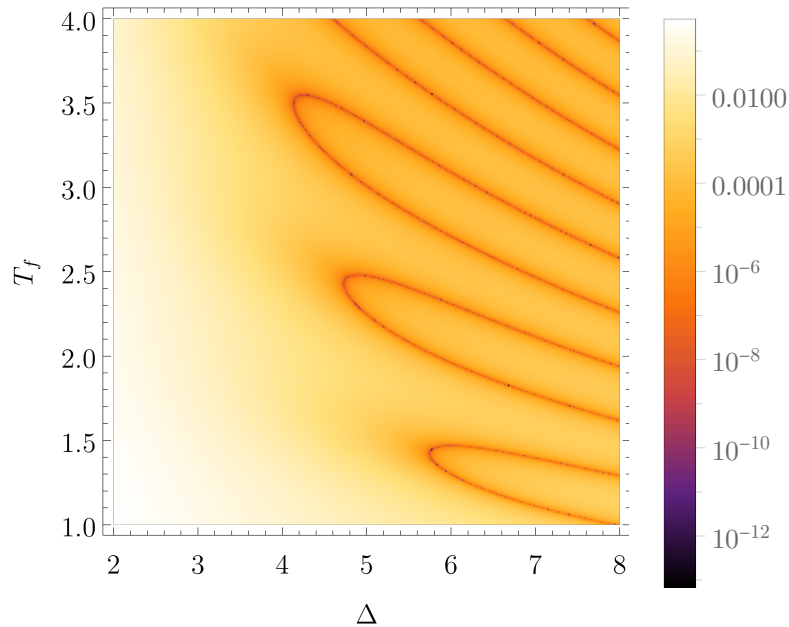


Figure 6.16: Fine structure of the boundary between fast-driving and adiabatic regimes of final infidelity.

6.2.4 Coefficients ξ and κ

TODO

6.2.5 Summary

Now we should understand all results separately, lets put it all together.

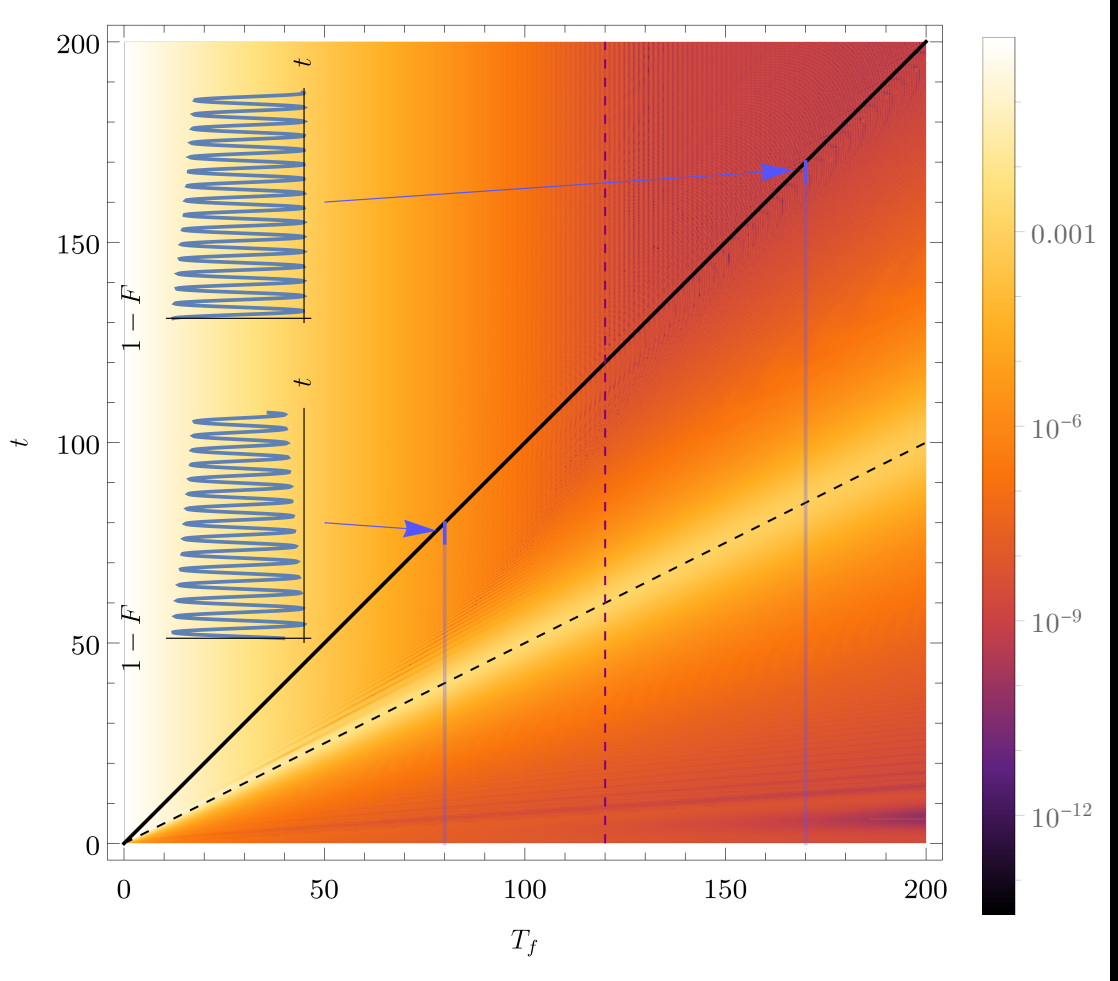


Figure 6.17: Fidelity dependence for linear driving with $\Delta = 1$. Black line marks $t = T_f$, dashed black line $t = T_f/2$ and purple dashed line is the approximate value of T_c . Blue lines marks driving from Fig. 6.13, 6.14, visualizing the final times of the driving.

6.2.6 Energy variance

Energy variance resembles structure similar to fidelity. Compare Fig. 6.18 with 6.6.

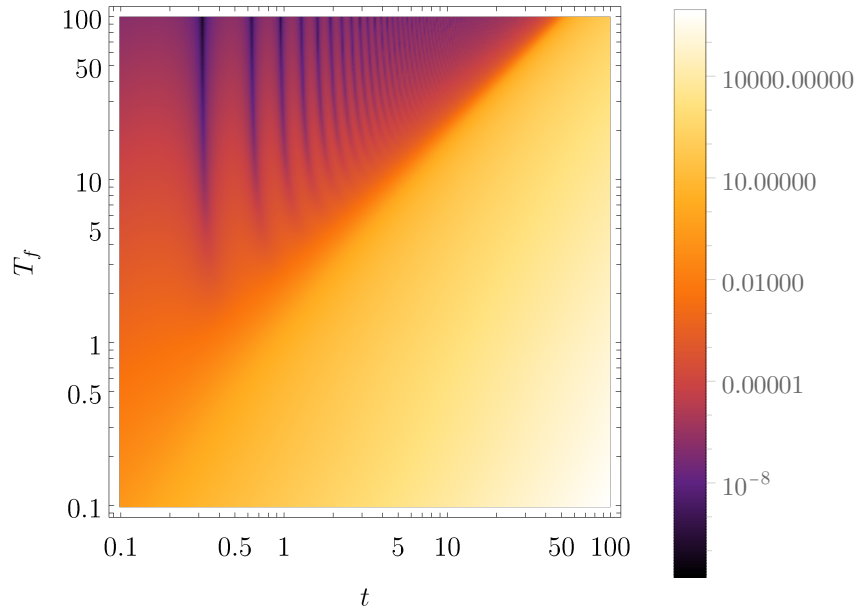


Figure 6.18: Energy variance for $\Delta_{sc} = 0.2$ for linear driving. Note that only $t < T_f$ has physical meaning.

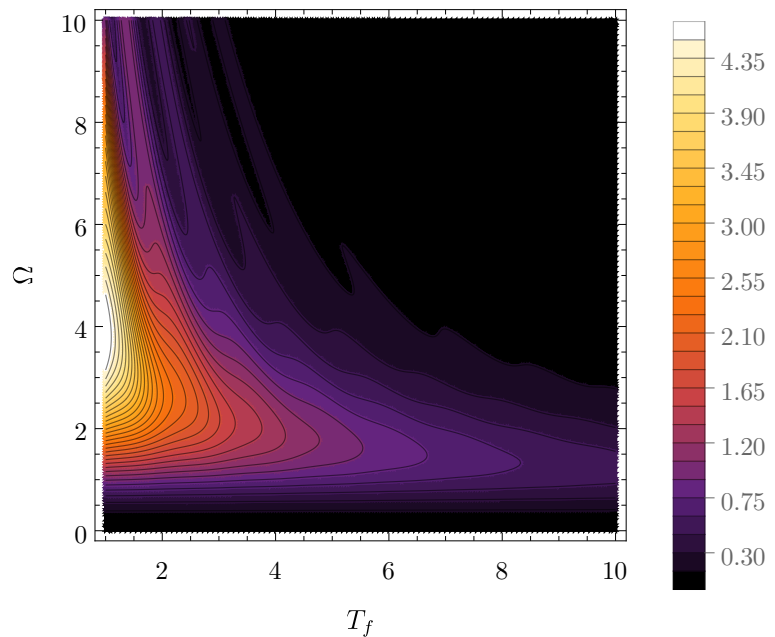


Figure 6.19: Energy variance for $t = T_f/2$ for linear driving.

6.3 Energy variance for two level system

For two level system, the variance

$$\delta E^2(t) := \langle \psi(t) | \hat{H}^2 | \psi(t) \rangle - \langle \psi(t) | \hat{H} | \psi(t) \rangle^2 \quad (6.40)$$

can be rewritten inserting identity $\mathbb{1} = |0\rangle\langle 0| + |1\rangle\langle 1|$ around Hamiltonian. Omitting the time dependence of every element we get

$$\begin{aligned} \delta E^2 &= \langle \psi | \mathbb{1} \hat{H}^2 \mathbb{1} | \psi \rangle - \langle \psi | \mathbb{1} \hat{H} \mathbb{1} | \psi \rangle^2 \\ &= \langle \psi | 0 \rangle \langle 0 | \hat{H}^2 | 0 \rangle \langle 0 | \psi \rangle + \langle \psi | 1 \rangle \langle 1 | \hat{H}^2 | 1 \rangle \langle 1 | \psi \rangle \\ &\quad + \langle \psi | 0 \rangle \langle 0 | \hat{H}^2 | 1 \rangle \langle 1 | \psi \rangle + \langle \psi | 1 \rangle \langle 1 | \hat{H}^2 | 0 \rangle \langle 0 | \psi \rangle \\ &\quad - \left(\langle \psi | 0 \rangle \langle 0 | \hat{H} | 0 \rangle \langle 0 | \psi \rangle + \langle \psi | 1 \rangle \langle 1 | \hat{H} | 1 \rangle \langle 1 | \psi \rangle \right. \\ &\quad \left. + \langle \psi | 0 \rangle \underbrace{\langle 0 | \hat{H} | 1 \rangle}_{\propto \langle 0 | 1 \rangle = 0} \langle 1 | \psi \rangle + \langle \psi | 1 \rangle \underbrace{\langle 1 | \hat{H} | 0 \rangle}_{\propto \langle 0 | 1 \rangle = 0} \langle 0 | \psi \rangle \right)^2. \end{aligned} \quad (6.41)$$

Using Fidelity definition $F(t) = |\langle 0(t) | \psi(t) \rangle|^2$ and Schrödinger equation $\hat{H} |k\rangle = E_k |k\rangle$ we have

$$\delta E^2 = F E_0^2 + (1 - F) E_1^2 - (F E_0 + (1 - F) E_1)^2 = F(1 - F)(E_0 - E_1)^2. \quad (6.42)$$

For three level system we have $\mathbb{1} = |0\rangle\langle 0| + |1\rangle\langle 1| + |2\rangle\langle 2|$ and

$$\delta E^2 = \sum_{k=1}^3 E_k^2 F_k (1 - F_k) - 4 \prod_{k=1}^3 E_k F_k - 2 F_0 F_1 E_0 E_1 - 2 F_0 F_2 E_0 E_2 - 2 F_1 F_2 E_1 E_2, \quad (6.43)$$

for $F_k := \langle k | \psi \rangle$, which has no practical simplification.

7. From the projective Hilbert space to state manifolds

7.1 Projective Hilbert space

Consider the Hilbert space \mathcal{H} to be a space of *bare states* and \mathcal{S} to be the space of *normalized bare states*. Physical observables are related to the *space of rays*, defined as $\mathcal{PH} := \mathcal{H}/U(1)$, for the factorization by elements of $U(1)$. This group consists of unitary transformations $e^{i\phi}$ for $\phi \in \mathbb{R}$, defining gauge symmetry between quantum states. \mathcal{PH} is then considered to be the *space of pure states*. For the sake of generality, let's not normalize our vectors yet, which would lead to the *space of unnormalized pure physical states*.

It can be shown, that \mathcal{PH} is of a Kähler structure, meaning it has two non-degenerate sesquilinear¹ 2-forms embedded along with operator complex unit

$$(J, G, \Omega),$$

such that

$$J^2 = \mathbb{1} \quad (7.1)$$

and any bracket of $|\psi_1\rangle, |\psi_2\rangle \in \mathcal{PH}$ can be decomposed into real and imaginary part[?]

$$\langle \psi_1 | \psi_2 \rangle = \frac{1}{2} G(\psi_1, \psi_2) - \frac{i}{2} \Omega(\psi_1, \psi_2). \quad (7.2)$$

From bracket sesquilinearity goes that G is symmetric and Ω antisymmetric form, thus they can be uniquely written into one 2-form called *Fubini-Study metric* with property

$$G = \text{Re}Q; \quad \Omega = \text{Im}Q. \quad (7.3)$$

Because $\langle \psi_1 | \psi_2 \rangle \in [0, 1]$ we say, that the metric is measuring the geodesic distance on the Bloch sphere. Here if we define

$$| \langle \psi_1 | \psi_2 \rangle | = \cos^2 \frac{\theta}{2}, \quad (7.4)$$

we get $d\theta = 2ds = 2\sqrt{|g_{\mu\nu} d\lambda^\mu d\lambda^\nu|}$, see ?.

To write the metric in a standard form, we need to realize how our space looks like. For finite $n+1$ -dimensional Hilbert space, one dimension is lost in the gauge transformation, leaving us with n -dimensional \mathcal{PH} . Another dimension is lost due to normalization, which is usually done by mapping to an n -dimensional complex sphere

$$CP^n = \left\{ \mathbb{Z} = (Z_0, Z_1, \dots, Z_n) \in \mathbb{C}^{n+1}/\{0\} \right\} / \{ \mathbb{Z} \sim c\mathbb{Z} \text{ for } c \in \mathbb{C} \}.$$

Natural property of such complex spaces is splitting of its tangent space to holonomic and anholonomic part²

$$T^{1,0}\mathcal{M} = \text{Span} \left\{ \frac{\partial}{\partial Z_i} \right\}; \quad T^{0,1}\mathcal{M} = \text{Span} \left\{ \frac{\partial}{\partial \bar{Z}_i} \right\}.$$

¹We are in physics, so complex conjugated is the first input of the 2-form.

² $T^{p,q}\mathcal{M}$ means $p+q$ - cotravariant space (the space of vectors) on \mathcal{M} . The line over letter means complex conjugation.

Distance on \mathbb{C}^{n+1} is standardly defined using Hermitean metric³

$$ds^2 = d\bar{Z} \otimes dZ. \quad (7.5)$$

For *normalized states* in quantum mechanics is $dZ = ??????$, which plugged into Eq. 7.5 yields

$$ds^2 = 1 - |\langle \psi + \delta\psi | \psi \rangle|^2. \quad (7.6)$$

7.2 Restriction to eigenstate manifolds

In quantum mechanics, one can examine a Hamiltonian $\hat{H}(\lambda)$, for some parameter $\lambda \in \mathbb{R}^n$. At every point λ we get projective Hilbert space $\mathcal{PH}(\lambda)$. This creates a fibre structure space, in which there are some section with interesting physical applications. Some of those sections are *eigenstate manifolds*, defined by setting only one non-zero coefficient Z_k in eigenbasis $|\psi\rangle = \sum_{k=0}^n Z_k |k\rangle$. From normalization goes automatically $Z_k = 1$. The distance is then

$$\begin{aligned} ds^2 &= 1 - \langle k + \delta k | k \rangle \langle k | k + \delta k \rangle = 1 - \langle k + \delta k | \left(1 - \sum_{j \neq k} |j\rangle \langle j| \right) |k + \delta k \rangle \\ &= \sum_{j \neq k} \langle k + \delta k | j \rangle \langle j | k + \delta k \rangle. \end{aligned} \quad (7.7)$$

Using the Schrödinger equation $\hat{H}|k\rangle = E_k|k\rangle$, distributivity of derivative and projection to some state $\langle j|$, we get

$$\begin{aligned} \hat{H}|k\rangle &= E_k|k\rangle \\ (\delta\hat{H})|k\rangle + \hat{H}|k + \delta k\rangle &= (\delta E_k)|k\rangle + E_k|k + \delta k\rangle \\ \langle j|(\delta\hat{H} - \delta E_k)|k\rangle &= \langle j|(\hat{H} - E_k)|k + \delta k\rangle = \langle j|(\hat{H} - E_j)|k + \delta k\rangle. \end{aligned} \quad (7.8)$$

We can set⁴ $\delta E_k = 0$, leading for $j \neq k$ to

$$\frac{\langle j | \delta\hat{H} | k \rangle}{(E_k - E_j)^2} = \langle j | k + \delta k \rangle. \quad (7.9)$$

Plugging to Equation 7.7 and considering $\hat{H} = \hat{H}(\lambda)$, we get metric on a ground state manifold

$$ds^2 = \text{Re} \sum_{j \neq k} \frac{\langle 0 | \partial_\mu \hat{H} | j \rangle \langle j | \partial_\nu \hat{H} | 0 \rangle}{(E_k - E_j)^2} d\lambda^\mu d\lambda^\nu \quad (7.10)$$

Definition of the k -state manifold is then

$$g_{\mu\nu}^{(k)} = \text{Re} \sum_{j \neq k} \frac{\langle k | \frac{\partial \hat{H}(\lambda)}{\partial \lambda^\mu} | j \rangle \langle j | \frac{\partial \hat{H}(\lambda)}{\partial \lambda^\nu} | k \rangle}{(E_k - E_j)^2}. \quad (7.11)$$

The Fubini-Study metric on the eigenstate manifold is sometimes called *Geometric tensor*. For the Lipkin-Meshkov Glick model, those can be seen on Fig. 7.2.

³which is by definition sesquilinear, as one would expect in quantum mechanics later on

⁴Can it be done only for E_0 ? It does not make sense generally, because $E = E(\lambda)$, even $E_0 = E_0(\lambda)$

If we compare first eigenstate manifold \mathcal{M}_1 with difference in infidelity transport done along ground state geodesic and along straight line, we can see they have one similarity. The higher curvature of \mathcal{M}_1 degrades geodesic even faster, making the straight line more advantageous. This is caused by the wavefunction running out from \mathcal{M}_0 to \mathcal{M}_1

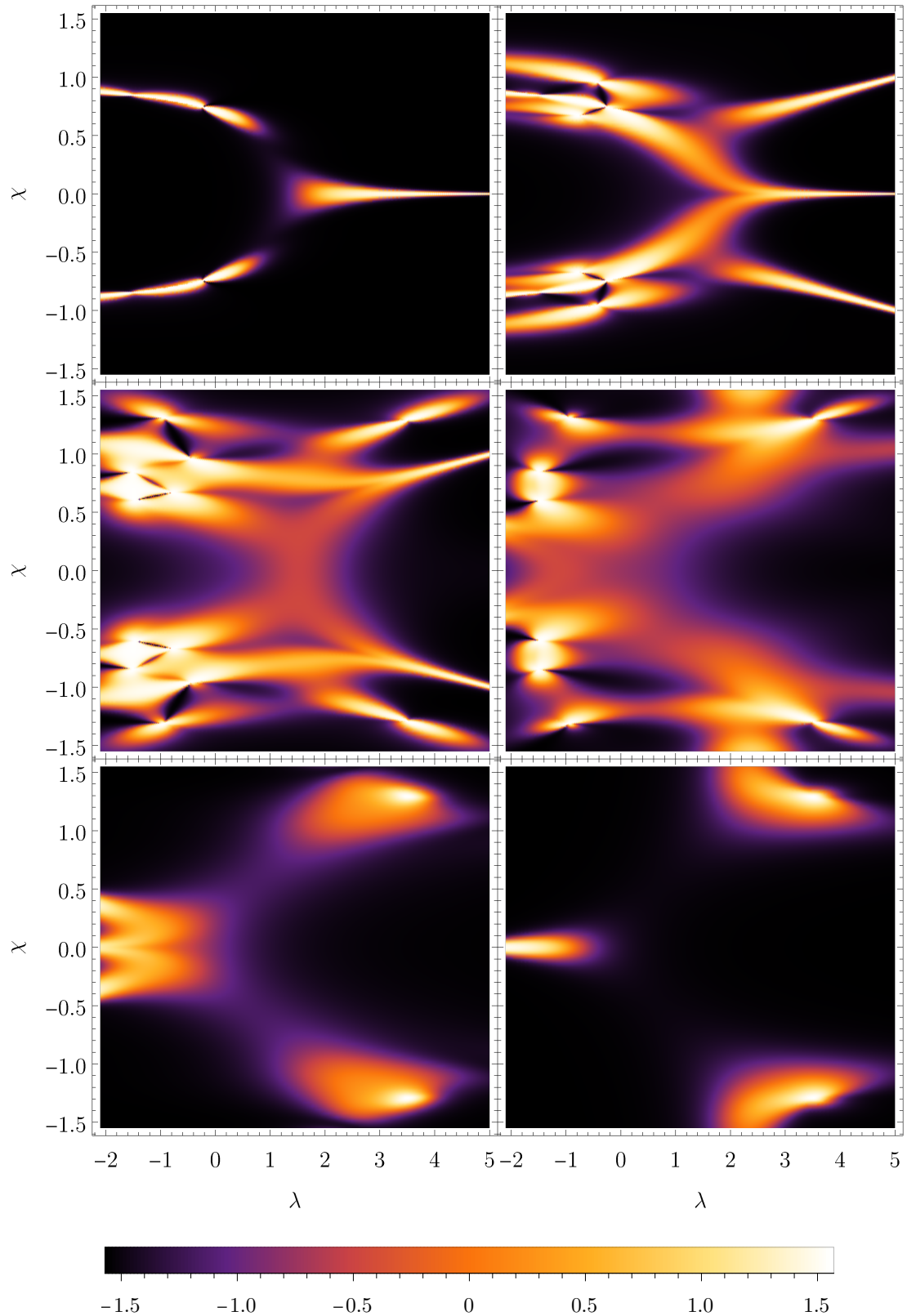


Figure 7.1: Arctangens of the metric tensor for higher state manifolds. By rows: $M_0, M_1; M_2, M_3; M_4, M_5$.

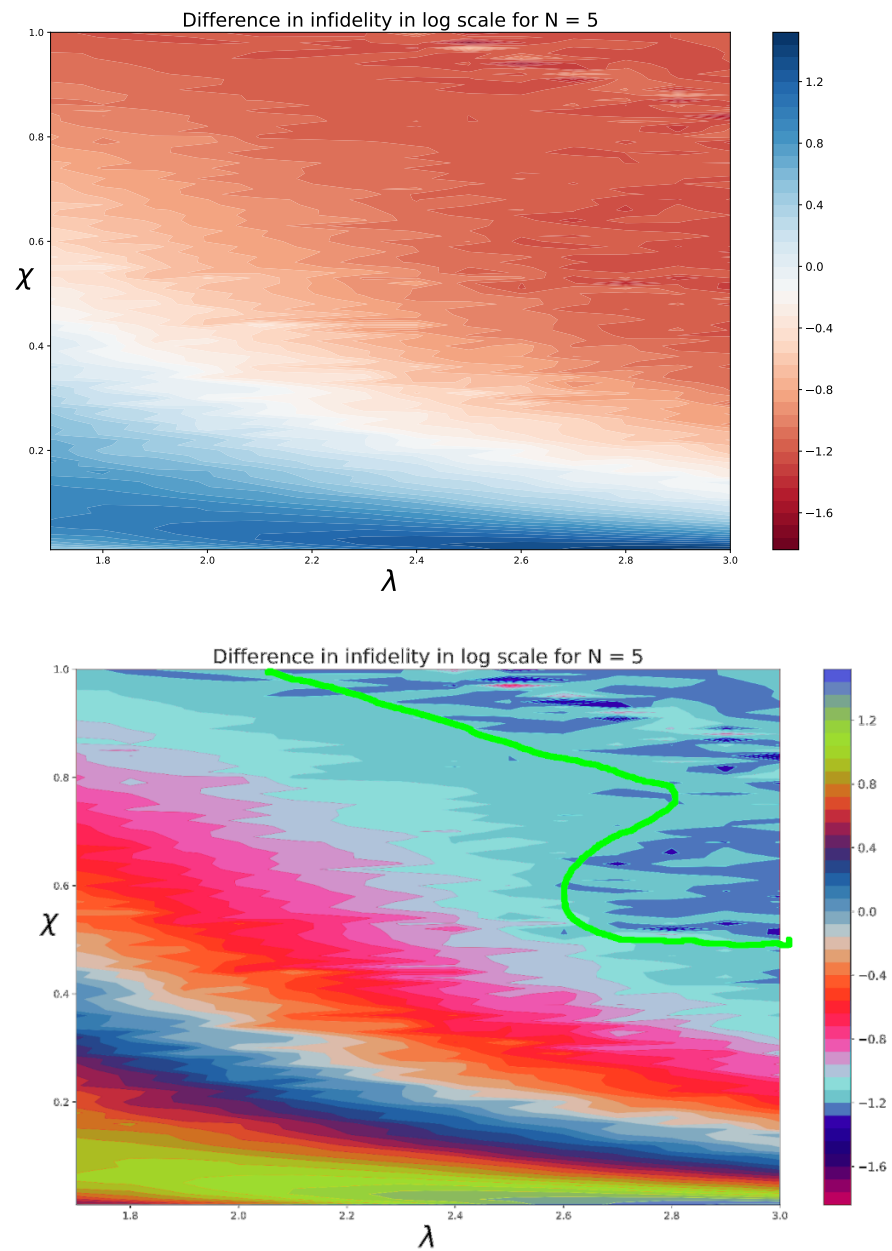


Figure 7.2: Infidelity difference between line and geodesic, above picture is original from Felipe, bottom one is edited in GIMP to see the difference more clearly.

8. The meaning of geodesics

8.1 Transport using quenches

Unifying the ground states $|o(\boldsymbol{\lambda})\rangle$ over all points $\boldsymbol{\lambda} \in \mathbb{R}^n$ in the parameter space, we get the ground state manifold. Here the fidelity f and distance s are defined

$$ds^2 \equiv 1 - f^2 \equiv 1 - |\langle o(\boldsymbol{\lambda} + \delta\boldsymbol{\lambda})|o(\boldsymbol{\lambda})\rangle|^2. \quad (8.1)$$

The final fidelity of transport on \mathcal{M} is then

$$F = \iint g_{\mu\nu} d\lambda^\mu d\lambda^\nu = \int_{t_i}^{t_f} \underbrace{\int_{t_i}^\tau g_{\mu\nu} \frac{d\lambda^\mu}{dt} \frac{d\lambda^\nu}{dt} dt d\tau}_{\mathcal{L}(\lambda^\mu, \dot{\lambda}^\mu, \tau)}. \quad (8.2)$$

Using Euler-Lagrange equations for time-independent $g_{\mu\nu} = g_{\mu\nu}(\lambda^\mu)$, leads to

$$\int_{t_i}^\tau \left[g_{\mu\nu,\kappa} \dot{\lambda}^\mu \dot{\lambda}^\nu - \frac{d}{dt} \left[g_{\mu\nu} (\delta_\kappa^\mu \dot{\lambda}^\nu + \dot{\lambda}^\mu \delta_\kappa^\nu) \right] \right] dt = 0, \quad (8.3)$$

which needs to be zero for integration over any subset (t_i, τ) . This can be achieved for any path only if the integrand itself is zero, which happens if the geodesic equation holds.

The fidelity f measures transition probability between two neighboring eigenstates of two different Hamiltonians. Those two states belong to the same Fibre space $\mathcal{PH}(\boldsymbol{\lambda}) \times \mathbb{R}^n$ from which the coefficients $(\mathbb{Z}, \boldsymbol{\lambda})$ are taken. Because all $\mathcal{PH}(\boldsymbol{\lambda})$ are canonically isomorphic, there is no problem in parallel transport from one space to another, which is needed for bracket¹.

The distance minimization runs into some interpretation problems. On one hand, minimalization of the distance is equivalent to maximalization of the sum of infinitesimal fidelities along the path (we say we *maximize the fidelity along the path*). On the other hand we are using only ground states in every step of the transport, therefore defining the fidelity to be one. There are actually two ways out of this confusion. *Perturbed adiabatic driving* and *Transport using quenches*.

Perturbed adiabatic driving

In the first case, we imagine at every point of transport, that the fidelity is small enough, such that in eigenbasis and some small parameters $\delta_i \in \mathbb{C}$ we get

$$|o(\boldsymbol{\lambda}_i)\rangle \equiv \begin{pmatrix} Z_0(\boldsymbol{\lambda}_i) \\ 0 \\ \vdots \\ 0 \end{pmatrix} \xrightarrow{\text{transport } ds} |o(\boldsymbol{\lambda}_i + \delta\boldsymbol{\lambda})\rangle \equiv \begin{pmatrix} Z_0(\boldsymbol{\lambda}_i + \delta\boldsymbol{\lambda}) \\ 0 \\ \vdots \\ 0 \end{pmatrix} + \underbrace{\begin{pmatrix} 0 \\ \delta_1(\boldsymbol{\lambda}_i + \delta\boldsymbol{\lambda}) \\ \vdots \\ \delta_n(\boldsymbol{\lambda}_i + \delta\boldsymbol{\lambda}) \end{pmatrix}}_{\Delta(\boldsymbol{\lambda}_i + \delta\boldsymbol{\lambda})},$$

¹This procedure is done without thinking in the back part of our brains such, that we don't even think about it. That's how trivial it is.

where the last term is neglected using

$$\langle \Delta(\lambda) | o(\lambda + \delta\lambda) \rangle \approx 0.$$

This might have interesting implication for slow transports, or small distance transports. For example when some slow thermalization is considered during a transport.

Transport using quenches

If we imagine $\delta\lambda$ to be finite (not infinitely small, as the notation suggests), the **transport** means **doing a sequence of quenches and measuring the system after every quench**.

Some notion of the space of our Hamiltonian can be seen by quenching from $(\lambda_i; \chi_i) = (0; 0)$ to $(\lambda; \chi)$, as can be seen in Figure 8.1.

In Figure 8.2 are marked equidistant points, meaning $\int_a^b ds = \text{const.}$ between every two neighboring points on curve. This means that if the system is measured periodically, the quenches jump smaller distances when closer to a singularity.

Decreasing time step Δt has no effect on the relative fidelity of quenches during the evolution but has an effect on their magnitude. As one would expect from *quantum Zeno effect*, when $\Delta t \rightarrow 0$, the transport becomes adiabatic, and the fidelity at any time will become 1. This can be observed in Figure 8.3, such that the shape of the point-like paths looks similar in the columns, and their magnitude decreases.

The quantum Zeno effect for this case can be shown directly by splitting the distance s to N equal pieces. The fidelity for N splits will then be

$$f(N) = (1 - \Delta s)^N = \left(1 - \left(\frac{s}{N}\right)^2\right)^N \xrightarrow{N \rightarrow \infty} 1, \quad (8.4)$$

meaning the consequent measurements will collapse the system to its instantenous eigenstate and the adiabatic condition for transport holds.

Such measurements can be achieved by fast thermalization of the system. If the finite speed thermalization with $N = T/\tau$ for the mean time between two measurements τ , we get

$$\begin{aligned} \log f(N) &= N \log \left(1 - \left(\frac{s}{N}\right)^2\right) = -\frac{s^2}{N} + o\left(\frac{s^4}{N^3}\right) \\ f(N) &= \exp\left(-s^2 \frac{\tau}{T} - \frac{s^4}{2N^3} \dots\right) = \exp\left(-s^2 \frac{\tau}{T}\right) \left(1 + o\left(\frac{s^4}{N^3}\right)\right) \end{aligned} \quad (8.5)$$

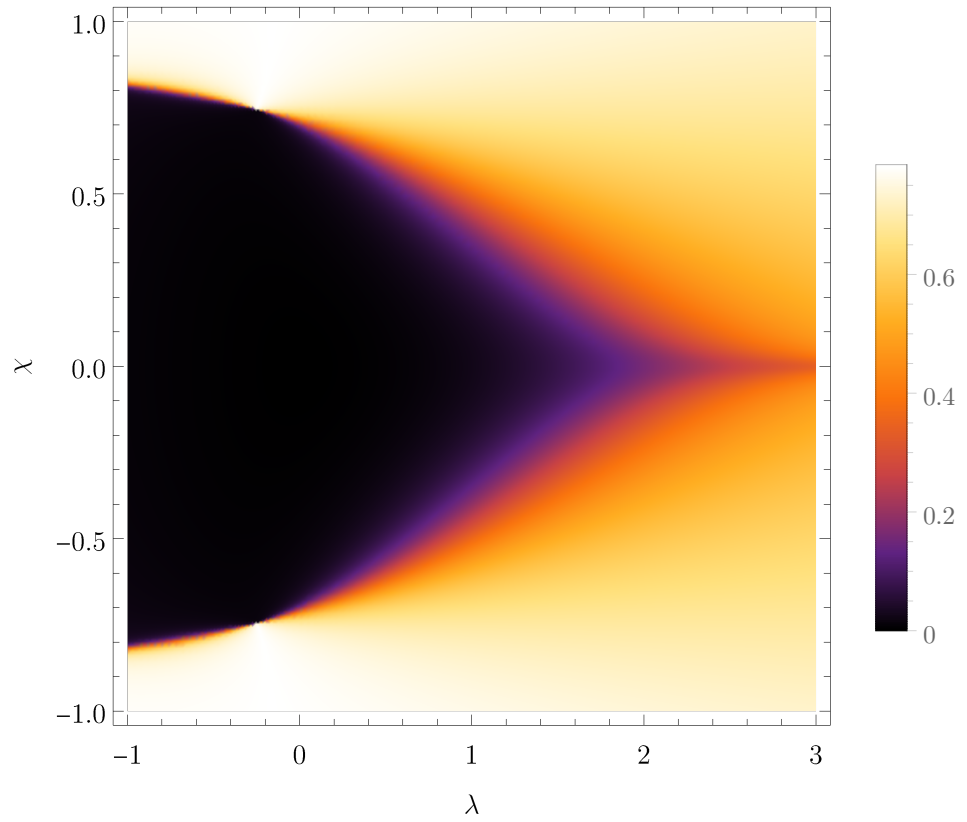


Figure 8.1: Arctangens of the fidelity of quenches from $(\lambda_i; \chi_i) = (0; 0)$ to $(\lambda; \chi)$.

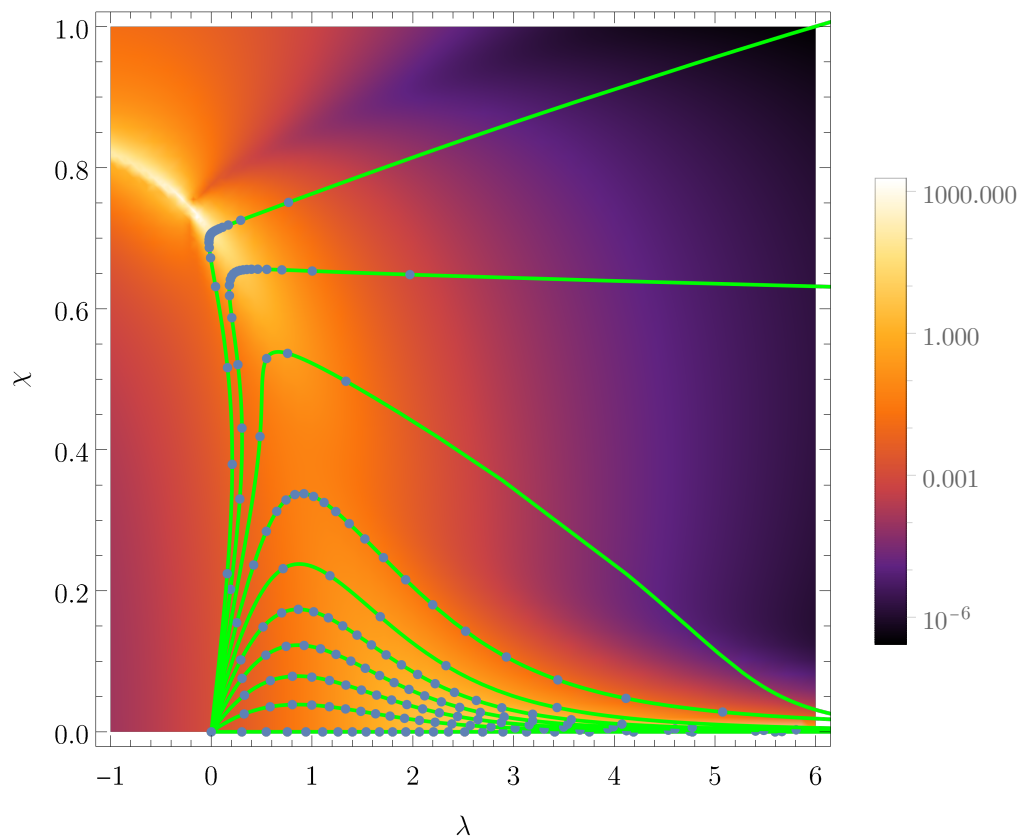
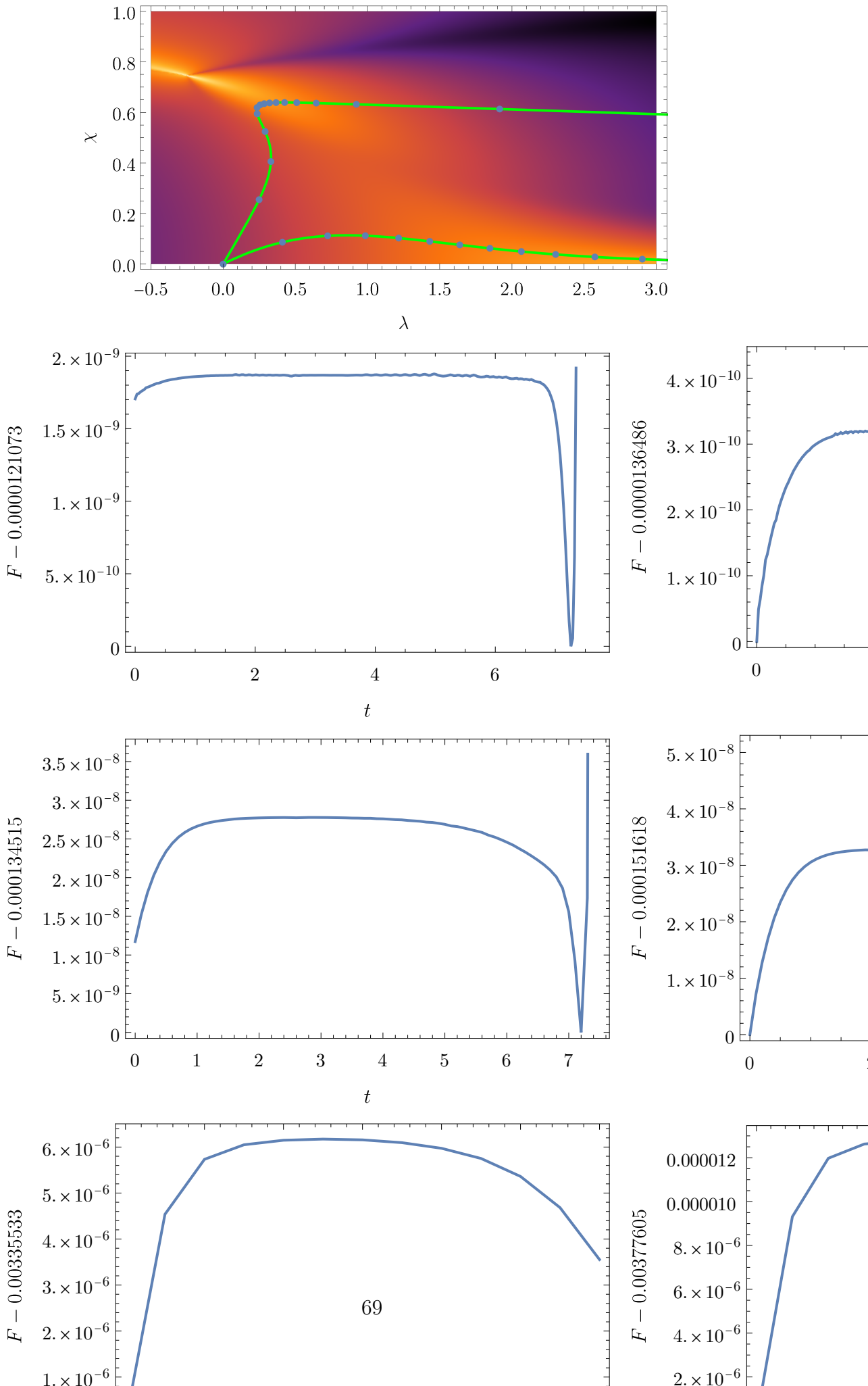


Figure 8.2: Equidistant points on geodesics of the ground state manifold.



9. The role of geodesics

9.1 Minimizing the energy variance

From ?. About transports using *fast forward* Hamiltonian means the system is driven to the target state in some fixed amount of time. The transport is done on the ground state manifold \mathcal{M} .

Conjecture 1. For any fast forward Hamiltonian $\hat{H}(\lambda(t))$ driven along one dimensional path $\lambda(t) : \mathbb{R} \mapsto \mathbb{R}$ using time t as parametrization, the energy fluctuations δE^2 , averaged along the path, are larger than the geodesic length l_λ

$$\int_0^T \sqrt{\delta E^2(t)} dt =: l_t \geq l_\lambda \int_{\lambda_i}^{\lambda_f} \sqrt{g_{\lambda\lambda}} d\lambda = \int_0^T \sqrt{g_{\lambda\lambda}} \frac{d\lambda}{dt} dt. \quad (9.1)$$

The length l_λ is defined in control space (with metric tensor $g_{\lambda\lambda}$) and is generally larger than the distance between wave functions, i.e. the absolute geodesic (defined with $G_{\mu\nu}$). From its definition, we can see that it corresponds to the metric tensor as we use it.

The energy variance is

$$\delta E^2 = \langle o(t) | \hat{H}(t)^2 | o(t) \rangle - \langle o(t) | \hat{H}(t) | o(t) \rangle^2 = \langle \partial_t(t) | \partial_t o(t) \rangle_c = G_{tt} \quad (9.2)$$

and the Metric tensor in control space is defined as

$$g_{\lambda\lambda} := \langle \partial_\lambda o(t) | \partial_\lambda o(t) \rangle_c \quad (9.3)$$

Proof.

$$\delta E^2 \equiv \langle o(t) | \hat{H}(t)^2 | o(t) \rangle_c = \dot{\lambda}^2 G_{\lambda\lambda} + \mathcal{O}(\dot{\lambda}^4), \quad (9.4)$$

where $\mathcal{O}(\dot{\lambda}^4)$ needs to be positive for any real-valued Hamiltonian. This comes from the fact, that it has instantaneous time-reversal symmetry. \square

The conjecture only applies to unit fidelity protocols ($F(t) = 1 \ \forall t \in [0, T_f]$) and can be extended to an arbitrary dimensional path.

Conclusion

Bibliography

- M. V. Berry. Quantal phase factors accompanying adiabatic changes. *Proc. R. Soc. Lond. A*, 392(1802):45–57, March 1984. URL <http://rspa.royalsocietypublishing.org/content/392/1802/45>.
- M V Berry. Transitionless quantum driving. *Journal of Physics A: Mathematical and Theoretical*, 42(36):365303, aug 2009. doi: 10.1088/1751-8113/42/36/365303. URL <https://doi.org/10.1088/1751-8113/42/36/365303>.
- Michael V. Berry. THE QUANTUM PHASE, FIVE YEARS AFTER. 1989.
- Marián Fecko. *Differential Geometry and Lie Groups for Physicists*. Cambridge University Press, 2006. doi: 10.1017/CBO9780511755590.
- C. Gorodski. *An introduction to Riemannian geometry*. 2012. Preliminary version.
- Daniel Gutiérrez-Ruiz, Diego Gonzalez, Jorge Chávez-Carlos, Jorge G. Hirsch, and J. David Vergara. Quantum geometric tensor and quantum phase transitions in the lipkin-meshkov-glick model. *Phys. Rev. B*, 103:174104, May 2021. doi: 10.1103/PhysRevB.103.174104. URL <https://link.aps.org/doi/10.1103/PhysRevB.103.174104>.
- Michael Kolodrubetz, Dries Sels, Pankaj Mehta, and Anatoli Polkovnikov. Geometry and non-adiabatic response in quantum and classical systems. *Physics Reports*, 697:1–87, 2017. ISSN 0370-1573. doi: <https://doi.org/10.1016/j.physrep.2017.07.001>. URL <https://www.sciencedirect.com/science/article/pii/S0370157317301989>. Geometry and non-adiabatic response in quantum and classical systems.
- W. Tu Loring. *Differential Geometry*. Springer International Publishing, 2017. doi: 10.1007/978-3-319-55084-8.
- P. Petersen. *Riemannian Geometry*. Springer Verlag, 1998. ISBN 978-0-387-29403-2.

List of Figures

| | | |
|------|--|----|
| 1.1 | Mappings needed for the bundle definition. | 6 |
| 2.1 | Fiber bundle over \mathbb{R}^n with Hilbert spaces $\mathcal{H}(\lambda)$ as individual fibers. | 11 |
| 2.2 | Geometrical intuition to transport on fiber manifold sections \mathcal{M}_i . | 12 |
| 2.3 | Space of bare states and its projection to space of rays $\mathcal{PH}(\lambda) := \mathcal{H}(\lambda/U(1))$ | 12 |
| 2.4 | Geometrical intuition to transport on fiber manifold sections \mathcal{M}_s . | 13 |
| 2.5 | Parallel transporting around some closed curve C with anholonomy drawn in yellow. | 14 |
| 4.1 | Bloch sphere for the eigenstate u_1 with the initial direction of magnetic field $\mathbf{B} = (0, 0, B_z)$ transported along $\gamma = \{(\phi, \sqrt{\phi}) \phi \in [0, 2\pi]\}$ (blue). The final orientation of the magnetic field is marked red and the states on the Bloch sphere correspond to initial eigenstate. | 27 |
| 4.2 | Bloch sphere for the eigenstate u_1 with the initial direction of magnetic field $\mathbf{B} = (0, 0, B_z)$ transported along $\gamma = \{(0, \theta) \theta \in [0, \pi/2]\}$ (blue). The final orientation of the magnetic field is marked red and the states on the Bloch sphere correspond to initial eigenstate. | 28 |
| 5.1 | Energy for the case $N = 3$, section $\lambda = 1$ | 30 |
| 5.2 | Energy for the case $N = 3$, section $\chi = 1$ | 31 |
| 5.3 | Arctangent of metric tensor elements for the case $N = 3$. From the top: $\text{Arctan}(g_{11})$, $\text{Arctan}(g_{12}) = \text{Arctan}(g_{21})$, $\text{Arctan}(g_{22})$. . . | 32 |
| 5.4 | Metric tensor determinant in a parameter space for $N = 3$ | 33 |
| 5.5 | 1.0 Arctangent of Christoffel symbols for the case $N = 3$. First row from left: $\text{Arctan}(\Gamma_{111})$, $\text{Arctan}(\Gamma_{121})$, $\text{Arctan}(\Gamma_{122})$. Second row from left: $\text{Arctan}(\Gamma_{211})$, $\text{Arctan}(\Gamma_{221})$, $\text{Arctan}(\Gamma_{222})$ | 33 |
| 5.6 | Arctangent of Ricci curvature for the case $N = 3$. <i>Excuse the resolution, I will make better calculation in Metacentrum later.</i> . . . | 34 |
| 5.7 | Ricci curvature sections for three different $\lambda = \text{const.}$ | 35 |
| 5.8 | Geodesics for the case $N = 3$ starting from $(\lambda_i; \chi_i) = (0; 0)$ with $(\lambda'_i; \chi'_i) = (\cos \theta; \sin \theta)$, parametrized by angle θ | 36 |
| 5.9 | Comparing geodesics with repulsing (blue) and attracting (red) metric tensor divergence in the spherical symmetrical space. | 36 |
| 5.10 | Energy differences between neighboring energy levels for $N = 5$. First row: $E_1 - E_0$, $E_2 - E_1$, second row: $E_3 - E_2$, $E_4 - E_3$, third row: $E_5 - E_4$, $E_6 - E_5$ | 37 |
| 5.11 | Metric tensor determinant for the case $N = 5$ | 38 |
| 5.12 | Geodesics for the case $N = 5$, starting from the point $(1; 0)$. <i>The numerics around the singularity breaks down, but the solution is close to the drawn one, i.e. they will pass close to the singularity and continue to the left.</i> | 39 |

| | | |
|------|--|----|
| 5.13 | Three possible solutions between points $(1; 0)$ and $(4; 0.5)$. The length of the yellow one is surely longer than other two, but the difference between green vs. blue solution is not clear on the first sight. | 39 |
| 5.14 | First order phase transition – Separatrix (red), second order transition (blue point) compared to minimum between the ground state and first excited state in $N=3$ case (black, dashed). | 40 |
| 5.15 | Energy spectrum as function of χ , for $\lambda = 1$ and $N = 10$ | 41 |
| 5.16 | Energy spectrum as a function of λ , for $\chi = 1$ and $N = 10$ | 41 |
| 5.17 | Spectrum degeneracy between E_0 and E_1 . Hamiltonian dimensions are 1,3,5,7 in the first column and 2,4,6,8 in the second column. Black crosses mark most left-wise and right-wise singularity and the background corresponds to the metric tensor determinant. Other singularities are also well visible in the determinant. | 43 |
| 6.1 | Driving along the geodesic. λ_i and λ_f are initial resp. final parameters. DensityPlot shows the difference between Hamiltonian eigenvalues. | 46 |
| 6.2 | Infidelity in time for final time $T_f = 1$ for geodesical driving. | 48 |
| 6.3 | Final infidelity dependence on final time T_f for geodesical driving. | 48 |
| 6.4 | Infidelity dependence on final time in log-log scale. We can observe difference in numerical evaluation of different firmulas in the height of spikes. | 48 |
| 6.5 | Rescaled final infidelity $T_s := 2sT_f$ dependence on final time. Red points are for $F = 1$ | 49 |
| 6.6 | Fidelity dependence on time and final time in log log scale. Note that only $t < T_f$ has physical meaning. | 49 |
| 6.7 | Energy variance for geodesical driving protocol. | 50 |
| 6.8 | Driving along the linear path. $\lambda_i = (-10; 1)$ and $\lambda_f = (10; 1)$ are initial resp. final parameters. DensityPlot shows the difference between Hamiltonian eigenvalues. | 51 |
| 6.9 | Infidelity in time for three final times $T_f \in \{1, 5, 20\}$ for the linear driving. | 52 |
| 6.10 | Value of first element of the ground state vector $\alpha \equiv 0(t)\rangle_1$ during linear driving. | 53 |
| 6.11 | Final infidelity as a function of T_f with zoom on transitional part. | 54 |
| 6.12 | Final infidelity as a function of T_f in log log scale wit linear scaled plot inserted. | 55 |
| 6.13 | Final infidelity as a function of t for fast-driving regime, $T_f = 80 < T_c$ | 55 |
| 6.14 | Final infidelity as a function of t for close-adiabatic regime. $T_f = 170 > T_c$ | 56 |
| 6.15 | Final infidelity as a function of Δ and T_f and its three regimes. Zoomed boundary between them can be seen on 6.16. | 57 |
| 6.16 | Fine structure of the boundary between fast-driving and adiabatic regimes of final infidelity. | 57 |

| | | |
|------|---|----|
| 6.17 | Fidelity dependence for linear driving with $\Delta = 1$. Black line marks $t = T_f$, dashed black line $t = T_f/2$ and purple dashed line is the approximate value of T_c . Blue lines marks driving from Fig. 6.13, 6.14, visualizing the final times of the driving. | 58 |
| 6.18 | Energy variance for $\Delta_{sc} = 0.2$ for linear driving. Note that only $t < T_f$ has physical meaning. | 59 |
| 6.19 | Energy variance for $t = T_f/2$ for linear driving. | 59 |
| 7.1 | Arctangens of the metric tensor for higher state manifolds. By rows: $M_0, M_1; M_2, M_3; M_4, M_5$ | 64 |
| 7.2 | Infidelity difference between line and geodesic, above picture is original from Felipe, bottom one is edited in GIMP to see the difference more clearly. | 65 |
| 8.1 | Arctangens of the fidelity of quenches from $(\lambda_i; \chi_i) = (0; 0)$ to $(\lambda; \chi)$ | 68 |
| 8.2 | Equidistant points on geodesics of the ground state manifold. | 68 |
| 8.3 | Fidelity for sequential quenches along geodesics (see green lines on top). Left (right) column corresponds to lower (upper) geodesic. Time steps from top are $\Delta t \in \{0.03, 0.1, 0.5\}$. Time difference between points in the plot on top is $\Delta t = 0.5$ | 69 |

A. Appendix 1

$$\begin{aligned}
A = & 16\sqrt[3]{2} \left(64\lambda^6 - 192\lambda^5\chi^2 + 24\lambda^4 (52\chi^4 - 93\chi^2 + 36) \right. \\
& - 8\lambda^3 (29\chi^4 + 414\chi^2 - 513) \chi^2 \\
& + 6\lambda^2 (1225\chi^8 - 10053\chi^6 + 17595\chi^4 - 10557\chi^2 + 1377) \\
& + \left((64\lambda^6 + 864\lambda^4 + 8262\lambda^2 + 3(818\lambda - 27285)\chi^{10} \right. \\
& + 6(\lambda(1225\lambda - 3198) + 27108)\chi^8 \\
& - (2\lambda(\lambda(116\lambda + 30159) - 89073) + 326727)\chi^6 \\
& + 6(\lambda(\lambda(8\lambda(26\lambda - 69) + 17595) - 42660) + 51516)\chi^4 \\
& - 3(2\lambda(\lambda(4\lambda(\lambda(8\lambda + 93) - 171) + 10557) - 16119) + 36207)\chi^2 \quad (A.1) \\
& + 24013\chi^{12} + 25515) \\
& - \left. (16\lambda^4 + 144\lambda^2 + 2(74\lambda - 1185)\chi^6 + 3(4\lambda(16\lambda - 77) + 1329)\chi^4 \right. \\
& - 2(2\lambda(\lambda(8\lambda + 93) - 207) + 1161)\chi^2 + 889\chi^8 + 1053) \right)^{1/2} \\
& + 6\lambda(409\chi^8 - 3198\chi^6 + 29691\chi^4 - 42660\chi^2 + 16119)\chi^2 + 24013\chi^{12} \\
& - 81855\chi^{10} + 162648\chi^8 - 326727\chi^6 + 309096\chi^4 \\
& \left. - 108621\chi^2 + 25515 \right)^{1/3}
\end{aligned}$$

$$\begin{aligned}
B = & \frac{256\sqrt[3]{2}}{3A} \left(16\lambda^4 + 144\lambda^2 + 2(74\lambda - 1185)\chi^6 + 3(4\lambda(16\lambda - 77) \right. \quad (A.2) \\
& \left. + 1329)\chi^4 - 2(2\lambda(\lambda(8\lambda + 93) - 207) + 1161)\chi^2 + 889\chi^8 + 1053 \right)
\end{aligned}$$

$$C = 4\sqrt{\frac{A}{3\sqrt[3]{2}}} + B + \frac{16}{3}(4\lambda^2 - (4\lambda + 33)\chi^2 + 49\chi^4 + 45) \quad (A.3)$$

$$\begin{aligned}
D = & -\frac{A}{3\sqrt[3]{2}} - B - \frac{8}{3}(59\lambda^2 + 436\lambda\chi^2 + 392\chi^4 + 132\chi^2 - 180) \\
& + 8(5\lambda + 14\chi^2)^2 \quad (A.4)
\end{aligned}$$

$$\begin{aligned}
E = & \frac{9216}{C} ((\lambda - 1)\chi^4 - 4(\lambda - 1)\chi^2 + \lambda - 2\chi^6) \\
F = & \frac{1}{2}\sqrt{\frac{A}{3\sqrt[3]{2}}} + B + \frac{16}{3}(4\lambda^2 - (4\lambda + 33)\chi^2 + 49\chi^4 + 45) \quad (A.5) \\
G = & -5\lambda - 14\chi^2
\end{aligned}$$

B. Attachments

B.1 First Attachment